12-2009

Structural Health Monitoring and Damage Evaluation of Full-Scale Bridges Using Triaxial Geophones: Controlled In-Situ Experiments and Finite Element Modeling

William S. Ragland II
University of Tennessee - Knoxville

To the Graduate Council:

I am submitting herewith a dissertation written by William S. Ragland II entitled "Structural Health Monitoring and Damage Evaluation of Full-Scale Bridges Using Triaxial Geophones: Controlled In-Situ Experiments and Finite Element Modeling." I have examined the final electronic copy of this dissertation for form and content and recommend that it be accepted in partial fulfillment of the requirements for the degree of Doctor of Philosophy, with a major in Civil Engineering.

Dayakar Penumadu, Major Professor

We have read this dissertation and recommend its acceptance:

Richard M. Bennett, Edwin G. Burdette, Richard T. Williams

Accepted for the Council:
Carolyn R. Hodges

Vice Provost and Dean of the Graduate School

(Original signatures are on file with official student records.)

To the Graduate Council:

I am submitting herewith a dissertation written by William Steven Ragland II entitled "Structural Health Monitoring and Damage Evaluation of Full-Scale Bridges Using Triaxial Geophones: Controlled In-Situ Experiments and Finite Element Modeling." I have examined the final electronic copy of this dissertation for form and content and recommend that it be accepted in partial fulfillment of the requirements for the degree of Doctor of Philosophy, with a major in Civil Engineering.

Dayakar Penumadu

Major Professor

We have read this dissertation
and recommend its acceptance:

Richard M. Bennett

Edwin G. Burdette

Richard T. Williams

Accepted for the Council:

Carolyn R. Hodges

Vice Provost and
Dean of the Graduate School

(Original signatures are on file with official student records)

Structural Health Monitoring and Damage Evaluation of Full-Scale Bridges Using Triaxial Geophones: Controlled In-Situ Experiments and Finite Element Modeling

A Dissertation
Presented for the
Doctor of Philosophy
Degree
The University of Tennessee, Knoxville

William Steven Ragland II
December 2009

Dedication

To Rachel
For her love, patience, and encouragement.

To Mom and Dad
For always believing in me.

Acknowledgements

There are several people who I wish to thank for their help in the completion of this research. I would like to thank Dr. Dayakar Penumadu for offering me the opportunity to work with him, for encouraging me throughout the study, for his help with field tests, for teaching courses I have taken, for discussing the research, for reviewing papers, for arranging financial support, and for chairing my committee. I want to thank Dr. Richard Williams for his encouragement, for his help with field tests, for numerous hours spent in the lab discussing the research, for reviewing papers, and for serving on my committee. I want to thank Dr. Edwin Burdette for serving on my committee, for his help contacting the correct people to obtain permission, bridge plans, and inspection reports, for discussing the research, and for teaching numerous courses I have taken. Had it not been for CE 361, I probably would not be in structures today. Dr. Richard Bennett has been a part of my experience at the University of Tennessee since my first day of class as a freshman in 2002, and I would like to thank him for serving on my committee, for discussing the research, and for teaching several courses I have taken.

I would like to thank the Joint Institute for Advanced Materials (JIAM) Fellowship Program for providing additional financial support during my doctoral studies.

I would like to extend a special thanks to Mr. Dave Lane for his help with countless hours of field testing. I would also like to thank Mr. Ken Thomas, Mr. Larry

Roberts, Mr. Aashish Sharma, and Mr. Eric Guffey for their help with field tests and countless times “dropping the sandbag”.

I would like to thank Mr. Phil Large of Wilbur Smith and Associates for his help in arranging the field tests on the SmartFix project and for finding plans when I needed them. I especially want to thank Mr. Jeff Walker of Bell and Associates Construction for his help and cooperation with the SmartFix field tests. Under immense pressure to finish a multimillion dollar project before a firm deadline, Mr. Walker found time to help me, and I am forever grateful.

Thanks are also extended to Terry Leatherwood, Henry Pate, and Ed Wasserman of the Tennessee Department of Transportation for their help and cooperation with permission, bridge plans, and bridge inspection reports. Special thanks are also extended to Dave Harrison and George Condjella of Seismic Surveys Inc. for their help and use of their equipment.

Last, but certainly not least, I want to thank my wife, Rachel, for her love, support, encouragement, and sacrifice during my doctoral studies. I also want to thank Mom and Dad for their encouragement and for helping me become the person I am today. Finally, I want to thank the rest of my family and friends for their support and encouragement throughout the journey that is, graduate school.

Abstract

The purpose of this study was to evaluate the effectiveness of various vibration-based damage detection methods using triaxial vibration records obtained using inexpensive geophones during in-situ, full-scale, damaged bridge tests.

Geophones are passive directional sensors and much cheaper than accelerometers which are typically used for structural vibration measurements. However, magnitude and phase errors associated with a geophone's output must be corrected for if they are implemented in bridge monitoring systems. This research discusses correction procedures for magnitude and phase errors associated with geophones. A simply supported beam was analyzed to verify that the correction procedures and modal parameter identification procedures used produced reliable results. A full-scale bridge test was also performed to further validate the correction and modal analysis procedures used. The results of the simple beam and full-scale bridge tests were validated using finite element modeling.

Vibration-based damage detection relies on changes in the dynamic properties of a structure to detect damage. Only one other study was found that compares various vibration-based damage detection techniques using full-scale damaged bridge tests. Thus, a need remains for further comparison of vibration-based damage detection techniques using vibration data collected entirely on full-scale bridges. This study compares various vibration-based damage detection techniques using triaxial vibration records obtained during separate in-situ, full-scale, damaged bridge tests. Furthermore, the damage detection techniques are extended to three dimensions to evaluate three

dimensional response of the bridge to damage. This is a unique aspect of the current research because no other three dimensional data sets obtained from in-situ, full-scale, damaged bridge tests have been reported in the literature.

Finite element modeling is perhaps the most widely relied upon method of structural and mechanical analysis. In the field of vibration-based damage detection, finite element models are often used to plan field tests, to verify field test results, and to produce damaged data sets when the actual structure is unable to be damaged. As part of this research, finite element models were constructed to lend credibility to the field test results and to investigate damage scenarios other than those inflicted during the field tests.

Table of Contents

List of Figures

List of Tables

Chapter 1. Introduction and Literature Review

1.1 Introduction

In recent years, much attention has been given to the state of infrastructure in the United States. In its *2009 Report Card for America's Infrastructure*, The American Society of Civil Engineers (ASCE) assessed the state of the nation's infrastructure with an overall poor grade of "D". While the condition of all infrastructure types remains an important issue, the focus of this study is the nation's bridge inventory. In the same report, ASCE assessed the nation's bridge inventory with an overall grade of "C" and estimated that it would take a $17 billion annual investment to significantly improve current bridge conditions in the United States.

As of 2008, the Federal Highway Administration (FHWA) reports that of the nation's 601,411 bridges, 79,922 are classified as functionally obsolete while 71,469 are classified as structurally deficient (FHWA 2008). In other words, one in four bridges in the United States is in need of some type of rehabilitation. Furthermore, according to the American Association of State Highway and Transportation Officials (AASHTO), the average age of bridges in the United States is 43 years old while most were only designed to last 50 years (AASHTO 2008).

As the nation's bridge inventory continues to age, methods of reliably assessing its overall health have become increasingly more important. Currently, bridges in the United States are inspected and rated during biennial inspections which rely heavily on visual techniques. However, in a recent report by the FHWA, visual inspections were deemed relatively unreliable (FHWA 2001). For this reason, researchers have been

working for several years on the development of more objective methods for nondestructively inspecting and rating bridge condition.

For the most part, the nondestructive evaluation methods that have been developed over the past several years fall into two major categories: local and global. Local damage detection methods used for assessing bridge health include techniques such as impact-echo, ground-penetrating radar, ultrasonic pulse velocity, spectral analysis of surface waves, infrared thermography, radar, and mechanical sounding (Gassman and Tawhed 2004). The problem with local damage detection techniques is that the location of the damage must be known before the test is conducted, and the area to be tested on the bridge must be accessible. Because of the limitations encountered when using local damage detection methods, global damage detection methods have been developed that rely on changes in the overall response of a bridge as an indication of damage. One area of global damage detection that has received much attention in the literature is often referred to as vibration-based damage detection.

Vibration-based damage detection focuses on changes in the dynamic characteristics of a structure, such as natural frequency, mode shape, etc., as indicators of damage. Several global evaluation techniques and indices have been derived and presented by various researchers over the past several years. Detailed reviews of these techniques as applied to bridges and other structures can be found in Doebling et al. (1996, 1998) and Sohn et al. (2004). It is left to the reader to further explore these reviews, but to summarize, the methods discussed monitor shifts in natural frequency, absolute changes in mode shapes, changes in mode shape curvature, changes in modal

strain energy, changes in calculated stiffness matrices, changes in calculated flexibility matrices, finite element model updating procedures, and neural network based methods.

The basic idea behind any global damage identification method that examines changes in the dynamic properties of a structure is that modal parameters (modal frequencies, modal damping ratios, mode shapes) are a function of the physical properties of the structure (mass, stiffness, boundary conditions). Therefore, a change in the physical characteristics of a structure should result in a change in its modal parameters. In a study by Farrar and Jauregui (1996), various vibration-based damage identification techniques were compared by evaluating a steel girder bridge that had been incrementally damaged by cutting one of the girders starting in the middle of the web and continuing through the bottom flange. Zhou et al. (2007) compared various vibration-based damage identification techniques using a laboratory model of a steel girder bridge to evaluate the effectiveness of various techniques at localizing small-scale damage on a bridge deck. The purpose of this study is to evaluate the effectiveness of various vibration-based damage detection methods using triaxial vibration records obtained using inexpensive geophones during in-situ, full-scale, damaged bridge tests.

1.2 Literature Review

Detailed reviews of structural health monitoring and vibration-based damage detection up to 1996 and from 1996 to 2001 can be found in Doebling et al. (1996, 1998) and Sohn et al. (2004) respectively. The purpose of this review is to summarize the parts

of these reviews that pertain to full-scale bridges and to review the literature relevant to the current research published after these reviews were completed.

Salane et al. (1981) observed a three-span highway bridge during a fatigue test and found that changes in the bridge's stiffness and vibration signatures could be used as indicators of damage.

Kato and Shimada (1986) measured ambient vibrations on a pre-stressed concrete bridge during a failure test. Using ambient vibrations, slight reductions in natural frequencies were observed as the load approached the ultimate load, but damping values were noted to be largely unaffected.

Biswas et al. (1990) observed a continuous, two-span composite bridge in a damaged and undamaged condition. Damage was induced by loosening bolts in a girder splice, and changes in frequency response functions calculated using a measured input were observed and found to be quantifiable. Consistent drops in modal frequencies as a result of the induced damage were also observed.

Jain (1991) studied a deteriorating railway bridge and found that modal parameters can only provide general information on the damage state of a bridge but not the location, extent, or cause of the damage.

Tang and Leu (1991) found that changes in the natural frequencies of a prestressed concrete bridge were not as reliable indicators of damage as changes in mode shapes. That authors state that a frequency shift on the order of 0.01 Hz must be detectable to identify damage using natural frequencies.

Raghavendrachar and Aktan (1992) evaluated a three-span reinforced concrete bridge using impact tests and found that modal parameters of higher modes of vibration are required for detecting small levels of damage.

Farrar et al. (1994) studied a double steel girder bridge on I-40 over the Rio Grande River in New Mexico. This particular study is perhaps the most cited study of vibration-based damage detection techniques applied to bridges. The bridge was tested in an undamaged condition followed by four incremental damage tests. The results from both forced and ambient vibration tests were used to calibrate detailed and simplified finite element models of the bridge. This report summarizes the experimental procedures and results obtained. It was determined that mode shapes are more sensitive indicators of damage than natural frequencies because of the large amount of damage necessary to cause a shift in the bridge's natural frequencies. A subsequent report by Farrar et al. (1996) summarizes the finite element models of the bridge and compares the results obtained with these models to the measured dynamic response of the bridge.

Alampalli et al. (1995) performed several tests on an undamaged single span steel girder bridge to evaluate the effects of test variations and environmental conditions on the bridge's modal properties. Damage was then introduced by cutting the steel girders at various locations. The authors found that changes in natural frequency could be used as indicators of damage because the change caused by the induced damage was greater than the observed statistical variation caused by test variations and environmental effects. It was also found that changes in mode shapes determined using modal assurance criterion (MAC) values were not sensitive enough to identify damage.

Farrar and Cone (1995) further analyzed the bridge tested by Farrar et al. (1994). Adequate estimates of natural frequencies and damping ratios were found using ambient vibration data. It was also reported that modal parameters may not be sensitive enough to identify damage in its early stages, perhaps making them unpractical damage indicators.

Liang et al. (1995) evaluated the repeatability of identified modal parameters and changes in modal parameters caused by repair work on the steel Peace Bridge over the Niagara River. Using accelerometer measurements, impact tests were found to provide better results than ambient input tests.

Salawu (1995) and Salawu and Williams (1995) studied a reinforced concrete bridge undergoing repairs. Using an integrity index, the repaired areas on the bridge were identified. Natural frequencies were found to slightly decrease after the repairs.

The MAC and coordinate modal assurance criterion (COMAC) were also used to identify the repaired areas. The MAC was found to indicate which modes were affected by the repairs, and the COMAC identified the location of the repairs. However, both the MAC and the COMAC falsely identified areas that were not actually repaired.

Stubbs et al. (1995) applied the damage index method to the bridge tested by Farrar, et al. (1994). The method was found to successfully identify the location of the induced damage without any knowledge of the bridge's material properties.

Farrar and Jauregui (1996, 1998 a, 1998 b) summarize the application of five damage identification techniques reported in the technical literature to experimental and numerical modal data obtained by Farrar et al. (1994) on the I-40 Bridge over the Rio Grande River. All methods studied correctly identified the damage location for a cut removing half the girder cross section. However, the authors state that if some of the methods had been applied without knowledge of the damage location, it would have been difficult to discern if damage had not actually occurred at locations other than the induced damage location. When applied to less severe damage scenarios, the methods were found to be inconsistent and did not clearly identify the induced damage location. Overall, the authors found that the damage index method (Stubbs et al. 1995) performed the best when the entire analysis was considered. The authors also point that that the damage index method was the only one studied that provided a specific criteria to quantify when observed changes in the calculated parameters were indicative of damage. The authors

point out that such a criteria is essential when trying to determine if damage has occurred at more than one location and suggest similar criteria could be developed for the other methods studied to help prevent false-positive readings.

De Stefano et al. (1997) describe the use of Auto-Regressive Moving Average (ARMAV) models to extract modal parameters from vibration data obtained under service conditions. Signal processing techniques used to minimize errors associated with noise are described, and the authors report overall reliable results.

Farrar et al. (1997) present results obtained from field tests on the Alamosa Canyon Bridge in New Mexico. The authors measured the bridge vibrations every 2 hours over a period of 24 hour period to assess the effects of temperature on modal parameters. A variation of 5% was noted in the first modal frequency over the 24 hour period.

Doebling and Farrar (1997) describe how to define statistical confidence limits for modal parameters. Using data from the I-40 bridge test described by Farrar, et al. (1994), the authors found that modal parameter variation from between tests can be more significant than those caused as a result of damage. The authors conclude that statistical analysis must be a part of any modal-based damage identification procedure.

Abe et al. (1999) studied the effects of varying wind loads and frictional forces on the modals properties of the Hakucho Bridge in Japan. The authors report that natural frequencies and damping ratios vary based on wind velocity which contradicted results obtained from wind tunnel testing performed on a model of the bridge. Discrepancies in modal the modal parameters obtained from the field test and the wind tunnel test are attributed to the model's inability to represent stick-slip behavior.

Ko et al. (1999) discuss the instrumentation of three large bridges (400+ meter main spans) in Hong Kong. A total of 900 sensors were installed on the three bridges to monitor accelerations, strains, wind speed, temperature, and displacements. The viability of detecting possible damage scenarios using modal parameters is discussed, and the authors conclude that dynamic monitoring should be able to detect most types of damage.

Krämer et al. (1999) describe the instrumentation, test setup, induced damage scenarios, and various other considerations in regard to the Z24 bridge damage detection tests. The Z24 bridge test is one of the most cited studies in the current literature. No results are provided in the current paper, only a description of the test procedure. The post-tensioned two box cell girder bridge is straight, slightly skewed, with three spans measuring 14 m, 30 m and 14 m resting on four piers. As part of an environmental monitoring system, sensors to measure air temperature, humidity, rain (true or false), wind speed, and wind direction were installed on the bridge. Sensors to measure the bridge's temperature, the approach pavement temperature, and temperature of the

surrounding soil were also installed. Inductive loops were also installed to monitor whether or not traffic was on the bridge. To measure bridge vibrations as part of the monitoring process, 16 force balanced accelerometers were installed on the bridge at various locations. During the damaged tests, a new measurement system recording 35 channels simultaneously was used to measure the vibrations over the entire bridge during 9 different test setups. Ambient vibrations as a result of traffic moving under the bridge were recorded, and force vibrations caused by two vertical shakers attached to the bridge were also recorded for the individual damaged tests.

Maeck and De Roeck (1999) investigated the prestressed Z24 Bridge in Switzerland. In this particular study, the authors were successful in locating and quantifying various induced damage scenarios using a direct stiffness approach. The direct stiffness approach uses calculations of modal bending moments and curvatures to derive the bending stiffness of the bridge at a particular location. Changes in the bending stiffness are considered to be indicative of damage.

Stubbs et al. (1999) use the damage index method to evaluate the integrity of a four-lane bridge spanning I-40. Modal parameters obtained from field test measurements are compared with those obtained from a finite element model constructed using as built plans. Possible damage locations and severity estimations were then made using the damage index method. The damage location and severity estimates were then compared

with surface crack patterns observed during a visual inspection of the bridge and were found to be in good agreement.

Wahab and De Roeck (1999) investigate changes in modal curvatures to detect damage induced in the Z24 Bridge. A damage indictor called the curvature damage factor is introduced in which the difference in mode shape curvatures for all modes is summarized by one number for each measured point. The authors found promise in using modal curvatures for damage detection in bridges. They also found modal curvature estimates to be more accurate for lower modes than higher modes. It is stated that a dense measurement grid is necessary to obtain good estimates of higher modal curvatures. Finally, the application of techniques to improve the quality of measured mode shapes in order to obtain better modal curvature estimates for higher modes is recommended.

Wang et al. (1999) present a summary of preliminary results obtained from monitoring the Kishwaukee Bridge in Illinois. The bridge is one of the first post-tensioned bridges constructed using the balanced cantilever technique. Baseline modal parameters obtained 13 years prior to the current test's modal parameters were found to be minimally different. Finite element modeling was used to assess the effects of identified cracking on the overall structural integrity of the bridge. Furthermore, results from the finite element model indicate that large localized damage only produced small changes in the overall modal properties of the bridge. The authors also note that a 30° F

decrease in temperature in a numerical simulation produced a 2% increase in natural frequency, and that strains induced to temperature variation can exceed those induced by traffic loading.

Bergmeister and Santa (2000) describe the instrumentation used to monitor part of the Colle di Sarco in Italy. Various measurement systems and their application to global monitoring are discussed. The instrumentation described includes several devices to measure environmental conditions, strain gauges on pre-stressing cables and reinforcement, and load cells on the bearings.

Choi and Kwon (2000) discuss a neural network damage detection method for a steel truss bridge. A finite element model of the bridge was calibrated using load test data. From the model, eight critical truss members were identified. Eight damage scenarios were simulated by reducing the stiffness of each identified critical member. The authors claim that the two-step neural network successfully located the damage in the finite element model.

Farrar et al. (2000) discussed the structural health monitoring studies performed on the Alamosa Canyon and I-40 Bridges. Both forced and ambient vibration tests are discussed. Tests performed to study the variability of modal parameters caused by thermal effects, vehicle weight, excitation source, and data reduction are also discussed. Finite element modeling of the Alamosa Canyon Bridge is discussed and modal

parameters are compared to those obtained from the field tests using the MAC. Attempts were made to damage the bridge, but the alterations permitted to be made did not cause a significant change in the measured modal properties. In another attempt to simulate damage, the bridge was locally stiffened by clamping a steel plate to the bottom flange of one of the girders. Of the damage identification methods studied, none were successful in locating the stiffened area of the bridge. Furthermore, particular emphasis is placed on the development of statistical confidence intervals for modal parameters used by damage detection techniques. The authors argue that damage must cause changes in modal parameters outside of developed confidence bounds for any definitive conclusion about the onset of damage to be made.

Peeters and De Roeck (2000) compare a direct stiffness approach and a sensitivity-based updating technique for locating damage induced on the Z24 Bridge. The authors noted numerical instabilities when trying to calculate curvatures directly from measured mode shapes. To prevent this, a smoothing procedure was first applied to the mode shapes, and then modal curvatures were calculated. It was concluded that the direct stiffness approach is a reliable alternative to the sensitivity-based updating technique.

Peeters et al. (2000) compare shaker excitation and ambient excitation of the Z24 Bridge. It was found that the additional cost of the shaker was not justifiable because ambient excitation provides comparable results. The authors extracted ten vibration

modes from the forced tests, most of which were consistently identified from the ambient tests.

Halling et al. (2001) present the results of seven forced vibration tests performed on an isolated single span of a freeway overpass structure. Furthermore, a series of states of damage and repair were performed as part of the testing program. Originally part of a nine-span overpass, the test span consisted of a 0.12 m asphalt layer atop a 0.18 m concrete deck supported by eight steel girders spanning between two concrete bents. Vibrations were measured at nine locations on the bridge and one location on the ground under the bridge using an array of force-balanced accelerometers. However, only five measurement locations on the bridge deck were considered in the present study. The authors noted decreases in natural frequencies for four damage tests, but they also note increases in natural frequencies for two damage tests. A finite element model of the bridge was constructed and calibrated to the field test results using a parameter optimization algorithm. Using the results from the finite element model, an agreement was found between the increase or decrease in natural frequency and the retrofit or damage applied to the bents. The authors also attempt to localize the damage inflicted on the bridge using the location of the point of rotation of the identified mode shapes with respect to the damage location. In concluding, the authors noted that changes in natural frequencies and mode shapes as indications in structural assessment were successfully identified. Also, the changes in natural frequencies and mode shapes (point of rotation) for each test are unique, and therefore could be used as indicators for structural

assessment. And finally, that the movement of the point of rotation from one test to the next can be used to locate damage or retrofit applied to the bridge bent.

Maeck et al. (2001) present a damage identification technique applied to the Z24 bridge data called the direct stiffness calculation based on the relation that the bending stiffness in each section of a structure can be written as the quotient of the bending moment to the corresponding curvature. Modal parameters were extracted from the collected data using the stochastic subspace identification procedure. In order to obtain internal bending moments, a finite element beam model of the bridge was constructed. A finite element model updating procedure is discussed. One interesting remark that the authors make is that cracks in the bridge could only be detected if they remained open. Finally, the direct stiffness calculation is deemed to be successful in locating damage despite numerical inaccuracies at some locations, and natural frequencies and modal displacements (and their derivatives) are also determined to be useful damage indicators.

Park et al. (2001) evaluate the correlation between predicted and observed damage locations on a two span reinforced-concrete box-girder bridge using the damage index method. Using a set of seven accelerometers and a specially designed impact hammer, bridge vibrations were measured at a total of 26 locations (13 on the east side and 13 on the west side) on the bridge deck and four locations on the column supporting the bridge at its midpoint. Vibrations were recorded in the vertical direction at all locations and in the transverse direction on the supporting column and the 13 locations on

the west side of the bridge deck. A finite element model of the bridge was then calibrated to the field test results using a sensitivity matrix and an updating technique. Nine months after the first test, another field test was performed. During this test, bridge vibrations caused by an impact hammer were recorded in the orthogonal coordinate directions at the same 30 locations previously described using five triaxial accelerometers. Another finite element model was then calibrated to the second set of field test results. Using the finite element models and the damage index method, the bridge was analyzed in effort to determine the existence of damage. In order to verify the correctness of the damage location predictions, a visual inspection of the bridge was completed, and observed cracking patterns in the bridge deck were compared with the predicted damage locations. The authors found a good agreement between the predicted and observed damage locations. Finally, the authors noted that environmental conditions might significantly affect the accuracy of the damage locations and baseline system identification. In a companion paper, Bolton et al. (2001) more thoroughly describe the bridge under investigation, the instrumentation setup, the test methodology, the modal analysis results, and discuss changes found in the measured bridge response characteristics during the period between the modal tests. Variations in bridge response characteristics due to environmental changes were not noted in either test.

Zhao and DeWolf (2002) used a modified flexibility method and ambient vibration data to evaluate a bridge subject to small changes in structural behavior. The bridge tested was a two-span (29.26 m each), continuous steel-girder bridge (7 total

girders) that was known to have partially restrained end bearings during cold weather. A total of 14 accelerometers were used to measure traffic induced vibrations over a two-year period. Response spectra were used to determine the three lowest natural frequencies and mode shapes. The natural frequencies were determined from the peaks in the spectrum, and the mode shapes were derived using the magnitude of the spectrum at each of the three natural frequencies. The bridge's natural frequencies were found to increase with decreasing temperature, in particular below 30° F. Modal displacements alone were found by the current authors to be unacceptable for structural monitoring due to large variations under the same temperature conditions. Finally, a modified modal flexibility method which incorporates both natural frequencies and modal displacements was found to provide a clear indication of a change in the bridge's structural behavior as a result of end bearing restraint due to temperature change.

Kim and Stubbs (2003) present a crack detection algorithm for full-scale bridges that not only locates the crack but also estimates the size of the crack. The paper is presented in two parts: 1. the theoretical development of the algorithm, and 2. a description of a field experiment to establish the feasibility of a real application. The algorithm is applied to modal test data collected on a full-scale steel girder bridge over the Rio Grande River on U.S. highway I-40 in New Mexico. The bridge was tested in an undamaged state and then again after each increment of damage (see Farrar et al. 1994). The authors were successful in locating the induced damage with a relatively small localization error. It was concluded that it is possible to accurately estimate crack sizes in

steel girder bridges with the knowledge of as few as three natural frequencies and mode shapes of both the undamaged and damaged bridge. Furthermore, it was shown that knowledge of material properties was not necessary for implementation of the algorithm.

Pothisiri and Hjelmstad (2003) present a global damage detection algorithm based on a parameter estimation method using a finite element model and measured modal properties from a structure. The proposed algorithm was examined using a numerical simulation of a planar truss bridge. Stating that the goal of the research was to formulate a practical approach for global damage detection from incomplete and noise-polluted data, random noise was added to the data obtained from the finite element model using known statistical parameters. Various damage scenarios were inflicted on the finite element model, and the results are discussed. Ultimately, the authors concluded that the proposed algorithm could detect and assess damage successfully in the face of noisy measurements provided that the noise is not too large. The authors refer to the proposed algorithm as the GPE (global parameter estimation) algorithm.

Ren et al. (2004 a) present the results of a seismic evaluation study of the Cumberland River Bridge in Western Kentucky. Parts of the study included an ambient vibration field test, finite element modeling, determination of site-specific ground motion, time history response to seismic excitation, and seismic evaluation and retrofitting. The Cumberland River Bridge consists of two identical six-span bridges, one in each direction. Each bridge consists of two, variable depth steel girders supporting

rolled steel stringers that support a reinforced concrete deck. Ambient vibrations were measured in three orthogonal coordinate directions using accelerometers at a total of 18 locations. Data was collected at the various locations through six different tests using four stationary sets of accelerometers and three roving sets of accelerometers. Modal properties were identified using two different methods: the peak picking method in the frequency domain and the stochastic subspace identification method in the time domain. A finite element model was then created and initially calibrated to the modal parameters identified from the field tests. A parametric study was then carried out to further calibrate the more sensitive parameters of the model, identified in the current study to be the inertial moment of the frame elements used to model the truss members of the superstructure, the bearing spring stiffness in the longitudinal direction, and the joint lumped masses used to model the concrete slab. In order to compensate for the reduction in transverse stiffness caused by the lumped mass approach used to model the concrete slab, the authors increased the transverse bending stiffness of the bridge girders using a multiplication factor. Using the calibrated finite element model, time history analyses of the bridge under 250 year and 500 year earthquakes were performed, and capacity/demand ratios were calculated for various components of the bridge. The results indicate that the bridge's bearings were in need of retrofit to meet seismic demand, the bridge would remain elastic under a 250 year earthquake, and that partial damage may be sustained under a 500 year earthquake but maintain accessibility for emergency vehicles.

Ren et al. (2004 b) discuss an experimental and analytical modal analysis of steel-girder arch bridge over the Tennessee River on highway I-24 in western Kentucky. The 643 m bridge consists of nine spans symmetric about the main arch span of 163 m. The arch span was the only portion of the bridge tested. Vibration data was collected at a total of 30 locations using triaxial accelerometers. The vibration data was gathered using three stationary accelerometers and four roving accelerometers. Two modal analysis methods were implemented to extract modal properties from the vibration data: the peak picking method in the frequency domain and the stochastic subspace identification method in the time domain. In comparing the two methods, good agreement was found in the identified natural frequencies, but the stochastic subspace identification method was found to produce much better mode shapes. Two different finite element models of the bridge were also constructed and compared. In Model-1 in the paper, the concrete slab elements are modeled as equivalent joint forces for static analysis or lumped joint masses for modal analysis. In Model-2, the concrete slab is modeled using shell elements. It was found that the results obtained using Model-1 agreed well with the field test results, and that this simplified model was suitable for the dynamic analysis of the bridge. Model-2 was found to only influence the transverse behavior of the bridge resulting in a higher transverse natural frequency.

Xia and Brownjohn (2004) present a method for quantitative damage assessment of a damaged reinforced concrete bridge deck structure using a systematically updated finite element model. The laboratory model used in the study was a lightly reinforced

concrete slab supported by two reinforced concrete beams. Finite element modeling of the structure was carried out in two steps. First, a finite element model was validated for the laboratory bridge model before any damage was induced. Second, the finite element model was validated after the damage was inflicted. This method was used to determine physical properties of the bridge in an undamaged state in order to establish a reliable finite element model prior to condition assessment of the damaged bridge. In order to validate the undamaged and damaged finite element models, vibration tests were conducted on both the undamaged and damaged laboratory bridge models. Vibrations caused by an instrumented hammer and an electrodynamic long stroke inertial shaker were measured at 22 locations using accelerometers. Data obtained from the hammer was used in the model updating procedure due to excessive noise in the data from the shaker. During the updating procedure for the undamaged bridge model, the stiffness of the boundary supports, the concrete's modulus of elasticity, and the mass density of the concrete were selected as the updating parameters. Due to cracking caused during the damage testing, the moment of inertia of the beams and the cross-sectional area were used as the updating parameters for the undamaged model. In order to assess the effectiveness of the updating procedure, experimental and analytical natural frequencies were compared directly, and experimental and analytical mode shapes were compared using a modal assurance criterion. A damage index based on a reduction in stiffness in the damaged model as compared to the undamaged model is presented. Finally, the authors present a method to estimate the load-carrying capacity of the damaged bridge model based on the moment of inertia and the steel ratio of the damaged cross section.

Bolton et al. (2005) document changes in the modal parameters of a bridge as a result of the Hector Mine Earthquake located 47 miles east-southeast of Barstow, California. The bridge discussed is a concrete box-girder bridge constructed in 1968 referred to as the Lavic Road Bridge. Originally, the bridge was to be monitored for reactive-aggregate induced deterioration. However, two weeks after a scheduled field test the earthquake damaged the bridge, and another unscheduled field test three days after the event was scheduled to capture any changes in the modal characteristics of the bridge. Pre-event and post-event vibration measurements were made at 30 locations on the bridge in three orthogonal coordinate directions using five orthogonal accelerometers. The bridge was excited using an instrumented weight drop hammer. Modal parameters were identified using a global polynomial curve-fitting method. Comparing the results from pre-event and post-event tests, the authors found significant changes in modal frequencies and damping ratios, but they noted that the modal order remained the same. In conclusion, the authors state that the modal properties of the superstructure remained relatively consistent and identifiable despite the large shifts in resonant frequencies and damping ratios as a result of earthquake induced damage.

Lauzon and DeWolf (2006) present results obtained from ambient vibration monitoring of a highway bridge undergoing destructive testing. The goal of the paper was to evaluate changes in vibration signatures that could possibly indicate that the stiffness of the bridge had changed in a way that could lead to the failure of the entire bridge or one of its major components. In its original state, the three-span bridge tested

consisted of eight simply supported rolled steel beams distributed across the bridge's width supporting a cast-in-place concrete deck. The bridge was replaced in phases, and during the final phase of construction a third of the bridge's cross section was made available for the tests described in the paper. A set of eight accelerometers was used to measure vibrations induced by a test vehicle. The bridge was tested first in an unaltered condition followed by a series of damaged tests as a result of incremental cutting of a fascia girder. At the end of the damage tests, the authors report no noticeable deflection of the bridge structure. Observing the response spectra, the authors note that the amplitude of lower frequencies may be more sensitive to a change in stiffness, and that changes in the amplitude of higher frequencies may be delayed until a more severe reduction in stiffness occurs. Shifts in resonant frequencies as a result of the induced damage were also noted, and that lower frequencies were more susceptible to shifting than higher frequencies. Finally, the signature assurance criterion (SAC) and the cross signature assurance criterion (CSAC) were found to be useful indicators of a stiffness reduction in the structure.

Sanayei et al. (2006) present a damage localization method focusing on the presence, location, and extent of structural damage using nondestructive test data. The proposed method provides an updated structural model representing the current state of the tested structure that can be used to simulate scenarios of damage or retrofitting. The University of Cincinnati Infrastructure Institute (UCII) bridge deck laboratory model was the tested structure discussed in the current paper. A finite element model of the bridge

deck grid was constructed to produce simulated data and to use in the model updating via parameter estimation study. Using simulated data, the proposed strain energy change ratio was able to identify simulated damage in the presence of noise using sparse measurement locations. The authors state that the primary goal of the research discussed in the paper was to update the finite element model of the UCII grid to closely match the nondestructive test data acquired. A parameter system identification program (PARIS) developed at Tufts University was used for all the parameter estimates presented in the paper. Using the calculated parameters, the finite element model was updated to better reflect the bridge deck grid model. The modal assurance criterion was used to compare mode shapes obtained from the updated model with those obtained from the nondestructive test data. The authors report successful parameter estimation due in part to the use of an error normalization function, multiresponse nondestructive test data, stiffness and mass parameter estimation, and use of selected subsets of measurements of static loads and modes of vibration.

Xu and Humar (2006) present an algorithm for structural damage identification by dividing the problem into what they call two distinct sub-problems. The first problem involves locating the damage, which is accomplished using modal energy-based damage index values. Second, the extent of the damage is evaluated using a back-propagation neural network. A neural network is a mathematical inverse model that can be used to find the implied relationship between a set of results and the causes that produced them. In this paper, the authors use a back-propagation neural network to examine the extent of

damage in a girder model of the Crowchild Bridge. The Crowchild Bridge is a continuous, three-span, two-lane, slab-on-steel girder bridge in Calgary, Alberta, Canada. One interesting aspect of this particular bridge is that its five steel girders support a steel-free concrete deck. The deck is reinforced using polypropylene fibers. The bridge is modeled as one continuous girder and then calibrated so that the first three natural frequencies matched those obtained from ambient vibration measurements. After comparing undamaged and damaged tests using the suggested procedure, the author came to the following conclusions. First, modal energy-based damage indices are quite effective in predicting the location of damage in a girder, and curvature modes are more useful in locating damage than translational modes. Second, that the back-propagation neural network used was effective in assessing the magnitude of the inflicted damage once the damage location had been identified, provided that the damage magnitude was not too small.

Liu and DeWolf (2007) present the variation of modal parameters as a function of temperature for a three-span curved post-tensioned box concrete bridge in Connecticut based on a multi-year monitoring program. The bridge was instrumented with accelerometers, tilt meters, and temperature sensors. The authors found that long-term variations in modal frequencies have a reciprocal relationship to the in-situ concrete temperature for all the measured modes. Linear regression models were also developed to simulate the change in modal frequency as a function of concrete temperature. It was also concluded that higher modes of vibration may be better suited for damage indicators

because they do not seem to be affected as much by changes in temperature. Furthermore, torsional modes of vibration were found to not be as easily affected by changes in temperature as bending modes. The authors conclude by stating that the use of natural frequencies alone is insufficient for damage detection because of their sensitivity to changes in temperature, and that the influence of temperature on natural frequency more than likely varies from structure to structure.

Samaan et al. (2007) present the results of free-vibration tests conducted on two continuous two-span bridge models. Two 1/8 scale bridge models were conducted as part of the experiment. One bridge model was straight, and the second bridge model was curved in plan with a span-to-radius of curvature ratio of 1. Free vibrations, both flexural and torsional, of the bridge models were measured using LVDTs and accelerometers. Using finite element models of both constructed bridge models, free vibration analyses were also conducted analytically. The finite element models, calibrated to the experimental results, were used in a parametric study of curved girder bridges. A total of 180 two-equal-span continuous curved bridges having a composite concrete deck-on-steel multiple-box cross section were examined. Evaluating span length, the first mode shape for straight bridges remains flexural, while the torsional contribution to the first mode shape decreases with increasing span length for curved bridges. An increase in the number of lanes had no effect on the straight bridge as its first mode shape remained purely flexural, but the torsional influence on the first mode shape of the curved bridge increased slightly with an increase in the number of lanes. Increasing the number of

boxes had no effect on the first mode shape of the straight bridge but increased the torsional effect on the first mode shape of the curved bridge. By increasing the span-to-radius of curvature ratio, the first mode shape is affected significantly. Changing the span-to-depth ratio was found to considerably affect the fundamental frequency of both straight and curved bridges. End-diaphragm thickness was found to have no effect on the lower modes of vibration but was found to increase the torsional stiffness of the bridge. The lower modes of vibration were not affected by the number of cross bracings, but the number of cross bracings was found to increase the torsional stiffness of the bridges. The value of the first natural frequency remained unchanged with an increase in the number of spans for both curved and straight bridges. Finally, the authors develop empirical expressions for the fundamental frequency of two-span straight and curved continuous multiple-box girder bridges.

Siddique et al. (2007) investigated vibration-based damaged detection techniques applied to an integral abutment bridge. The bridge discussed is the Attridge Drive overpass in Saskatoon, Saskatchewan. Constructed in 2001, the concrete slab on steel girder bridge is six lanes wide, consists of two spans, and has a 16° skew. Vibrations as a result of ambient traffic loading were recorded using five roving accelerometers and one fixed accelerometer. The vibration data was then used to calibrate a finite element model. Because the bridge is in service, damage tests on the real bridge were not possible, and the calibrated finite element model was used to generate damaged data. Damage was induced in the model by removal of selected elements from the bridge deck.

Five vibration-based damage detection techniques were then applied to the undamaged and damaged data: change in mode shape, mode shape curvature, change in flexibility, damage index, and change in uniform flexibility curvature. Using only the fundamental mode, the authors found that all the methods evaluated were cable of detecting damage as long as a sufficient number of sensors were used to characterize the mode shapes. The change in mode shape and change in flexibility methods were determined to offer the greatest potential in detecting damage not located near a sensor. It is also suggested that controlled excitation sources may greatly enhance the effectiveness of vibration-based damage detection techniques. Temperature effects on the bridge's natural frequencies were also discussed, and it was concluded that shifts in natural frequency are not reliable indicators of damage because temperature induced shifts are much greater than those induced by damage.

Zhou et al. (2007) describe a numerical and laboratory-based study evaluating the ability of vibration-based damage detection techniques to detect small-scale damage on a bridge deck. A half-scale laboratory model of a two-girder, simple-span, slab-on-girder bridge deck was constructed in the laboratory for the experimental portion of the work. Accelerometers were used to measure vibrations induced by a mechanical shaker attached directly to the bridge. Damage was induced in the bridge by physically removing small blocks of concrete from the bridge deck. Five different vibration-based damage detection techniques were then evaluated using the undamaged and damaged data: mode shape curvature, change in flexibility, damage index, change in uniform

flexibility curvature, and a change in mode shape method. A finite element model was also constructed and calibrated to extend the investigation to consider additional damage scenarios. The authors found that damage could be detected and localized within a distance equal to the sensor spacing using only the fundamental mode of vibration and as few as five measurement points. It was also noted that the performance of all the techniques evaluated declined when damage was located near a support. Finally, the authors concluded that an increase in the number of measurement points provides a proportional improvement in the localization resolution for the three curvature-based methods, but not as significant an improvement for the other methods mentioned.

Conte et al. (2008) describe dynamic field tests performed on the Alfred Zampa Memorial Bridge (AZMB). Located northeast of San Francisco, the AZMB is a suspension bridge crossing the Carquinez Strait as part of highway I-80. The first major suspension bridge built in the U.S. since the 1960's, AZMB has a main span of 728 m and sides spans of 147 m and 181 m. Other characteristics of the AZMB that are of note include an orthotropic steel deck, reinforced concrete towers, and large-diameter drilled shaft foundations. The authors describe both ambient vibration testing and forced vibration testing performed on the bridge just prior to its opening to traffic in 2003. Ambient vibration was induced mainly by wind, while the forced vibration tests were based on controlled traffic loads and vehicle-induced traffic loads. Vibration measurements were made using an array of 34 uniaxial and 10 triaxial accelerometers dispersed over the length of the bridge. The paper concludes by presenting modal

parameters for the bridge obtained from ambient vibration data using the data-driven stochastic subspace identification method.

Morassi and Tonon (2008) present a study on the use of vibration data for structural identification of a three-span, two-lane post-tensioned reinforced concrete bridge in Italy. Vibrations induced by a mechanical shaker were measured by a set of 10 accelerometers. Additionally, 2 seismometers were placed at each pier support location. Modal parameters were identified by curve fitting frequency response functions using a numerical algorithm based on an iterative least-squared method. When the algorithm provided no significant response, the peak picking method was used. A finite element model of the bridge was constructed using a two-step process. First, the model was calibrated manually to provide a good estimate of the studied bridge. Second, an automated process based on an extended sensitivity analysis was used to improve the identification. The authors note that one of the most significant parameters impacting the natural frequencies appeared to be the flexibility of the boundary conditions at the piers and abutments. The identification procedure used in the current paper minimized an objective function based only on the difference in experimental and finite element frequencies. In order to evaluate the sensitivity of the identified model to various parameters, a parametric study was conducted in which the following quantities were studied: the stiffness of the springs simulating the boundary conditions at the piers, modulus of elasticity for the reinforced concrete elements, and the mass of the concrete. The authors found that the sensitivity of measured frequencies to changes in foundation

stiffness is not negligible. When evaluating the sensitivity of natural frequencies to changes in the modulus of elasticity, the authors report the model results: 1) in the central span, the fundamental mode has the highest sensitivity, especially in the thicker part of the transverse cross section 2) the highest sensitivity values for the second mode are obtained in the lateral regions of the central span, and 3) the third mode has high sensitivity in the middle region of all three spans, but low sensitivity near the piers. To further verify the correctness of the finite element model, the results were also compared to those obtained from a static load test. In concluding, the authors note that the accuracy of the finite element model was significantly affected by the modeling of the transverse profile of the deck.

1.3 References

Abe, M., Fujino, Y., Kajimura, M., Yanagihara, M., and Sato, M. (1999). "Monitoring of a long span suspension bridge by ambient vibration measurement." *Structural Health Monitoring 2000*, Stanford University, Palo Alto, California, 400–407.

Alampalli, S., Fu, G., and Dillon, E.W. (1995). "On the use of measured vibration for detecting bridge damage." *Proceedings of the 4th International Bridge Engineering Conference*, 125–137.

American Association of State Highway and Transportation Officials. (2008). *Bridging the Gap: Restoring and Rebuilding the Nation's Bridges*. Washington, D.C.

American Society of Civil Engineers. (2009). *2009 Report Card for America's Infrastructure*. Reston, Virginia.

Bergmeister, K. and Santa, U. (2000). “Global monitoring concept for bridges.” *Nondestructive Evaluation of Highways, Utilities, and Pipelines*, *Proceedings of SPIE*, 3,995, 14–25.

Biswas, M., Pandey, A.K., and Samman, M.M. (1990). “Diagnostic experimental spectral/modal analysis of a highway bridge.” *Modal Analysis: The International Journal of Analytical and Experimental Modal Analysis*, 5(1), 33–42.

Bolton, R., Stubbs, N., Park, S., Choi, S., and Sikorsky, C. (2001). "Documentation of changes in modal properties of a concrete box-girder bridge due to environmental and internal conditions." *Computer-Aided Civil and Infrastructure Engineering*, 16(1), 42-57.

Bolton, R., Sikorsky, C., Park, S., Choi, S., and Stubbs, N. (2005). "Modal property changes of a seismically damaged concrete bridge." *Journal of Bridge Engineering*, 10(4), 415-428.

Choi, M.Y. and Kwon, I.B. (2000). “Damage detection system of a real steel truss Bridge by neural networks.” *Smart Structures and Materials 2000: Smart Systems for Bridges, Structures, and Highways*, *Proceedings of SPIE*, 3,988, Newport Beach, California, 295–306.

Conte, J.P., He, X.F., Moaveni, B., Masri, S.F., Caffrey, J.P., Wahbeh, M., Tasbihgoo, F., Whang, D.H., and Elgamal, A. (2008). "Dynamic testing of Alfred Zampa Memorial Bridge." *Journal of Structural Engineering*, 134(6), 1006-1015.

De Stefano, A., Sabia, D, and Sabia, L. (1997). “Structural identification using ARMAV models from noisy dynamic response under unknown random excitation.”

Structural Damage Assessment Using Advanced Signal Processing Procedures, *Proceedings of the International Conference on Damage Assessment of Structures* (*DAMAS 97*), University of Sheffield, UK, 419–428.

Doebling, S.W., Farrar, C.R., Prime, M.B., and Shevitz, D.W. (1996). *Damage Identification and Health Monitoring of Structural and Mechanical Systems from Changes in their Vibration Characteristics: A Literature Review.* Rep. No. LA 13070-MS, Los Alamos National Laboratory, Los Alamos, N.M.

Doebling, S.W. and Farrar, C.R. (1997). "Using statistical analysis to enhance modal-based damage identification." *Structural Damage Assessment Using Advanced Signal Processing Procedures*, *Proceedings of the International Conference on Damage Assessment of Structures* (*DAMAS 97*), University of Sheffield, UK, 199–210.

Doebling, S.W., Farrar, C.R., and Prime, M.B. (1998). "A summary review of vibration-based damage identification methods." *The Shock and Vibration Digest*, 30(2), 91–105.

Farrar, C.R., Baker, W.E., Bell, T.M., Cone, K.M., Darling, T.W., Duffey, T.A., Eklund, A., and Migliori, A. (1994). *Dynamic Characterization and Damage Detection in the I-40 Bridge Over the Rio Grande.* Rep. No. LA-12767-MS, Los Alamos National Laboratory, Los Alamos, N.M.

Farrar, C.R. and Cone, K.M. (1995). "Vibration testing of the I-40 bridge before and after the introduction of damage." *Proceedings of the 13th International Modal Analysis Conference*, Bethel, CT., 203–209.

Farrar, C.R., Duffey, T.A., Goldman, P.A., Jauregui, D.V., and Vigil, J.S. (1996). *Finite Element Analysis of the I-40 Bridge Over the Rio Grande.* Rep. No. LA-12979-MS, Los Alamos National Laboratory, Los Alamos, N.M.

Farrar, C.R. and Jauregui, D.A. (1996). *Damage Detection Algorithms Applied to Experimental and Numerical Modal Data from the I-40 Bridge*. Rep. No. LA-13074-MS, Los Alamos National Laboratory, Los Alamos, N.M.

Farrar, C.R., Doebling, S.W., Cornwell, P.J., and Straser, E.G. (1997). "Variability of modal parameters measured on the Alamosa Canyon bridge." *Proceedings of the 15th International Modal Analysis Conference*, Orlando, FL, 257–263.

Farrar, C.R. and Jauregui, D.A. (1998 a). "Comparative study of damage identification algorithms applied to a bridge: I. experiment." *Smart Materials and Structures*, 7(5), 704-719.

Farrar, C.R. and Jauregui, D.A. (1998 b). "Comparative study of damage identification algorithms applied to a bridge: II. numerical study." *Smart Materials and Structures*, 7(5), 720-731.

Farrar, C.R., Cornwell, P.J., Doebling, S. W., and Prime, M.B. (2000). *Structural Health Monitoring Studies of the Alamosa Canyon and I-40 Bridges.* Rep. No. LA-13635-MS, Los Alamos National Laboratory, Los Alamos, N.M.

Federal Highway Administration (FHWA) (2001). *Reliability of visual inspection*. Rep. No. FHWA-RD-01–020, Washington, D.C.

Federal Highway Administration (FHWA) (2009). *Deficient Bridges by State and Highway System.* Washington, D.C. Accessed October 10, 2009. <http://www.fhwa.dot.gov/bridge/deficient.htm>

Gassman, S.L. and Tawhed, W.F. (2004). "Nondestructive assessment of damage in concrete bridge decks." *Journal of Performance of Constructed Facilities*, 18(4), 220-231.

Halling, M.W., Muhammad, I., and Womack, K.C. (2001). "Dynamic field testing for condition assessment of bridge bents." *Journal of Structural Engineering*, 127(2), 161-167.

Jain, B.K. (1991). "Diagnostics through experimental vibration signature analysis of prestressed concrete bridges." *International Symposium on Fracture in Steel and Concrete Structures*, Madras, India, 1123–1136.

Kato, M. and Shimada, S. (1986). "Vibration of PC bridge during failure process." *Journal of Structural Engineering*, 112(7), 1692–1703.

Kim, J. T. and Stubbs, N. (2003). "Nondestructive crack detection algorithm for full-scale bridges." *Journal of Structural Engineering*, 129(10), 1358-1366.

Ko, J., Ni, Y., and Chan, T. (1999). "Dynamic monitoring of structural health in cable-supported bridges." *Smart Structures and Materials 1999: Smart Systems for Bridges, Structures, and Highways*, *Proceedings of SPIE*, 3,671(161), 161–172.

Krämer, C., De Smet, C.A.M., and De Roeck, G. (1999). "Z24 bridge damage detection tests." *Proceedings of the 17th International Modal Analysis Conference,* Kissimmee, FL, USA.

Lauzon, R.G. and DeWolf, J.T. (2006). "Ambient vibration monitoring of a highway bridge undergoing a destructive test." *Journal of Bridge Engineering*, 11(5), 602-610.

Liang, Z., Tong, M., and Lee, G.C. (1995). "Modal energy measurement of a long steel bridge." *Proceedings of the 13th International Modal Analysis Conference*, Bethel, CT, 226–232.

Liu, C.Y. and DeWolf, J.T. (2007). "Effect of temperature on modal variability of a curved concrete bridge under ambient loads." *Journal of Structural Engineering*, 133(12), 1742-1751.

Maeck, J. and De Roeck, G. (1999). "Damage detection on a prestressed concrete bridge and RC beams using dynamic system identification." *Damage Assessment of Structures*, *Proceedings of the International Conference on Damage Assessment of Structures* (DAMAS 99), Dublin, Ireland, 320–327.

Maeck, J., Peeters, B., and De Roeck, G. (2001). "Damage identification on the Z24 bridge using vibration monitoring." *Smart Materials and Structures*, 10(3), 512-517.

Morassi, A. and Tonon, S. (2008). "Dynamic testing for structural identification of a bridge." *Journal of Bridge Engineering*, 13(6), 573-585.

Park, S., Stubbs, N., Bolton, R., Choi, S., and Sikorsky, C. (2001). "Field verification of the damage index method in a concrete box-girder bridge via visual inspection." *Computer-Aided Civil and Infrastructure Engineering*, 16(1), 58-70.

Peeters, J.M.B. and De Roeck, D. (2000). “Damage identification on the Z24 bridge using vibration monitoring.” *European COST F3 Conference on System Identification and Structural Health Monitoring*, Madrid, Spain, 233–242.

Peeters, J.M.B., Maeck, J., and De Roeck, G. (2000). “Excitation sources and dynamic system identification in civil engineering.” *European COST F3 Conference on System Identification and Structural Health Monitoring*, Madrid, Spain, 341–350.

Pothisiri, T. and Hjelmstad, K.D. (2003). "Structural damage detection and assessment from modal response." *Journal of Engineering Mechanics*, 129(2), 135-145.

Raghavendrachar, M. and Aktan, A.E. (1992), “Flexibility by multireference impact testing for bridge diagnostics.” *Journal of Structural Engineering*, 118(8), 2186–2203.

Ren, W.X., Zatar, W., and Harik, I.E. (2004 a). "Ambient vibration-based seismic evaluation of a continuous girder bridge." *Engineering Structures*, 26(5), 631-640.

Ren, W.X., Zhao, T., and Harik, I.E. (2004 b). "Experimental and analytical modal analysis of steel arch bridge." *Journal of Structural Engineering*, 130(7), 1022-1031.

Salane, H.J., Baldwin, J.W., and Duffield, R.C. (1981). “Dynamics approach for monitoring bridge deterioration.” *Transportation Research Record*, 832, 21–28.

Salawu, O.S. (1995). “Nondestructive assessment of structures using the integrity index method applied to a concrete highway bridge.” *Insight*, 37(11), 875–878.

Salawu, O.S. and Williams, C. (1995). “Bridge assessment using forced-vibration testing.” *Journal of Structural Engineering*, 121(2), 161–173.

Samaan, M., Kennedy, J.B., and Sennah, K. (2007). “Dynamic analysis of curved continuous multiple-box girder bridges.” *Journal of Bridge Engineering*, 12(2), 184-193.

Sanayei, M., Bell, E.S., Javdekar, C.N., Edelmann, J.L., and Slavsky, E. (2006). "Damage localization and finite-element model updating using multiresponse NDT data." *Journal of Bridge Engineering*, 11(6), 688-698.

Siddique, A.B., Sparling, B.F., and Wegner, L.D. (2007). "Assessment of vibration-based damage detection for an integral abutment bridge." *Canadian Journal of Civil Engineering*, 34(3), 438-452.

Sohn, H., Farrar, C.R., Hemez, F.M., Shunk, D.D., Stinemates, D.W., and Nadler, B.R. (2004). *A Review of Structural Health Monitoring Literature: 1996–2001*. Rep. No. LA-13976-MS, Los Alamos National Laboratory, Los Alamos, N.M.

Stubbs, N., Kim, Y.I., and Farrar, C.R. (1995). “Field verification of a nondestructive damage localization and severity estimation algorithm.” *Proceedings of the 13th International Modal Analysis Conference*, Bethel, CT, 210-218.

Stubbs, N., Sikorsky, C., Park, S.C., and Bolton, R. (1999). “Verification of a methodology to nondestructively evaluate the structural properties of bridges.” *Structural Health Monitoring 2000*, Stanford University, Palo Alto, California, 440-449.

Tang, J.P. and Leu, K.M. (1991). “Vibration tests and damage detection of P/C bridges.” *Journal of the Chinese Institute of Engineers*, 14(5), 531–536.

Wahab, M. and De Roeck, G. (1999). “Damage detection in bridges using modal curvatures: application to a real damage scenario.” *Journal of Sound and Vibration, 226*(2), 217-235.

Wang, M.L., Satpathi, D., Lloyd, G.M., Chen, Z.L., and Xu, F.L. (1999). *Monitoring and Damage Assessment of the Kishwaukee Bridge*. A Preliminary Investigative Report submitted to the Illinois Department of Transportation, Bridge Research Center, University of Illinois at Chicago.

Xia, P.Q. and Brownjohn, J.M.W. (2004). "Bridge structural condition assessment using systematically validated finite-element model." *Journal of Bridge Engineering*, 9(5), 418-423.

Xu, H.P. and Humar, J. (2006). "Damage detection in a girder bridge by artificial neural network technique." *Computer-Aided Civil and Infrastructure Engineering*, 21(6), 450-464.

Zhao, J. and DeWolf, J.T. (2002). "Dynamic monitoring of steel girder highway bridge." *Journal of Bridge Engineering*, 7(6), 350-356.

Zhou, Z., Wegner, L.D., and Sparling, B.F. (2007). “Vibration-based detection of small-scale damage on a bridge deck.” *Journal of Structural Engineering*, 133(9), 1257-1267.

Chapter 2. Geophones

2.1 What is a geophone?

A geophone is a passive directional sensor that measures the speed of motion in the direction of its sensitive axis. In basic terms, a geophone is a coil suspended by springs around a permanent magnet, all of which is contained in a protective casing. When the coil moves relative to the magnet as a result of an external excitation, a voltage is induced in the coil that can be recorded. Because the output voltage is directly proportional to the velocity of the coil, geophones are referred to as velocity transducers.

Traditionally, seismologists, not bridge engineers, use geophones. Because of their extreme sensitivity, seismologists often use geophones to measure wave energy propagating through several kilometers of geologic materials. The petroleum industry, for example, uses arrays of geophones to aid in locating pockets of hydrocarbons deep inside the earth. One may also find geophones being used in mining industries, as well as by security companies because of their high sensitivity to vibration and passive response.

Typically, when one thinks of dynamic testing of civil engineering structures, accelerometers come to mind. However, geophones offer some key advantages over accelerometers when considered for implementation in bridge monitoring systems. To begin, the signal produced by an accelerometer often requires charge amplification before recording, and thus a power source is needed for the amplifier and associated hardware. Geophones are passive devices and continually produce a voltage that can be recorded without any additional amplification or conditioning. The lack of a need for an external power supply overcomes one of the obstacles in implementing remote bridge monitoring systems and makes geophones ideal candidates for implementation in such systems due

to their passive nature. Furthermore, geophones may play an invaluable role in the effort to develop wireless sensor systems for bridge monitoring. If the continuous voltage produced by a geophone could be used to power or recharge the wireless transmitter, the use of geophones would eliminate the need to change batteries or provide some other type of power source for the wireless transmitters.

Another important advantage geophones have over accelerometers is their price. Geophones comparable to those used in this study can be purchased for around fifty dollars each. When compared to several hundreds of dollars for an accelerometer and the related conditioning electronics, geophones provide a more economical choice. For the same investment in sensors, more locations on a single bridge can be monitored or more bridges can be monitored with the additional sensors. Because the effectiveness of vibration-based damage detection techniques increases with a decrease in sensor spacing, the additional sensors provide valuable information at a reduced cost.

Geophones with low resonant frequencies (<1 Hz) may also cost several hundred dollars. Therefore, for structures such as long span bridges where many of the bridge's resonant frequencies are less than one hertz, geophones may not provide an economical advantage over accelerometers. However, this study demonstrates that the more moderately priced geophones discussed herein can provide an accurate dynamic characterization of highway bridges with fundamental frequencies greater than 2 Hz, making them excellent candidates for most remote bridge monitoring systems.

2.2 Geophone Theory

Geophones can be modeled as a single degree of freedom (SDOF) system as shown in Figure 2.1. The governing differential equation for the SDOF system is shown in Eq. 2.1.

$$m\ddot{y} + c\dot{y} + ky = -m\ddot{x}_g \tag{2.1}$$

The transfer function of Eq. 2.1, *H(s)*, can be obtained from the ratio of the Laplace transform of the output function *y(t)* to the input function $x_g(t)$. This relationship is critical in understanding the magnitude and phase errors that may be associated with the output of a sensor, accelerometers and geophones alike.

A geophone's output signal is a voltage resulting from a coil moving through a magnetic field. According to Faraday's Law, the voltage across the coil is proportional to the change in flux through the coil with respect to time. For small displacements, the change in flux, Φ, is constant, and thus the voltage, V, across the coil is directly proportional to the velocity of the coil as shown in Eq. 2.2 in the Laplace domain, where G is a transduction constant referred to as the sensitivity of the geophone.

$$V = -\frac{\partial \Phi}{\partial t} = -\frac{\partial \Phi}{\partial y}\frac{\partial y}{\partial t} = -G\dot{Y}(s) = -GsY(s) \tag{2.2}$$

Because a geophone's output is constant with respect to velocity at frequencies above its natural frequency, it is helpful to represent the geophone's transfer function in this manner. This is accomplished by integrating the external acceleration term once in the Laplace domain.

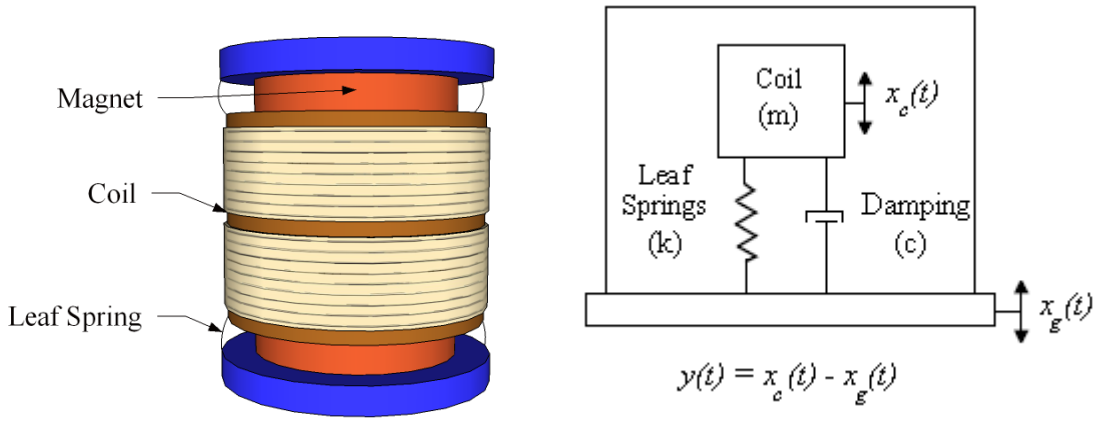

Figure 2.1. Geophone and idealized single degree of freedom system

After substituting for conventional notation, evaluating at $s=i\omega$, and simplifying, the common form of a geophone's transfer function is obtained as shown in Eq. 2.3 where ω is the frequency of vibration, ω_n is the natural frequency of the geophone, and ς is the damping ratio of the geophone.

$$H(\omega,\varsigma) = \frac{-G\left(\frac{\omega}{\omega_n}\right)^2}{\left(1-\left(\frac{\omega}{\omega_n}\right)^2\right)+2i\varsigma\left(\frac{\omega}{\omega_n}\right)} \qquad 2.3$$

Using Eq. 2.3, the magnitude and phase response of a geophone as a function of frequency and damping ratio can be calculated as shown in Eqs. 2.4 and 2.5 respectively.

$$\left|H(i\omega)\right| = \frac{G\left(\frac{\omega}{\omega_n}\right)^2}{\sqrt{\left(1-\left(\frac{\omega}{\omega}\right)^2\right)^2+\left(2\varsigma\frac{\omega}{\omega_n}\right)^2}} \qquad 2.4$$

$$PHASE\left(H(\omega,\varsigma)\right) = \tan^{-1}\left(\frac{2\varsigma\left(\frac{\omega}{\omega_n}\right)}{1-\left(\frac{\omega}{\omega_n}\right)^2}\right) \qquad 2.5$$

Plots of a geophone's magnitude and phase response, Figure 2.2 and Figure 2.3 respectively, as a function of frequency for various damping ratios are useful in understanding the data obtained using geophones. In order to convert recorded voltages to velocities, the voltages are divided by the geophone sensitivity. Observing Figure 2.2, it can be seen that the output voltage of a geophone tapers off below its natural frequency. If this taper is not accounted for, the actual magnitude of input signals with frequency components in this range will be underestimated. In other words, the data needs to be normalized if its frequency content is below the natural frequency of the geophone.

From Figure 2.3, it can be seen that data collected using geophones is subject to considerable phase shifts when its frequency content is around the natural frequency of the geophone. Thus, there is a corresponding time lag associated with a geophone's output when compared to the input at frequencies near the natural frequency of the geophone. In order to ensure that the data being analyzed is accurate, the phase errors associated with the geophone must be removed. This correction is particularly important if geophones with varying response characteristics are used to characterize a structure's dynamic response. Otherwise, the data from different geophone types will be out of phase with one another ultimately resulting in unintelligible mode shapes.

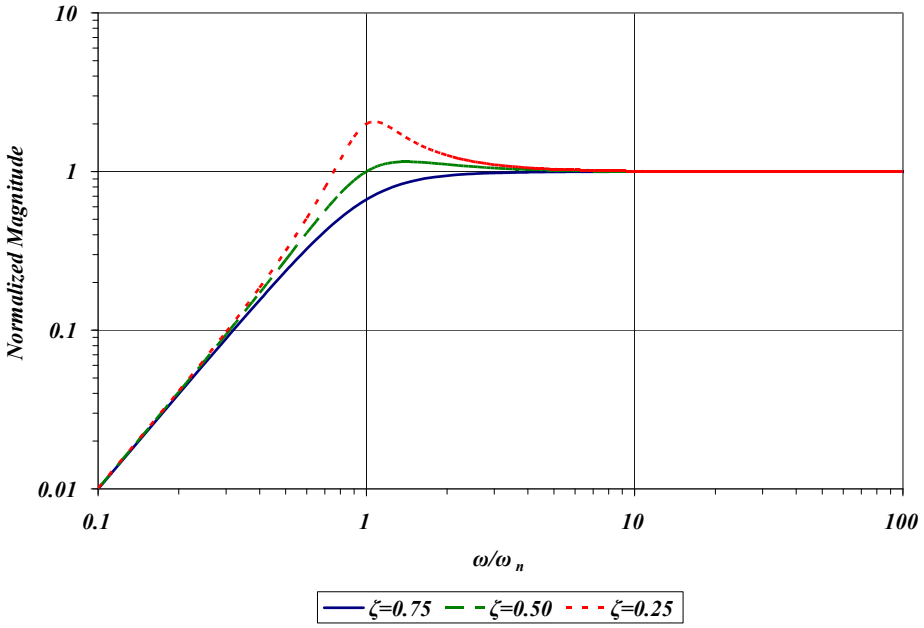

Figure 2.2. Geophone output magnitude for various damping ratios

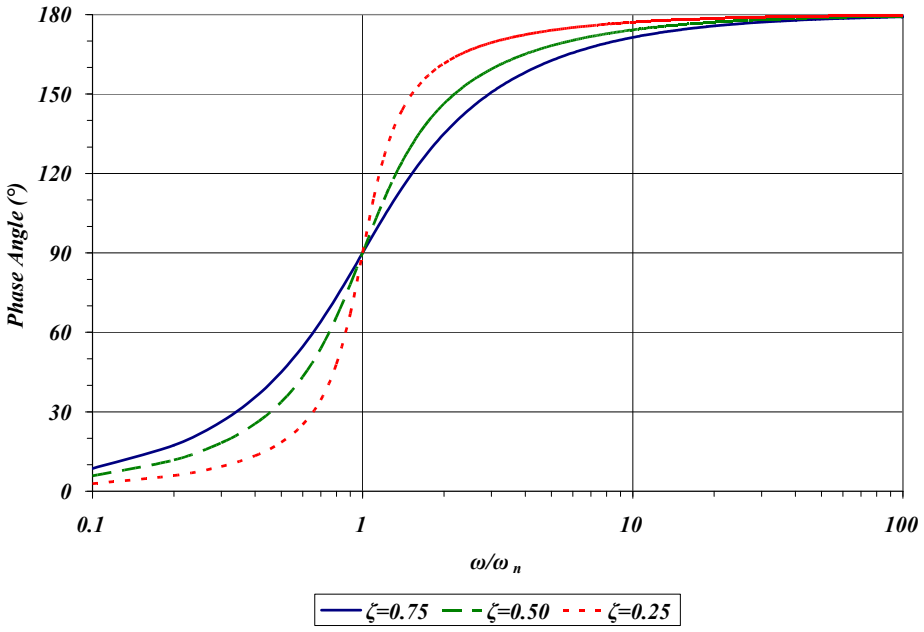

Figure 2.3. Geophone output phase for various damping ratios

2.3 Geophone Calibration

In order to correct the geophone's output for magnitude and phase errors, three parameters associated with the geophone's transfer function need to be determined: the geophone's sensitivity, G, natural frequency, ω_n, and damping ratio, ζ. In order to determine these geophone parameters, a Mark Products LRS-1000 10Hz vertical geophone, a Mark Products L-28LBH 4.5Hz horizontal geophone, and a Brüel & Kjær 4371V accelerometer were all mounted to a steel plate which was attached to an MTS 858 Table Top System capable of producing controlled vertical oscillations. Horizontal geophones can not accurately measure vertical oscillations, and for this reason the horizontal geophone was mounted at a slight angle to induce vertical and horizontal components of motion. The test setup can be seen in Figure 2.4.

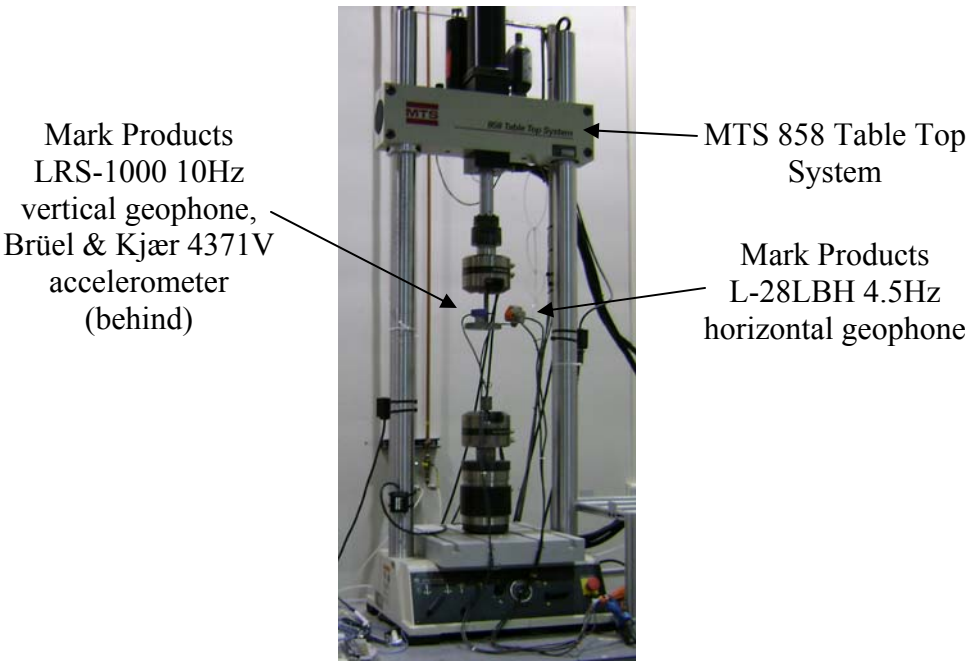

Figure 2.4. Geophone calibration setup

Once the sensors were securely in place, the setup was incrementally subjected to known frequencies ranging from 2 to 30 Hz. Output measurements were recorded using a Geometrics 48-channel StrataView® seismograph with a 24-bit A/D converter. Each time series was then analyzed to determine the peak output value at each test frequency for each geophone and the accelerometer. The accelerometer used during the calibration process is known to provide reference data free of magnitude and phase errors over the frequency range tested. Therefore, dividing the maximum geophone output by the maximum accelerometer output (recall that each is a voltage) at each frequency increment provides a data set that can be analyzed to determine the geophone parameters.

The experimental data set was evaluated using Eq. 2.6 and the Levenberg-Marquardt algorithm in MATLAB® (Mathworks 2007) to determine the geophone's sensitivity, natural frequency, and damping ratio as shown in Figure 2.5. The identified geophone parameters are presented in Table 2.1.

$$\left|\frac{V}{\ddot{X}(i\omega)}\right| = \frac{G\left(\frac{\omega}{\omega_n^2}\right)}{\sqrt{\left(1-\left(\frac{\omega}{\omega_n}\right)^2\right)^2 + \left(2\varsigma\frac{\omega}{\omega_n}\right)^2}} \qquad 2.6$$

Once the geophones had been calibrated, the systematic correction of measured output signals was implemented using a MATLAB® routine developed to remove magnitude and phase errors from each frequency component of the measured data. An example of the corrected geophone output compared to the accelerometer output for a 10Hz input motion is shown in Figure 2.6. Observing Figure 2.6, one can see that there

is no difference in the data obtained from the corrected geophones compared to the accelerometer. Note that the vertical component of the horizontal geophone output is plotted in Figure 2.6.

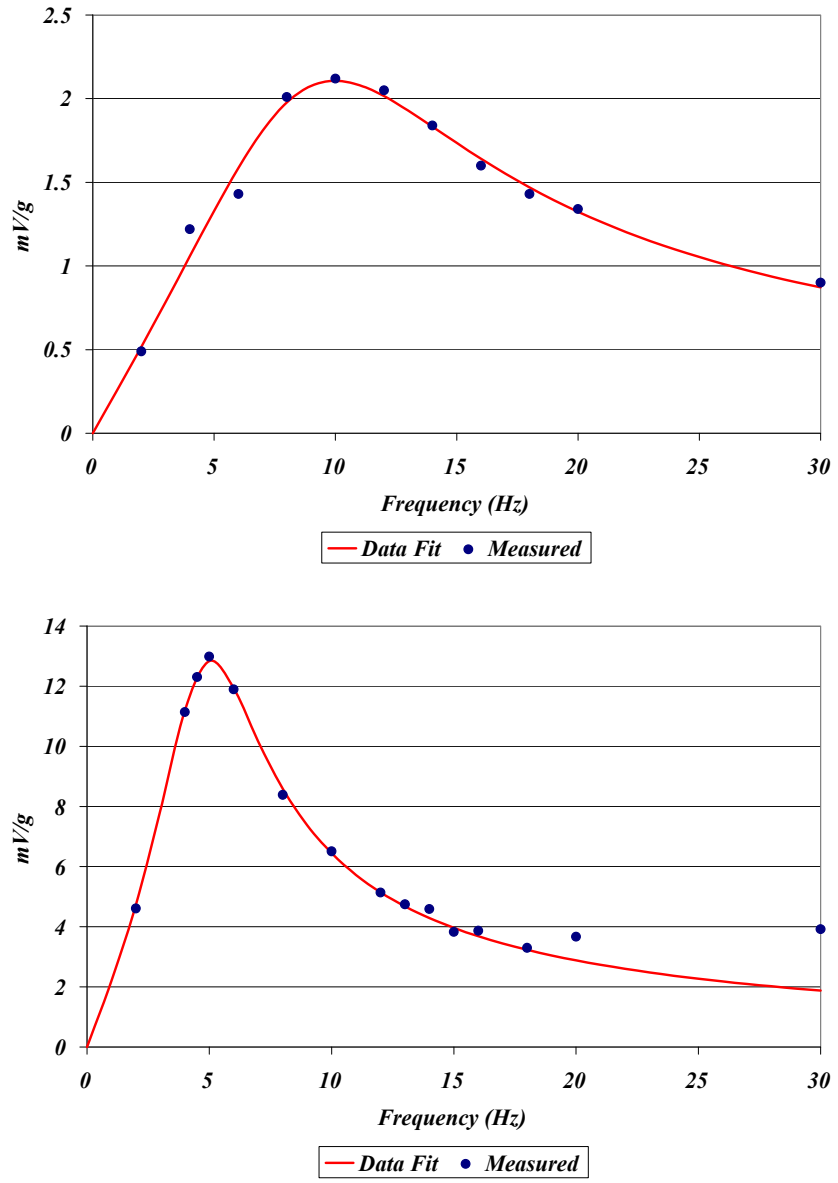

Figure 2.5. Geophone parameter determination using the Levenberg-Marquardt algorithm: vertical (top), horizontal (bottom)

Table 2.1. Experimentally determined geophone parameters

Parameter	Mark Products LRS-1000 Vertical Geophone	Mark Products L-28LBH Horizontal Geophone
ω_n (Hz)	9.984	5.070
Damping Ratio, ζ	0.6076	0.4252
Sensitivity (mV/(cm/s))	160.6	348.0
R^2	0.9773	0.9984

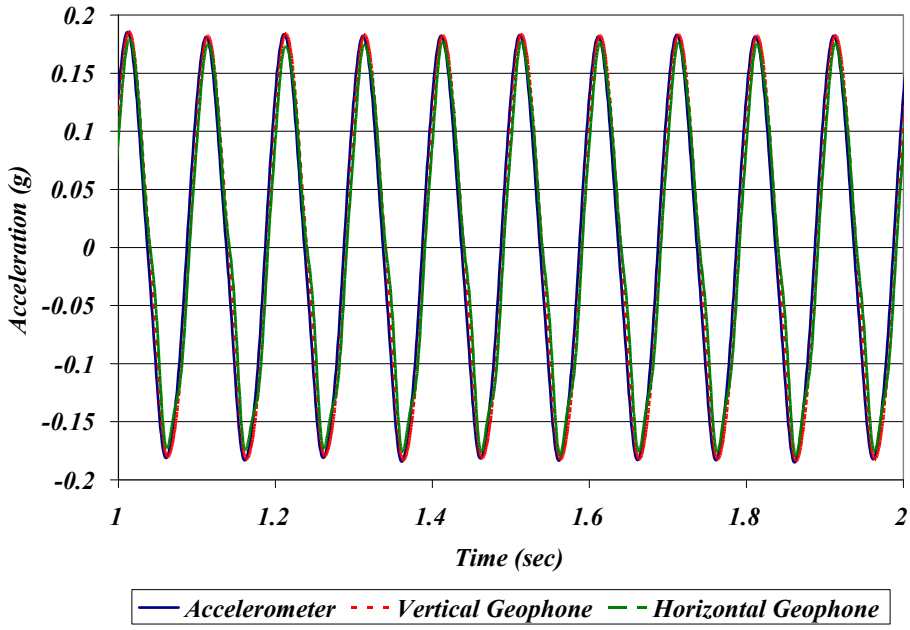

Figure 2.6. Calibrated horizontal and vertical geophone signals compared to measured accelerations for a 10 Hz input signal

2.4 References

The Mathworks, Inc. (2007). MATLAB®. Version R2007a.

Chapter 3. Nondestructive Evaluation of a Full-Scale Bridge Using an Array of Triaxial Geophones

This chapter is revised based on a paper submitted to the ASCE *Journal of Structural Engineering* by William Ragland, Dayakar Penumadu, and Richard Williams:

Ragland, W.S., Penumadu, D., and Williams, R.T. (In review). "Nondestructive evaluation of a full-scale bridge using an array of triaxial geophones." *Journal of Structural Engineering*.

My primary contributions to the paper included: (i) development of the problem into a work, (ii) gathering and reviewing literature, (iii) design and conduction of the field tests on the simple beam and full-scale bridge, (iv) processing, analyzing, and interpretation of the experimental data, (v) development and calibration of the finite element models, and (vi) most of the writing.

3.1 Abstract

Vibration-based damage detection is a nondestructive structural health monitoring approach that focuses on changes in the dynamic characteristics of a structure, such as its natural frequencies and mode shapes, as indicators of damage. Because vibration-based damage detection techniques require data with a high signal to noise ratio for analysis, the choice of sensors used to measure the vibrations is an important consideration. The objective of this paper is to demonstrate the use of inexpensive geophones for determining the modal parameters of civil engineering structures, particularly bridges, for use with vibration-based damage detection techniques. A geophone is a velocity

transducer commonly used by seismologists for subsurface exploration, and their use for bridge vibration measurement provides some advantages over accelerometers. In most cases, engineers employ accelerometers for the purpose of measuring bridge vibrations. However, compared to geophones, accelerometers are relatively expensive, have lower sensitivity, and require a power supply and amplifier in addition to the signal recorder. In comparison geophones are passive sensors, they connect directly to the recording system, and provide an economical way to acquire vibration data simultaneously at a large number of measurement points. In order to validate the use of geophones for modal parameter identification, a simple beam experiment was conducted, and the results compared with theoretical values and a finite element model. Finally, modal parameters extracted from vibration data acquired using geophones during testing of a full-scale reinforced concrete bridge located in Knoxville, TN, are presented. The results show that modal parameters obtained using geophones are reliable and could be used with vibration-based damage detection techniques.

3.2 Introduction

Researchers have been using vibration testing as a means of assessing the structural health of buildings and bridges for several years. Results obtained through vibration testing have proved useful for structural health monitoring (Zhao and DeWolf 2002, He et al. 2009), finite element model updating and calibration (Bell et al. 2007, Catbas et al. 2007), condition assessment of structures (Halling et al. 2001, Ren et al. 2004), and structural damage detection (Kim and Stubbs 2003, Huth et al. 2005). The

focus of this paper is nondestructive evaluation of bridges by means of a new approach for obtaining vibration records using highly sensitive geophones that are passive in nature and relatively inexpensive for large scale implementation in practice.

The nondestructive evaluation methods that have been developed over the past several years for the purpose of assessing structural health fall into two major categories: local and global. Local damage detection methods used for assessing bridge health include techniques such as impact-echo, ground-penetrating radar, ultrasonic pulse velocity, spectral analysis of surface waves, infrared thermography, and mechanical sounding (Gassman and Tawhed 2004). One of the drawbacks associated with local damage detection techniques is that the location of the damage must be known or guessed before a test is conducted, and the area to be tested on the bridge must be accessible. Because of such drawbacks, global damage detection methods have been developed that instead rely on changes in the overall response of a bridge as an indication of damage. Vibration-based methods are one class of global damage detection that has received much attention in the literature.

Vibration-based damage detection focuses on changes in the dynamic characteristics of a structure, such as natural frequency and mode shape, as indicators of damage. Several different global evaluation techniques and associated quantitative damage indices have been published in recent years. Detailed reviews of these techniques as applied to bridges and other structures can be found in Doebling et al. (1996, 1998) and Sohn et al. (2004). In summary, the methods discussed monitor shifts in natural frequency, absolute changes in mode shapes, changes in mode shape curvature

or strain energy, and variations in stiffness and flexibility matrices. Numerical methods that involve experimental data and the updated response of boundary value problems using the finite element method (FEM) or artificial neural networks (Xu and Humar 2006) are also in the literature.

The premise for the implementation of all vibration-based damage detection techniques is that vibration data is available for analysis. In most cases, engineers employ accelerometers for the purpose of measuring bridge vibrations. Other instruments and techniques that appear in the literature include the use of anemometers, temperature sensors, strain gauges, displacement transducers, global positioning systems, weigh-in-motion systems, corrosion sensors, elasto-magnetic sensors, optic fiber sensors, tiltmeters, level sensors, total stations, seismometers, barometers, hygrometers, pluviometers, and video cameras (Ko and Ni 2005).

Several factors influence the selection of sensors, but often times cost and ease of installation play significant roles in the process. Accelerometers, for example, are often relatively expensive. Thus, the number of accelerometers available to a single research group for use in vibration testing is often limited. It has been shown by researchers that the effectiveness of vibration-based damage detection techniques decreases with an increase in sensor spacing (Zhou et al. 2007). Therefore, the number of sensors used and their placement are important considerations when acquiring vibration data for implementation with vibration-based damage detection techniques. Strain gauges, on the other hand, are relatively inexpensive. However, their installation process is time consuming, and their location is fixed. This leads to the fact that the sensors used for

bridge vibration testing should be easy to move to facilitate vibration measurements at various locations on the bridge and optimal sensor placement. Considering these factors, the purpose of the current research is to demonstrate the use of inexpensive and highly sensitive passive sensors, geophones, for determining modal parameters of full-scale bridges for use with vibration-based damage detection techniques.

3.3 Geophones as Sensors

A geophone is a passive directional sensor that measures the speed of motion in the direction of its sensitive axis. In basic terms, a geophone is a coil suspended by springs around a permanent magnet, all of which is contained in a protective casing. When the coil moves relative to the magnet, a voltage is induced in the coil that depends on the relative velocity between the coil and magnet.

Traditionally, geophysicists, rather than bridge engineers, use geophones to measure elastic waves propagating through several kilometers of geologic materials. Detailed technical descriptions of the various types of geophones can be found in geophysical textbooks (Dobrin and Savit 1988, Robinson and Coruh 1988).

Accelerometers are commonly used for dynamic testing of civil engineering structures. However, geophones offer important advantages over accelerometers when considered for implementation in bridge monitoring systems. First of all, an accelerometer generally requires charge amplification electronics to produce a signal suitable for recording, and thus a power source is needed for the amplifier and associated hardware. In comparison, geophones are passive devices that produce a voltage that can

be recorded without additional amplification or conditioning. The lack of a requirement for an external power supply and amplifier overcomes one of the obstacles in implementing remote bridge monitoring systems, and makes geophones ideal candidates for implementation in such systems. Furthermore, geophones may be more easily incorporated into a wireless sensor system for bridge monitoring.

3.4 Modal Analysis

In this research, the rational polynomial method (Richardson et al. 1985) as implemented in DIAMOND (Farrar et al. 1998) was used for extracting natural frequencies and mode shapes from measured field data. DIAMOND (Damage Identification and Modal Analysis of Data) is a MATLAB® (Mathworks 2007) based software package developed at Los Alamos National Laboratories for modal analysis, damage identification, and finite element model refinement. Briefly, the rational polynomial method uses orthogonal polynomials to estimate the coefficients of a polynomial approximation to the frequency response function (FRF). The FRF of a system is the ratio of the Fourier transform of the measured input and response signals. Thus, the rational polynomial method is intended for use with measured inputs. Because input forces were not recorded in this research, an assumption was made in order to implement the rational polynomial method. If an input force is known to have a flat spectrum, then any peaks in the response spectrum are caused by structural resonances. Therefore, it was assumed that the impulsive sources used during tests possessed a flat spectrum, at least over the frequency range of interest. This assumption allows the

response spectrum matrix created from Fourier amplitude spectra to be analyzed instead of the FRF matrix. This modal analysis procedure produces reliable results, as demonstrated by the results obtained in this research.

3.5 Simply Supported Beam Test

Perhaps one of the easiest structures to characterize dynamically is the simply supported beam. It is well known that the n^{th} natural frequency of a beam with length L, mass per unit length, m, modulus of elasticity, E, and moment of inertia, I, is given by Eq. 3.1 while the corresponding natural vibration mode is given by Eq. 3.2.

$$\omega_n = \frac{n^2\pi^2}{L^2}\sqrt{\frac{EI}{m}} \qquad 3.1$$

$$\phi_n = \sin\frac{n\pi x}{L} \qquad 3.2$$

Observing Eqs. 1 and 2 it becomes apparent that the first natural vibration mode is a half sine wave with a frequency ω_1, the second natural vibration mode is a complete sine wave with a frequency $\omega_2=4\omega_1$, the third vibration mode is one and a half sine waves with a frequency $\omega_3=9\omega_1$, and so on.

In order to validate the geophone correction and modal analysis procedures used, a simply supported beam was tested and analyzed. The test beam was a HP12x53 (Figure 3.1) simply supported at each end by a 45 cm length of 2x6 pine resulting in a center-to-center support span of 12.4 m. Mark Products LRS-1000 10 Hz vertical geophones and Mark Products L-28LBH 4.5 Hz horizontal geophones were used to measure the vibrations during the tests. To connect the geophones to the beam, one vertical geophone and one horizontal geophone were rigidly attached to a 1.6 cm thick 11.5 cm diameter

steel plate which rested along the top flange centerline at a spacing of 53.3 cm with the horizontal geophones oriented perpendicular to the length of the beam. A total of 24 plates (48 geophones) were used for the test. Each geophone was connected to a conductor cable, which was connected to a Geometrics 48-channel StrataView® seismograph containing a 24-bit A/D converter.

For an excitation source, a rubber mallet was used to strike the center of the top flange at various locations along the beam's length. A piezoelectric sensor was attached to the rubber mallet to trigger the seismograph to begin recording the instant the beam was struck. During each test, data was sampled at a rate of 1000 Hz for a total of three seconds which results in a measurable bandwidth of 0 to 500 Hz with a resolution of 0.33 Hz in the frequency domain. Frequency response spectra for the geophones used on the test beam are presented in Figure 3.2.

Figure 3.1. Simply supported test beam (HP12x53) instrumented with geophones

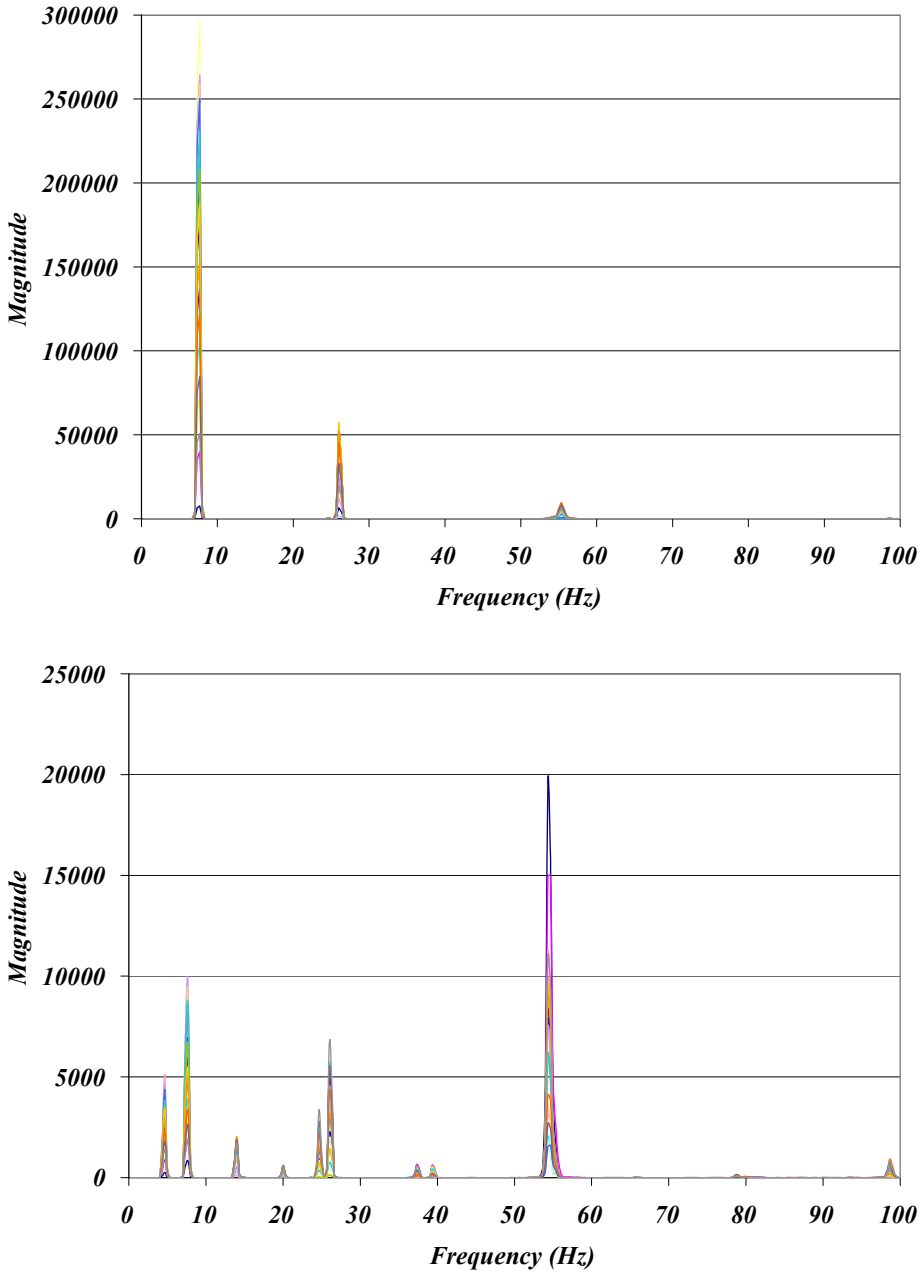

Figure 3.2. Frequency response spectra for the HP12x53 test beam vertical geophones (top), horizontal geophones (bottom)

Observing Figure 3.2, it can be seen that the same response spectra is obtained for each geophone. The varying magnitude between geophones is caused by the difference in modal amplitude at each geophone location. Vertical and horizontal geophones are separated into separate spectra to prevent the vertical response from dominating the spectra. Otherwise, the frequency information contained in the horizontal spectra would not be visible. Observing the horizontal spectra, additional modes are observed in addition to those contained in the vertical spectra.

In order to evaluate the accuracy of the results, the natural frequencies were compared with theoretical values as well as results from two different finite element models constructed using the finite element program ABAQUS® (Dassault 2008). Generic values for the material properties of steel were used in each model: E_s = 200 GPa (29,000 ksi), υ_s = 0.30, and ρ_s = 7.85 g/cm^3 (490 lb/ft^3). In both models, the beam flanges and web were modeled using 4-node, reduced integration shell elements, S4R in ABAQUS. To connect the flanges to the web, the beam connector element in ABAQUS was used which provides a rigid connection between nodes. In the first finite element model, support conditions were simulated as follows: one end of the beam was modeled as a pin support by restraining displacements of the bottom flange in all three coordinate directions at the bearing location, while the other end of the beam was modeled as a roller by allowing displacement of the bottom flange parallel to the length of the beam and restraining displacements in the other two coordinate directions at the bearing location. In the second model, springs were used to simulate the boundary conditions in all coordinate directions at each bearing location. The stiffness of the springs was adjusted

until the finite element model frequencies matched the test frequencies. A comparison of the first three fundamental natural frequencies of the test beam obtained theoretically, from field test data, and using ABAQUS is shown in Table 3.1.

Observing Table 3.1, the importance of accurately modeling the boundary conditions of a physical system (beam in this study) is apparent. The first natural frequency is underestimated and the third natural frequency is overestimated theoretically. The same observation is also true when using the simple support finite element model although the third mode is in much better agreement with the field test result. However, using springs to model the boundary conditions provides a model that more closely represents the field test results.

Through the modeling process, it was found that the vertical spring stiffness had a greater effect on the second and third modes than the first mode. However, the first mode was affected more by the longitudinal (parallel to the beam's length) spring stiffness than the higher modes. Changing the stiffness of the transverse spring (perpendicular to the beam's length) had little effect on any of the first three modes.

In order to further verify that the modal analysis procedure used produces reliable results, mode shapes obtained from the finite element model were compared with those obtained from the field test. As shown in Figure 3.3, the mode shapes obtained from the field tests are the correct shape and very similar to those obtained from the finite element model and are oriented as if the reader where facing the beam's web. Observing the results obtained using DIAMOND and the field test data, note that each dot represents a plate location containing one vertical and one horizontal geophone.

Table 3.1. Comparison of HP12x53 fundamental natural frequencies (Hz)

Mode	Theoretical	Field Test (Rational Polynomial)	ABAQUS Shell Elements	
			Simple Support	Spring Support
1	6.60	7.17	6.59	7.17
2	26.41	25.53	25.82	25.42
3	59.42	55.24	55.91	55.24

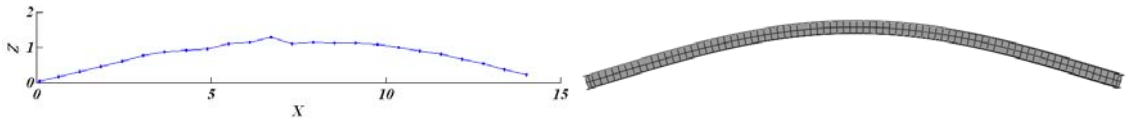

Mode 1

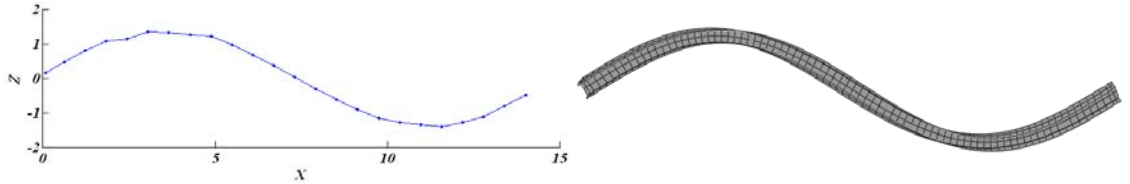

Mode 2

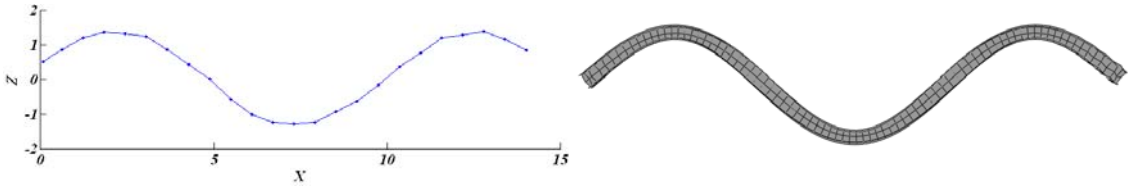

Mode 3

Figure 3.3. First three vertical bending modes of the HP12x53 test beam (m) DIAMOND using geophone data (left), ABAQUS (right)

Perhaps the most compelling argument for the importance of correctly modeling the beam's support conditions is observed in the horizontal data. As shown in Table 3.2, the natural frequencies obtained using the finite element model incorporating springs to simulate the beam supports are in much better agreement with the field test results than the model that uses a traditional simple support scheme.

The corresponding mode shapes to the natural frequencies presented in Table 3.2 are shown in Figure 3.4 and are oriented as if the reader were looking down of the beam, perpendicular to the top flange. Observing Figure 3.4, a great deal of detail can be seen in the identified mode shapes. What is particularly impressive about the identified modes is that they were not meant to be excited. The beam was struck in the center of the top flange with hopes of exciting the fundamental bending modes of vibration. However, small horizontal and torsional vibrations were induced which were captured by the horizontal geophones because of their high sensitivity. The ability of geophones to detect small amplitude, high frequency vibrations lends credibility to their use for dynamic characterization of structures.

Table 3.2. Comparison of horizontal HP12x53 natural frequencies (Hz)

Mode	Field Test (Rational Polynomial)	ABAQUS Shell Elements	
		Simple Support	Spring Support
4	4.40	4.07	4.40
5	13.74	12.20	13.31
6	25.60	21.10	25.18
7	37.89	31.18	38.06
8	53.76	47.22	53.69
9	78.50	70.77	75.42
10	98.21	100.73	98.44

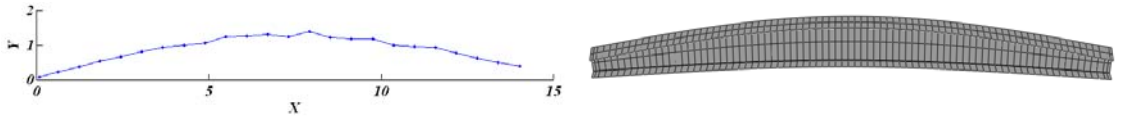

Mode 4

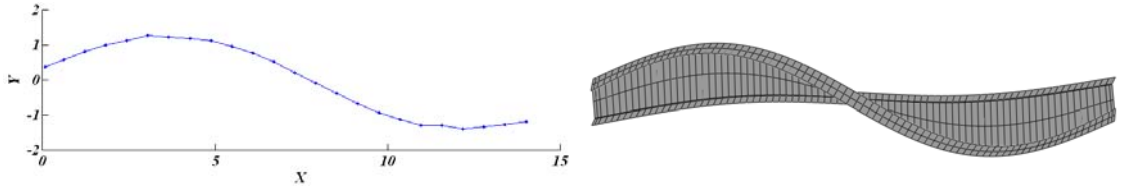

Mode 5

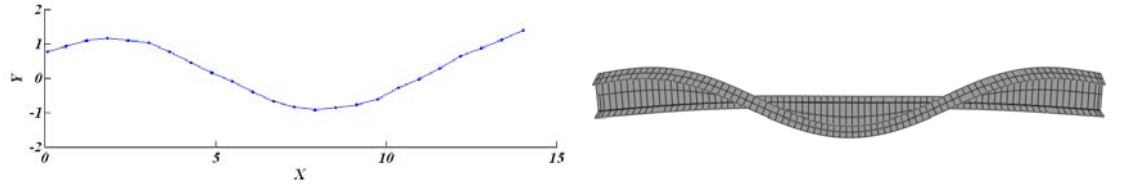

Mode 6

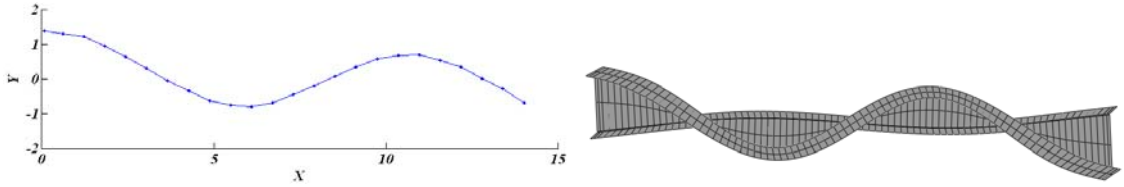

Mode 7

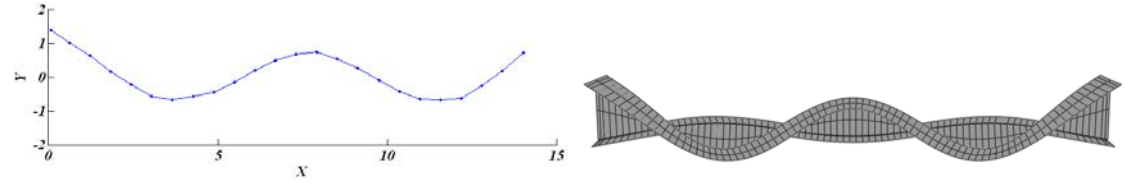

Mode 8

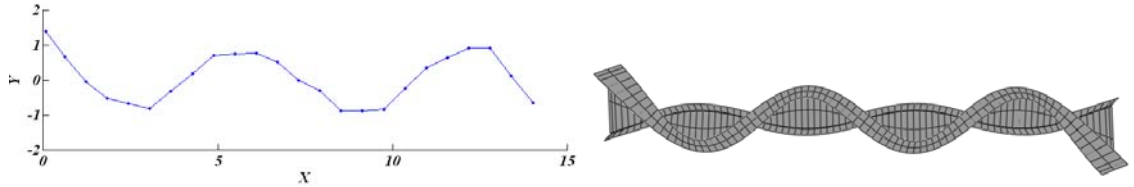

Mode 9

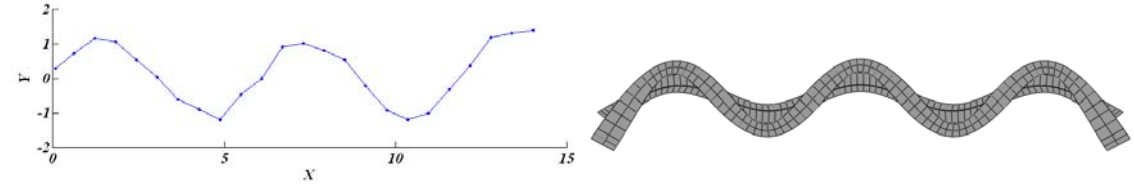

Mode 10

Figure 3.4. Horizontal modes of the HP12x53 (m)
DIAMOND using geophone data (left), ABAQUS (right)

3.6 Full-Scale Bridge Test

If geophones are to gain recognition as a viable sensor for implementation in bridge monitoring programs, it is important that their use be demonstrated on full-scale bridges. The obstacle that must be overcome when using geophones is that the fundamental frequencies of most bridges fall near the resonant frequency of the geophones, where amplitude and phase errors are possible. Conducting a field experiment on a relatively simple test bridge provides verification that geophones, when corrected for amplitude and phase response, can be used to accurately characterize the dynamic response of a bridge.

The bridge tested is located on the University of Tennessee campus and is shown in Figure 3.5. It is believed the bridge was constructed around 1982 for the World's Fair and crosses Second Creek in two spans as shown in Figure 3.6. Each span consists of two reinforced concrete beams supporting a concrete deck constructed using 1.22 m wide precast panels with a monolithic concrete topping reinforced with woven wire fabric as shown in Figure 3.7. It is not known if the deck panels are solid or hollow-core. The bridge is supported at midspan by a reinforced concrete pier consisting to two columns connected by a single tie beam. Each end of the bridge rests on a reinforced concrete abutment. All dimensions shown in Figure 3.6 and Figure 3.7 were measured in the field.

Figure 3.5. Test bridge at the University of Tennessee

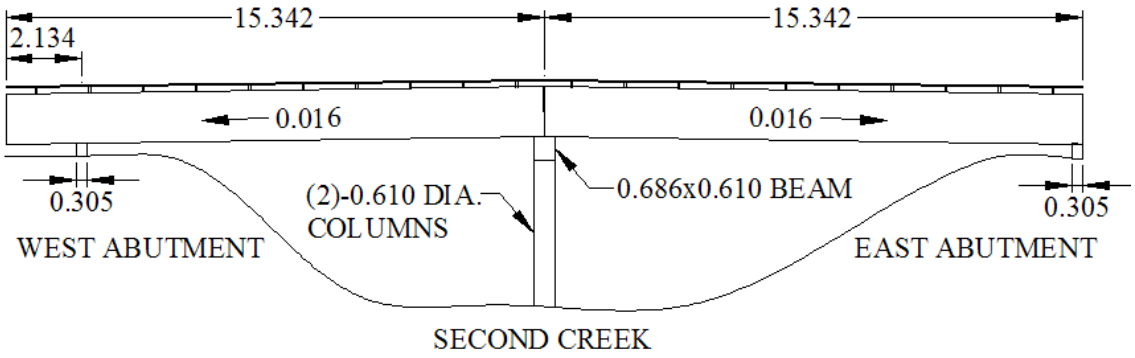

Figure 3.6. UT test bridge: elevation (m)

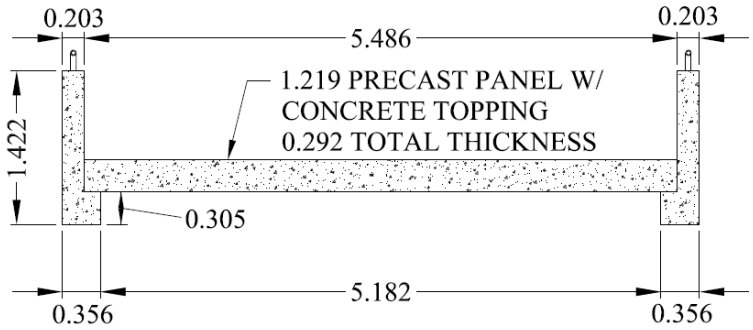

Figure 3.7. UT test bridge: typical cross section (m)

Mark Products LRS-1000 10Hz vertical geophones and Mark Products L-28LBH 4.5Hz horizontal geophones were used to measure the vibrations during the test. To secure the geophones to the bridge, one vertical geophone and one horizontal geophone were rigidly attached to a 1.6 cm thick 11.5 cm diameter steel plate which rested on the bridge.

Throughout the test, data was recorded in the three global coordinate directions at a total of 144 measurement locations using a Geometrics 48-channel StrataView® seismograph containing a 24-bit A/D converter. Because the seismograph was only able to record 48 geophone signals at once (24 vertical and 24 horizontal each time), the 144 measurements locations were divided into six groups, each in a straight line as shown in Figure 3.8. In Figure 3.8, lines 1 and 6 are resting on top of each support beam, and the remaining lines are resting on the bridge deck.

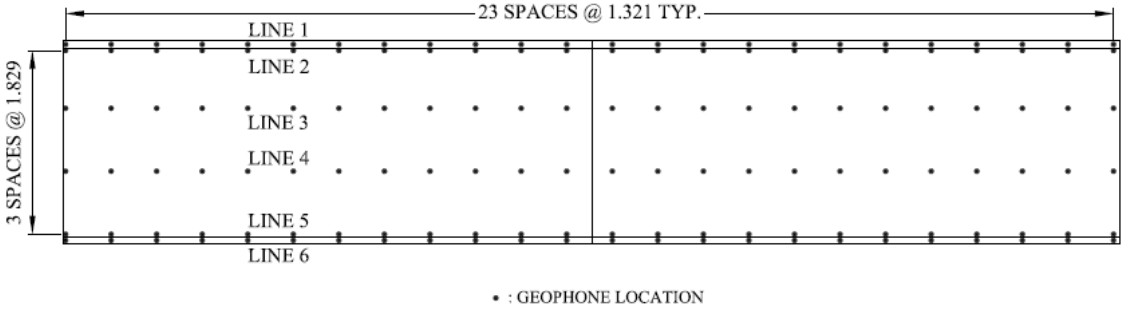

Figure 3.8. UT test bridge: geophone layout (m)

In order to obtain triaxial vibration records, the sandbag was dropped and then dropped again after rotating the horizontal geophones by 90°. Once the data had been recorded in three directions, the line of geophones was shifted to the next position. This process was repeated until all 144 measurement locations were covered.

An important consideration during the field test was the repeatability of the sandbag source. If multiple test setups were to be used to acquire the data, it was important to verify that the same amount of energy was passed to the bridge each time the sandbag was dropped. If the source proved to be unrepeatable, the magnitude and phase relationship between various sensor setups would vary resulting in unintelligible mode shapes. However, as shown in Figure 3.9, dropping a sandbag at the same location imparts approximately the same amount of energy into the bridge each time, and the magnitude and phase relationships are preserved between various sensor setups. This would not be the case if ambient loading such as wind or traffic was used to characterize the bridge. Because of the randomness of ambient loads, the magnitude and phase relationship between various sensor setups would vary widely making the identification of mode shapes difficult. Under working conditions, a bridge will most likely be excited by traffic. Therefore, all the sensors used to characterize the dynamic response of the bridge need to be recorded simultaneously, and the use of geophones provides an economical way to accomplish this task.

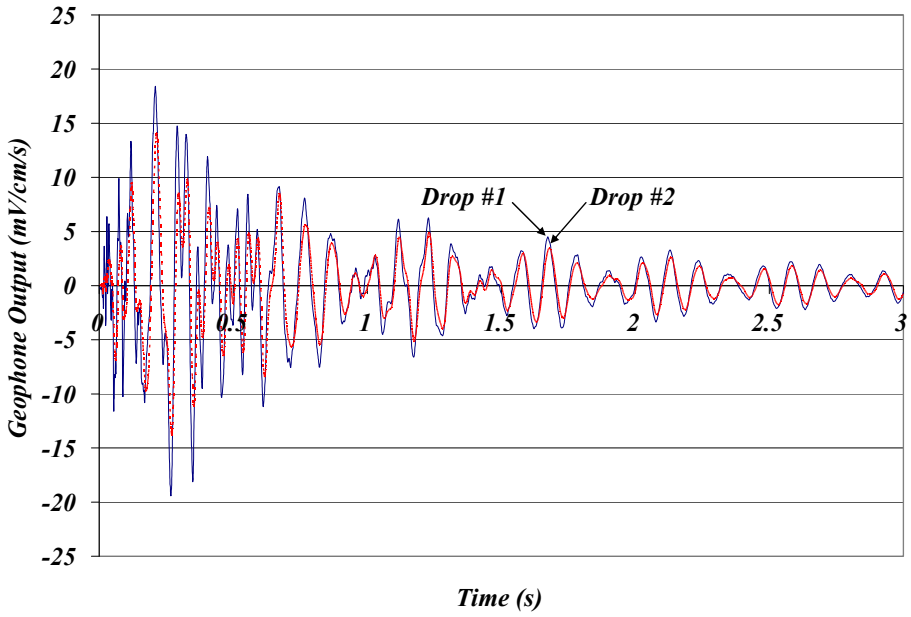

Figure 3.9. Comparison of vertical geophone signals from repeated drops

3.7 Finite Element Model

A finite element model of the UT test bridge was constructed using ABAQUS to verify the field test results. With the exception of the bent columns and handrail on top of each beam, the entire bridge was modeled using 4-node reduced integration shell elements, S4R in ABAQUS. The columns and handrail were modeled using 3-node quadratic beam elements, B32 in ABAQUS.

In order to model the L-shaped support beams, each leg was modeled as a separate shell element. The interior surfaces of each shell were then tied together using the tie constraint in ABAQUS to form a single beam. Using the tie constraint, the displacements and rotations of a slave surface, the short leg here, are tied to the displacements and rotations of a master surface, the long leg here.

At each abutment, the bridge support was modeled as a pin by restricting displacement in all directions but allowing rotation. At the center of the bridge, the interaction between the main beams and the pier was modeled using a join connector in ABAQUS. The join connector ties the displacements of two nodes together but allows independent rotation.

The interaction between the individual precast panels that make up the bridge deck was modeled by tying the displacement between individual panels but allowing for independent rotation. The interaction between the deck and support beams was also modeled using this approach.

Material properties used to model the bridge deck were different than those used to model the support beams and the center pier. When inspecting the underside of the bridge, it was noted that the precast panels were made of a masonry type material. Considering that the bridge deck has a concrete topping, and that little else is known about its construction, median material properties between those for masonry and concrete were used to model the bridge deck: E_d = 17.9 GPa (2,600 ksi), υ_d = 0.18, and ρ_d = 1.36 g/cm^3 (85 lb/ft^3). The support beams and center pier were modeled using the following material properties for concrete: E_c = 27.8 GPa (4,030 ksi), υ_c = 0.18, and ρ_c = 2.32 g/cm^3 (145 lb/ft^3). The steel handrail was modeled using the following material properties: E_s = 200 GPa (29,000 ksi), υ_s = 0.30, and ρ_s = 7.85 g/cm^3 (490 lb/ft^3).

3.8 Model Correlation

In order to quantify the correlation between mode shapes measured in the field and those obtained from the finite element model, the modal assurance criterion (MAC) (Ewins 1985) was used. The MAC, 3.3, takes advantage of the orthogonal property of mode shapes to compare two modes. If the modes are identical, a value of one will be obtained. If the modes are dissimilar, a value of zero will be obtained. In practice, modes are considered correlated if a value greater than 0.9 is calculated and uncorrelated if a value less than 0.05 is calculated. The MAC that compares mode *i* and *j* has the form given in Eq. 3.3 where $(\Phi)_k$ is an element of the mode shape vector and *n* represents the number of points at which the two mode shapes are compared.

$$MAC(i,j) = \frac{\left|\sum_{k=1}^{n}(\phi_j)_k(\phi_i)_k\right|^2}{\left(\sum_{k=1}^{n}(\phi_j)_k(\phi_j)_k\right)\left(\sum_{k=1}^{n}(\phi_i)_k(\phi_i)_k\right)} \qquad 3.3$$

3.9 Results and Discussion

MAC results comparing the mode shapes identified from the field test and those obtained from the finite element model are shown in Table 3.3. Observing Table 3.3, it can be seen that the first two modes are highly correlated. Modes 3 and 4 are also well correlated, but exhibit a fairly high degree of coupling as evidenced by the higher values in the 3,4 and 4,3 locations.

Overall, the finite element model of the test bridge is considered to be reasonably correlated to the field test results. It is expected that the correlation between the field test results and the bridge model could be improved using a finite element model updating

procedure which is beyond the scope of this research. As a part of this research, the purpose of the finite element model was simply to verify that the data collection and modal analysis procedures used produced reliable results.

The first four identified natural frequencies for the test bridge are presented in Table 3.3. Notice that the first two frequencies fall near the natural frequency of the vertical geophones used to characterize the bridge. Therefore, magnitude errors and phase shifts would be expected had the data not been corrected to account for the geophone response. Undoubtedly, no intelligible mode shapes incorporating both the vertical and horizontal geophones would be obtained.

The corresponding mode shapes for the first four identified natural frequencies are presented in Figure 3.10. In Figure 3.10, each grid intersection represents a triaxial measurement location. Because of the density of sensors used during the bridge test, an amount of mode shape detail exceeding what is normally reported in the literature is presented here. In Figure 3.10, modes 1 and 2 are obviously the fundamental bending modes of each span while modes 3 and 4 are higher order bending modes.

Observing the mode shapes, it can be seen that the magnitude and phase relationships between various sensor setups are preserved. Although it can not be seen in Figure 3.10, when animated the vertical and horizontal motion of the bridge is in phase with one another. This would not be the case had the geophone output not been corrected to account for the differing dynamic characteristics of the vertical and horizontal geophones, and the mode shapes would be difficult to identify.

Table 3.3. UT bridge: comparison of field test and finite element results

Natural Frequencies (Hz)			MAC			
Mode	Test	FE Model	Mode 1	Mode 2	Mode 3	Mode 4
1	8.78	8.78	0.9704	0.0007	0.0099	0.0003
2	11.40	11.20	0.0000	0.9506	0.0017	0.0065
3	25.79	26.25	0.0056	0.0095	0.8487	0.1387
4	27.90	27.69	0.0006	0.0135	0.1895	0.8752

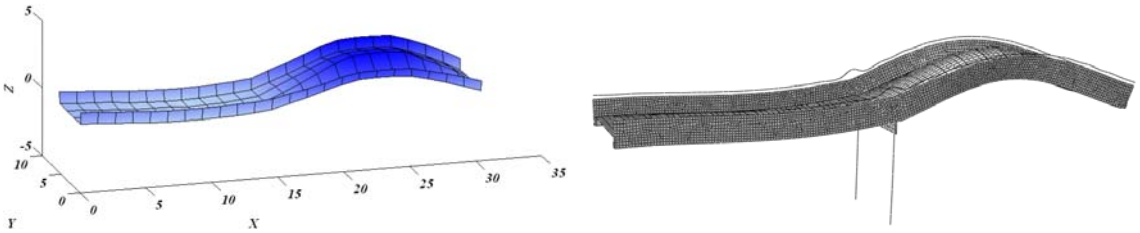

Mode 1

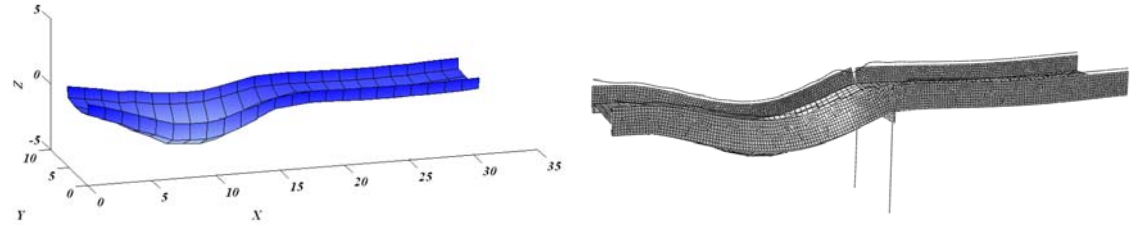

Mode 2

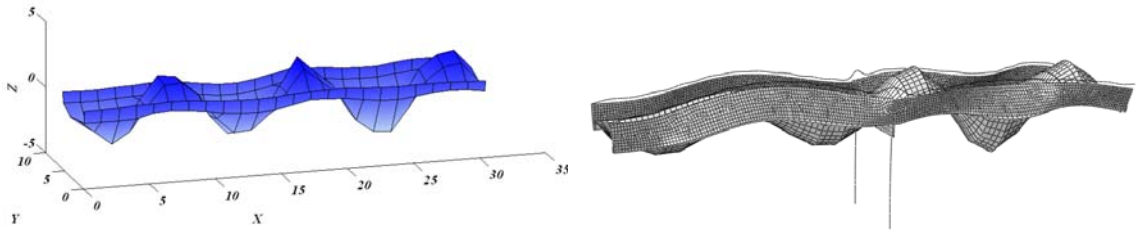

Mode 3

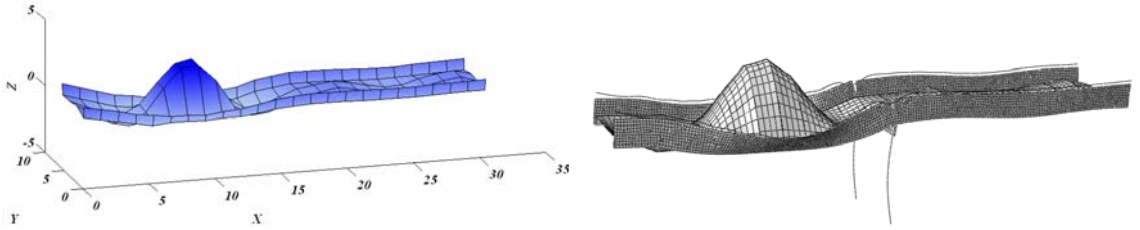

Mode 4

Figure 3.10. UT test bridge: modes of vibration (m)
DIAMOND using geophone data (left), ABAQUS (right)

Another interesting observation from Figure 3.10 is the complexity of the bridge deck displacement, particularly in modes 3 and 4. Because researchers are often times only able to place sensors along the edge of a bridge due to traffic, this type of mode shape complexity is often missed. Noting that the more effective vibration-based damage detection techniques rely on changes to mode shapes and their derivatives, the added mode shape detail may prove invaluable in implementing these techniques in remote bridge monitoring systems. Again, the use of geophones provides an economical way to acquire additional mode shape detail.

3.10 Conclusions

The goal of this study was to evaluate the use of inexpensive geophones for the purpose of dynamically characterizing full-scale bridges using output only data. The motivation behind the study was to determine a reliable and inexpensive method to accurately determine modal parameters for use with vibration-based damage detection techniques.

One of the significant obstacles in implementing continuous monitoring systems is the cost of the sensors. The results of this study have demonstrated that low-cost geophones can be used to characterize the dynamic response of a bridge. Furthermore, geophones do not require a power source which eliminates another obstacle in implementing remote monitoring systems. Throughout the described tests, the only power source used was a battery to power the seismograph.

The current study has demonstrated that the rational polynomial method can be used for modal parameter identification with output-only data. Assuming the input function has a relatively flat response over the frequency range of interest allows the response spectrum matrix created by multiplying the spectrum of each measured response by the conjugate spectrum of a reference response to be analyzed instead of a measured FRF matrix. As demonstrated by this research, this method of modal analysis produces accurate and reliable results. Furthermore, the method is fairly straightforward and easy to understand making it more user friendly for parameter estimation than some of the other methods reported in the literature.

The density of sensors used in the current study resulted in mode shapes that are more defined than those often reported in the literature. Thus, mode shape detail that may have been missed by other researchers has been identified in the current study. Because the more effective vibration-based damage detection techniques rely on changes in mode shapes and their derivatives, additional mode shape detail may prove to be invaluable in implementing these techniques in remote monitoring systems, and geophones provide an economical way to obtain the additional detail.

3.11 References

Bell, E.S., Sanayei, M., Javdekar, C.N., and Slavsky, E. (2007). "Multiresponse parameter estimation for finite-element model updating using nondestructive test data." *Journal of Structural Engineering*, 133(8), 1067-1079.

Catbas, F.N., Ciloglu, S.K., Hasancebi, O., Grimmelsman, K., and Aktan, A.E. (2007). "Limitations in structural identification of large constructed structures." *Journal of Structural Engineering*, 133(8), 1051-1066.

Dassault Systèmes, Inc., SIMULIA Corp. (2008). ABAQUS®. Version 6.8.

Dobrin, M.B. and Savit C.H. (1988). *Introduction to Geophysical Prospecting*, 4th Ed., McGraw-Hill, New York.

Doebling, S.W., Farrar, C.R., Prime, M.B., and Shevitz, D.W. (1996). *Damage Identification and Health Monitoring of Structural and Mechanical Systems from Changes in Their Vibration Characteristics: A Literature Review.* Rep. No. LA 13070-MS, Los Alamos National Laboratory, Los Alamos, N.M.

Doebling, S.W., Farrar, C.R., and Prime, M.B. (1998). "A summary review of vibration-based damage identification methods." *The Shock and Vibration Digest*, 30(2), 91–105.

Ewins, D.J. (1985). *Modal Testing: Theory and Practice*. John Wiley, New York.

Farrar, C.R., Doebling, S.W., and Prime, M.B. Cornwell, P.J., Kam, M., Straser, E.G., Hoerst, B.C., Shevitz, D.W., and Jauregui, D.A. (1998). *A Comprehensive Monitoring System for Damage Identification and Location in Large Structural and Mechanical Systems.* Rep. No. LA-UR-98-233, Los Alamos National Laboratory, Los Alamos, N.M.

Gassman, S.L. and Tawhed, W.F. (2004). "Nondestructive assessment of damage in concrete bridge decks." *Journal of Performance of Constructed Facilities*, 18(4), 220-231.

Halling, M. W., Muhammad, I., and Womack, K. C. (2001). "Dynamic field testing for condition assessment of bridge bents." *Journal of Structural Engineering*, 127(2), 161-167.

He, X., Moaveni, B., Conte, J.P., Elgamal, A., and Masri, S.F. (2009). "System identification of Alfred Zampa Memorial Bridge using dynamic field test data." *Journal of Structural Engineering*, 135(1), 54-66.

Huth, O., Feltrin, G., Maeck, J., Kilic, N., and Motavalli, M. (2005). "Damage identification using modal data: experiences on a prestressed concrete bridge." *Journal of Structural Engineering*, 131(12), 1898-1910.

Kim, J.T. and Stubbs, N. (2003). "Nondestructive crack detection algorithm for full-scale bridges." *Journal of Structural Engineering*, 129(10), 1358-1366.

Ko, J.M. and Ni, Y.Q. (2005). "Technology developments in structural health monitoring of large-scale bridges." *Engineering Structures,* 27(12), 1715-1725.

The Mathworks, Inc. (2007). MATLAB®. Version R2007a.

Ren, W.X., Zatar, W., and Harik, I.E. (2004). "Ambient vibration-based seismic evaluation of a continuous girder bridge." *Engineering Structures*, 26(5), 631-640.

Richardson, M.H. and Formenti, D.L. (1985). "Parameter estimation from frequency response measurements using rational fraction polynomials." *Structural Measurement Systems Technical Note 85-3*.

Robinson, E.S. and Coruh, C. (1988). *Basic Exploration Geophysics*, John Wiley & Sons, New York.

Sohn, H., Farrar, C.R., Hemez, F.M., Shunk, D.D., Stinemates, D.W., and Nadler, B.R. (2004). *A Review of Structural Health Monitoring Literature: 1996–2001*. Rep. No. LA-13976-MS, Los Alamos National Laboratory, Los Alamos, N.M.

Xu, H.P. and Humar, J. (2006). "Damage detection in a girder bridge by artificial neural network technique." *Computer-Aided Civil and Infrastructure Engineering*, 21(6), 450-464.

Zhao, J. and DeWolf, J.T. (2002). "Dynamic monitoring of steel girder highway bridge." *Journal of Bridge Engineering*, 7(6), 350-356.

Zhou, Z., Wegner, L.D., and Sparling, B.F. (2007). "Vibration-based detection of small-scale damage on a bridge deck." *Journal of Structural Engineering*, 133(9), 1257-1267.

Chapter 4. Damage Detection on a Full-Scale Three-Girder Bridge Using an Array of Triaxial Geophones

This chapter is revised based on a paper submitted to the ASCE *Journal of Structural Engineering* by William Ragland, Dayakar Penumadu, and Richard Williams:

Ragland, W.S., Penumadu, D., and Williams, R.T. (In review). "Damage detection on a full-scale three-girder bridge using an array of triaxial geophones." *Journal of Structural Engineering*.

My primary contributions to the paper included: (i) development of the problem into a work, (ii) gathering and reviewing literature, (iii) arrangement, design and conduction of the field tests, (iv) processing, analyzing, and interpretation of the experimental data, (v) development of computer codes for implementation of the damage detection techniques, and (vi) most of the writing.

4.1 Abstract

Nondestructive damage evaluation of structures has received the attention of many researchers over the past several years. Vibration-based damage detection is a nondestructive evaluation approach based on structural damage being reflected in a structure's dynamic response. Varying levels of success have been reported when applying various vibration-based damage detection techniques to bridges. However, previous studies typically incorporate a calibrated finite element model of a real bridge, a scaled laboratory model, or a partial bridge where a substantial portion of the bridge has already been removed to provide a damaged data set for damage detection and analysis.

This paper describes results from an in-situ, full-scale bridge test that was subjected to controlled levels of known damage and evaluates various vibration-based damage detection techniques on their ability to locate the induced damage both locally and globally. One of the challenges involved when implementing vibration-based damage detection techniques with full scale bridges is obtaining inexpensive, detailed modal parameters from vibration measurements. To overcome this obstacle, inexpensive geophones are proposed to obtain spatially resolved and temporally coupled triaxial vibration records over a relatively dense measurement grid. A unique aspect of this work is the extension of established damage detection techniques to include the three dimensional response of a bridge using triaxial vibration records. Results show that each of the damage detection methods used for analysis is capable of successfully locating the induced damage, but with poor spatial resolution. Contrary to expectations, it was observed from the present test that the horizontal response of the bridge, particularly in the longitudinal direction, is more sensitive to induced damage than the vertical response. Finally, the first torsional mode was found to be more sensitive to induced damage than the fundamental bending mode.

4.2 Introduction

As the nation's infrastructure continues to age, methods of reliably assessing its overall health have become increasingly more important. While the condition of all types of infrastructure is important, the primary focus of this work is the nation's bridge inventory. Currently, bridges in the United States are inspected and rated during biennial

inspections which rely heavily on visual techniques. However, in a report released by the Federal Highway Administration, visual inspections were found to be relatively unreliable (FHWA 2001). For this reason, researchers have been working on the development of more objective methods for nondestructively inspecting and rating bridge condition.

Researchers have been using vibration testing as a means of assessing structural health for some time. Results obtained through vibration testing serve as the basis for several areas of research and structural analysis such as structural health monitoring (Krämer et al. 1999, Zhao and DeWolf 2002), finite element model updating and calibration (Xia and Brownjohn 2004, Morassi and Tonon 2008), condition assessment of structures (Halling et al. 2001, Ren et al. 2004), and structural damage detection (Farrar and Jauregui 1996, Maeck et al. 2001, Pothisiri and Hjelmstad 2003). The focus of this paper is vibration-based damage detection on in-situ, full-scale bridges.

Vibration-based damage detection focuses on changes in the dynamic characteristics of a structure, such as natural frequency and mode shape, as indicators of damage. Several different global evaluation techniques and associated quantitative damage indices have been published in recent years. Detailed reviews of these techniques as applied to bridges and other structures can be found in Doebling et al. (1996, 1998) and Sohn et al. (2004). In summary, the methods discussed monitor shifts in natural frequency, absolute changes in mode shapes, changes in mode shape curvature or strain energy, and variations in stiffness and flexibility matrices.

After careful review of the literature, the authors found that studies which compare different vibration-based damage detection techniques in an objective manner to a common data set collected entirely on a full-scale bridge are scarce. Often times the damaged data set is obtained from a calibrated finite element model (Siddique et al. 2007) or a scaled laboratory model of the real bridge (Zhou et al. 2007). One of the more cited studies that compared different damage detection techniques using data collected entirely on a full-scale bridge was performed by Farrar and Jauregui (1996) on the I-40 eastbound bridge over the Rio Grande River in New Mexico. Using an array of vertical accelerometers, the vibration response of the bridge was measured in an undamaged state and after each progressive damage scenario was inflicted (Farrar et al. 1994).

In Farrar and Jauregui's study, only the three eastern spans of the eastbound bridge were tested while the western spans of the bridge were being demolished. Because the superstructures of the eastern and western spans of the eastbound bridge were independent, it is not expected that either span greatly affected the dynamic response of the other, except through a common pier. Portions of the foundation at the east abutment had also been removed to construct an access road for construction activities. While it is agreed that the demolition and foundation removal can be viewed as changes to the boundary conditions of the test bridge, it remains that the bridge was not in an in-situ operating state when the tests were performed.

One aspect of the bridge studied by Farrar and Jauregui (1996) that would seem to lend ease to damage identification is its lack of redundancy. Two welded-steel plate girders support the bridge between piers (40 m, 50 m, and 40 m spans), one on each side

of the deck with a center-to-center spacing of approximately 9 m. Obviously any significant damage to either girder would dramatically alter the bridge's behavior do to the lack of redundant load paths between piers. It is therefore expected, and confirmed in the report, that most of the damage detection techniques evaluated would be successful in locating the induced damage.

Another well known and highly cited full-scale damaged bridge test is the Z24 Bridge in Switzerland (Krämer et al. 1999). The Z24 Bridge was a post-tensioned two box cell girder bridge with spans of 14, 30, and 14 m supported by four concrete piers. Various damage scenarios were inflicted on the bridge, and its vibration response was measured using a fairly dense array of accelerometers. One of the drawbacks to the Z24 Bridge study is that the bridge was not in an in-situ operating state when some of the damage tests were performed. Due to the amount of modification to the bridge needed to simulate some of the damage scenarios, it is debatable if changes in the bridge's dynamic response are due to the simulated damage or the modifications. Finally, Krämer et al. (1999) state that "if high sensitivity, low frequency sensors were cheap, and only a small amount of data was to be acquired, stored, and processed, then a large number of sensors would be desirable." The current study directly addresses this concern by implementing high sensitivity, low frequency, inexpensive geophones to obtain triaxial vibration records.

Recently, a large construction project often referred to as SmartFix 40 realigned I-40 through downtown Knoxville, TN, while increasing the roadway's capacity to meet current demand. In order to decrease the amount of time required for construction, a

small section of I-40 was closed for a period of 14 months. Due to the closing, the rare opportunity to perform full-scale bridge testing in an in-situ state and subjected to controlled amounts of damage at a chosen location became a reality. The experimental testing methods, analysis procedures, and results obtained for one of the SmartFix bridges are presented in this paper.

The testing of the bridge discussed in this paper is of interest for several reasons. First, the bridge was tested in an in-situ, full-scale, operating condition before any structural demolition or removal of the surrounding soil had taken place. Second, all vibration records were obtained using inexpensive geophones which provide some advantages over accelerometers which are traditionally used to measure bridge vibrations. Furthermore, unlike previous studies that relied heavily on the vertical response of the bridge, triaxial vibration records were obtained in this study which has allowed the use of vibration-based damage detection techniques to be extended to three dimensions. Third, the bridge tested has direct practical relevance because it is of a similar design to many existing bridges and new bridges being constructed in Tennessee. Thus, results obtained in this study may prove applicable in the implementation of monitoring systems for a large number of bridges. Finally, the method used to induce damage is believed to simulate a realistic crack that has a high probability of occurring on an in-service bridge which could threaten the bridge's overall structural integrity. Not all damage types are immediately threatening to the structural integrity of a bridge (e.g. bridge deck spalling), or the damage occurs in a location likely to be visually noticed and reported by bridge users (e.g. a significant hole in the bridge deck). While the ideal

damage detection method would identify all types of damage, the goal of this research is to identify superstructure damage in its early stages that is capable of going unnoticed by bridge users and potentially collapsing a significant portion of a bridge. Considering these points, the purpose of this paper is to propose a new three-dimensional approach to vibration-based damage detection using triaxial vibration measurements obtained using highly sensitive, inexpensive geophones on an incrementally damaged, in-situ, full-scale bridge.

4.3 Geophones as Sensors

One of the challenges involved when implementing vibration-based damage detection techniques with full scale bridges is obtaining inexpensive, detailed modal parameters from vibration measurements. To overcome this obstacle, inexpensive geophones (approximately $50 each) are used in this study to obtain triaxial vibration records over a relatively dense measurement grid.

A geophone is a passive directional sensor that measures the speed of motion in the direction of its sensitive axis. In basic terms, a geophone is a coil suspended by springs around a permanent magnet, all of which is contained in a protective casing. When the coil moves relative to the magnet, a voltage is induced in the coil that depends on the relative velocity between the coil and magnet.

Traditionally, geophysicists, rather than bridge engineers, use geophones to measure elastic waves propagating through several kilometers of geologic materials.

Detailed technical descriptions of the various types of geophones can be found in geophysical textbooks (Dobrin and Savit 1988, Robinson and Coruh 1988).

Accelerometers are commonly used for dynamic testing of civil engineering structures. However, geophones offer important advantages over accelerometers when considered for implementation in bridge monitoring systems. First of all, an accelerometer generally requires charge amplification electronics to produce a signal suitable for recording, and thus a power source is needed for the amplifier and associated hardware. In comparison, geophones are passive devices that produce a voltage that can be recorded without additional amplification or conditioning. Because they do not require an external power supply or an amplifier, geophones are ideal candidates for implementation in remote bridge monitoring systems. Furthermore, geophones may more easily be incorporated into a wireless sensor system for bridge monitoring in the future.

4.4 Damage Detection Methods

Various damage detection techniques have been presented in the literature, but most are simply a variation of a much smaller number. For this study, the methods compared by both Farrar and Jauregui (1996) and Zhou et al. (2007) are evaluated. By comparing the same methods as previous researchers a better understanding of these methods when applied to different bridge structures can be obtained. The various methods are briefly described in the following paragraphs.

Given mode shapes obtained before and after damage, the damage index method (Stubbs et al. 1995) attempts to identify damage in a structure using changes in modal

strain energy between the undamaged and damaged structure. The damage index, β_{ij}, relates the change in modal strain energy at location *j* in the *i*th mode using mode shape curvatures as shown in Eq. 4.1.

$$\beta_{ij} = \frac{\left(\int_a^b \left[\Phi_i'' * (x)\right]^2 dx + \int_a^L \left[\Phi_i'' * (x)\right]^2 dx \right) \int_a^L \left[\Phi_i''(x)\right]^2 dx}{\left(\int_a^b \left[\Phi_i''(x)\right]^2 dx + \int_a^L \left[\Phi_i''(x)\right]^2 dx \right) \int_a^L \left[\Phi_i'' * (x)\right]^2 dx} \tag{4.1}$$

In Eq. 4.1, $\Phi_i''(x)$ and $\Phi_i''^*(x)$ are the second derivatives of the *i*th mode shape of the undamaged and damaged structure, respectively. L is the length of the beam, and a and b are the end points of the segment of the beam being analyzed. Multiple modes can be used, in which case the damage index is calculated by summing damage indices from each mode. Upon calculating the damage index at each location on the beam, a normal distribution is fit to the indices, and values falling two or more standard deviations from the mean are considered likely damage locations.

The mode shape curvature method (Pandey et al. 1991) assumes that damage to a structure only affects its stiffness and mass. Mode shapes are determined for the structure before and after damage, and mode shape curvatures are estimated using some type of numerical differentiation. In order to develop this method, consider an example of a beam with uniform bending stiffness, *EI*, subjected to a bending moment, *M(x)*. The curvature, $v(x)$, of the beam at location x is then given by Eq. 4.2.

$$v(x) = \frac{M(x)}{EI} \tag{4.2}$$

$$\Delta\Phi'' = \left|\Phi_i'' *\right| - \left|\Phi_i''\right| \tag{4.3}$$

Observing Eq. 4.2, it is clear that curvature is inversely proportional to flexural stiffness and that a reduction in stiffness will result in an increase in curvature. Therefore, differences in undamaged and damaged mode shape curvatures, Eq. 4.3, should be greatest near damaged locations. When multiple modes are used, the absolute value of the difference in curvatures for each mode is summed to obtain a damage parameter for each location.

The change in flexibility method (Pandey and Biswas 1994) first approximates the flexibility matrix of the undamaged structure, Eq. 4.4, and the damaged structure, Eq. 4.5, using a given number, n, of modal frequencies, ω_i, and unit-mass-normalized mode shapes, φ_i.

$$[F] \approx \sum_{i=1}^{n} \frac{1}{\omega_i^2} \{\varphi_i\}\{\varphi_i\}^T \tag{4.4}$$

$$[F]^* \approx \sum_{i=1}^{n} \frac{1}{\omega_i^{*2}} \{\varphi_i\}^* \{\varphi_i\}^{*T} \tag{4.5}$$

$$[\Delta F] = [F] - [F]^* \tag{4.6}$$

The two flexibility matrices are then subtracted which results in the change in flexibility matrix, Eq. 4.6. The absolute maximum value of each column of the change in flexibility matrix is then determined, and the column corresponding to the largest change in flexibility is indicative of the damaged degree of freedom.

The uniform load surface, U_i, is obtained by summing all the columns of the flexibility matrix. The result is the deformed shape of the structure caused by applying a unit load to each degree of freedom on the structure simultaneously. The change in

uniform load surface curvature method (Zhang and Aktan 1995) identifies damage as the location where the absolute difference between the undamaged and damaged uniform load surface curvatures is greatest, Eq. 4.7.

$$\Delta U_i'' = \left| U_i''^* - U_i'' \right| \tag{4.7}$$

4.5 Full-Scale Bridge Used for Experiments

Constructed in 1967, the bridge tested was a part of the entrance ramp to James White Parkway from I-40 westbound, Figure 4.1, and consisted of three spans comprised of a concrete deck supported by three steel girders. Cross bracing in the form of steel channels was provided between all the girders. The bridge was constructed on a thirty degree skew and within a horizontal curve with a radius of 853.44 m, which added a slight curve and super elevation to the bridge. There is also a decrease in elevation from the east abutment (#2) to the west abutment (#1). When in operation, the bridge carried a single lane of traffic. An elevation of the bridge is shown in Figure 4.2, and a typical cross section is shown in Figure 4.3.

From east to west, the bridge spanned approximately 13, 22, and 10 m as shown in Figure 4.2. Three rolled W-shapes were connected with bolted splice plates to form one continuous beam over the entire bridge length. The ends of each beam were W30x108, while the center was a W30x124. Cover plates, 2.9 cm thick, were added to the top and bottom of each beam in the end spans. For the center span, headed studs were used on top of the beam to promote composite action with the concrete deck. Connections that allowed for longitudinal (parallel to the bridge length) movement,

marked “Exp” in Figure 4.2, and connections that prevented longitudinal movement, marked “Fix” in Figure 4.2, were installed at each location where a beam was supported by either a concrete bent or abutment. Intermediate diaphragms, C12x20.7, were located at 7.6 m on center perpendicular to each beam, and end diaphragms, C15x33.9, were provided at each end of the bridge parallel to the bridge skew.

Figure 4.1. Entrance ramp to James White Parkway
(47SR1580031)

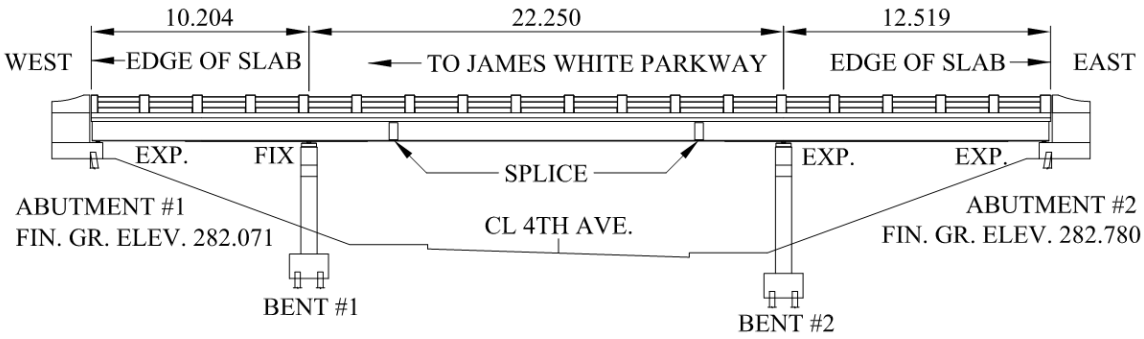

Figure 4.2. Entrance ramp to James White Parkway: elevation (m)

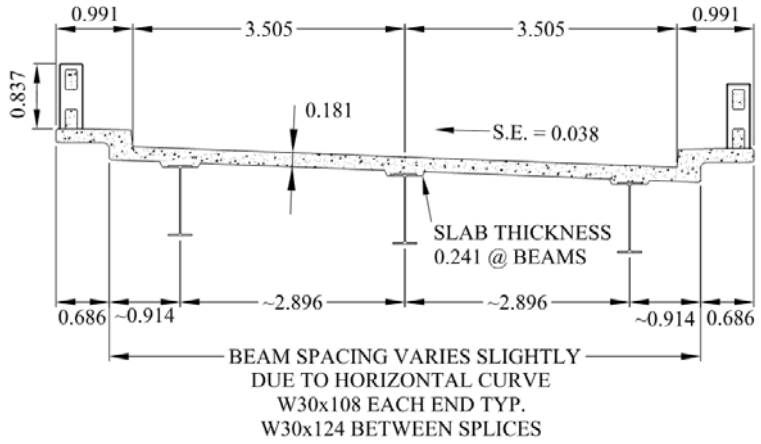

Figure 4.3. Entrance ramp to James White Parkway: typical cross-section (m)

4.6 Field Test Setup

Mark Products LRS-1000 10Hz vertical geophones and Mark Products L-28LBH 4.5Hz horizontal geophones were used for the vibration measurements. One vertical and one horizontal geophone were rigidly attached to a 1.6 cm thick, 11.5 cm diameter steel plate which rested on the bridge deck. The bridge was excited by dropping a 22.7 kg sandbag at a total of 6 different locations corresponding to the third points of the center span along beams 1,2, and 3 in Figure 4.4.

Throughout the test, data was recorded in the three global coordinate directions at a total of 72 measurement locations using a Geometrics 48-channel StrataView seismograph containing a 24-bit A/D converter. Because the seismograph was only able to record 48 geophone signals at once (24 vertical and 24 horizontal each time), the 72 measurements locations were divided into three groups. For each group, the geophones were spaced at 1.98 m center-to-center (except for the last pair of plates, which was 1.37 m) on the bridge deck along the beam line below as shown in Figure 4.4.

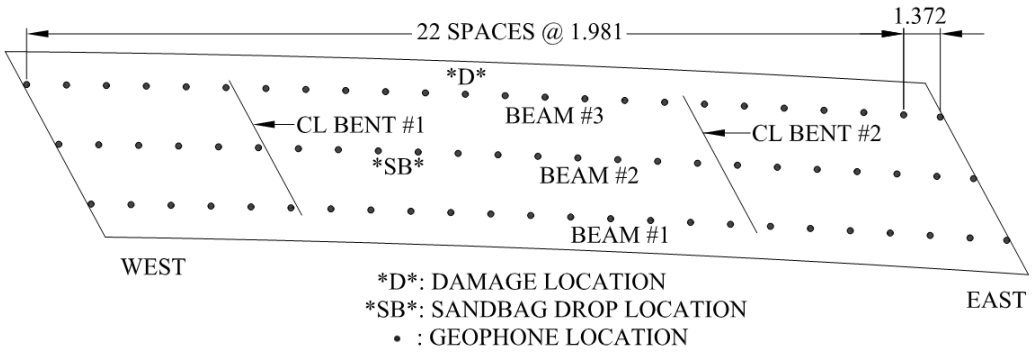

Figure 4.4. Entrance ramp to James White Parkway: geophone layout

In order to obtain triaxial vibration records, the sandbag was dropped and then dropped again after rotating the horizontal geophones by 90°. Once the data had been recorded in three directions, the line of geophones was shifted to the next position. This process was repeated until all 72 measurement locations were covered. During each test, data was sampled at a rate of 1000 Hz for a total of four seconds. Using these sampling parameters, a frequency resolution of 0.25 Hz was obtained over a frequency range of 0-500 Hz. All results presented in this paper were obtained from the data set collected when the sandbag was dropped on beam #2 closest to bent #1 as shown in Figure 4.4.

An important consideration during the field test was the repeatability of the sandbag source. If multiple test setups were to be used to acquire the data, it was important to verify that the same amount of energy was passed to the bridge each time the sandbag was dropped. If the source proved to be unrepeatable, the magnitude and phase relationship between various sensor setups would vary resulting in unintelligible mode shapes. However, it was verified that dropping a sandbag at the same location imparts approximately the same amount of energy into the bridge each time, and the magnitude

and phase relationships are preserved between various sensor setups. This would not be the case if ambient loading such as wind or traffic was used to characterize the bridge. Because of the randomness of ambient loads, the magnitude and phase relationship between various sensor setups would vary widely making the identification of mode shapes difficult. Under service conditions, a bridge will most likely be excited by traffic. Therefore, all the sensors used to characterize the dynamic response of the bridge need to be recorded simultaneously, and the use of geophones provides an economical way to accomplish this task.

4.7 Damage Scenarios

While the test bridge exhibited some defects, the first test performed is considered to represent an undamaged or initial reference state. The goal of this study is to identify the additional damage induced as part of the experiment based on comparisons with a baseline measurement. Additional studies could be performed to assess the overall condition of the bridge using only the baseline measurement by comparing the field test results with bridge inspection reports and/or a finite element model.

For this research, damage was induced by incrementally cutting a main girder upward from the bottom flange as shown in Figure 4.5. The cut was located on beam #3 at mid-span of the bridge's center span as indicated in Figure 4.4. This method of inducing damage was meant to simulate a crack that may occur due to fatigue or excessive vehicle weight and that is capable of compromising the structural integrity of the bridge.

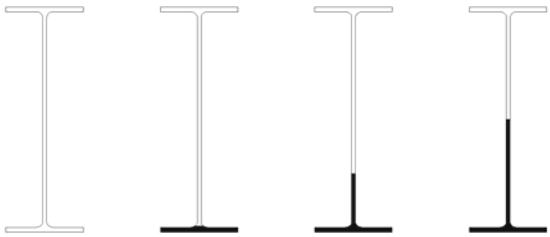

Figure 4.5. Damage scenarios
From left to right, undamaged (D0), bottom flange cut (D1),
bottom flange plus ¼ of the web cut (D2), bottom flange plus ½ the web cut (D3)

4.8 Modal Analysis

For this study, the rational polynomial method (Richardson et al. 1985) as implemented in DIAMOND (Farrar et al. 1998) was used for extracting natural frequencies and mode shapes from measured field data. DIAMOND (Damage Identification and Modal Analysis of Data) is a MATLAB® (Mathworks 2007) based software package developed at Los Alamos National Laboratories for modal analysis, damage identification, and finite element model refinement.

Briefly, the rational polynomial method uses orthogonal polynomials to estimate the coefficients of a polynomial approximation to the frequency response function (FRF). The FRF of a system is the ratio of the Fourier transform of the measured input and response signals. Thus, the rational polynomial method is intended for use with measured inputs. However, recording the input excitation for an in-service bridge under ambient loading, such as wind or traffic, would be nearly impossible. For this reason, it was decided not to record input excitations as a part of this research. Because the input was not recorded, an assumption was made in order to implement the rational polynomial method. If an input force is known to have a flat spectrum, as would be the case for wind

or traffic, then any peaks in the response spectrum are caused by structural resonances. Therefore, it was assumed that the impulsive loading source used during tests possessed a flat spectrum, at least over the frequency range of interest. This assumption allows the response spectrum matrix created by multiplying the spectrum of each measured response by the conjugate spectrum of a reference response to be analyzed instead of the FRF matrix.

This method of modal analysis is meant to simulate what would have to be used in an actual bridge monitoring system where inputs due to ambient sources, such as wind and traffic, are not easily measured. The results of this study indicate that the natural frequencies and operating shapes obtained using this procedure can be successfully combined with vibration-based damage detection techniques to locate damage on a full-scale bridge.

4.9 Damage Effects on Conventional Modal Properties

A summary of the identified natural frequencies for undamaged and damaged bridge tests is presented in Table 4.1. It was expected that the natural frequencies would decrease with each progressive increase in damage (Figure 4.5), but no discernable pattern is observed in Table 4.1. Furthermore, natural frequencies are observed to at times increase with an increase in damage. Because resolution in the frequency domain is directly proportional to the length of measured time series ($\Delta f=1/t$, where t is the length of the measured time series in seconds), it is expected that these results would slightly improve had longer vibration records been recorded. However, similar changes in natural

frequencies were observed when comparing the results obtained from different sandbag drop locations. Thus, the observed changes in natural frequencies are considered to be reliable due to their repeatability.

After the final damage scenario was induced, the largest decrease in natural frequency occurred in the first torsional mode (mode 1). The fundamental bending mode (mode 2) experienced a decrease in natural frequency after damage scenario D1 was induced, but after damage scenario D2 was induced, it experienced an increase in natural frequency. Overall, the observed changes in natural frequency are not considered to be significant because researchers have shown that environmental conditions can cause changes in natural frequencies of similar order to those caused by the induced damage in this study (Farrar et al. 1997, Zhao and DeWolf 2002). Therefore, similar observations noted by previous researchers (Liu and DeWolf 2007, Siddique et al. 2007) are confirmed by this study, and changes in natural frequencies alone are deemed to be unreliable indicators of damage.

Table 4.1. Comparison of natural frequencies (Hz)

Damage Test	Mode 1	Mode 2	Mode 3	Mode 4	Mode 5	Mode 6
D0, Undamaged	4.20	5.04	8.14	10.28	15.42	30.06
D1, Flange Cut	4.34 (3.28%)	4.80 (-4.85%)	8.29 (1.75%)	10.39 (1.09%)	15.43 (0.04%)	29.66 (-1.33%)
D2, Flange + ¼ Web Cut	4.18 (-0.35%)	5.31 (5.31%)	8.24 (1.12%)	10.31 (0.27%)	15.35 (-0.48%)	29.92 (-0.48%)
D3, Flange + ½ Web Cut	4.14 (-1.37%)	5.12 (1.41%)	8.08 (-0.81%)	10.28 (0.01%)	15.42 (0.00%)	29.98 (-0.29%)

Note: Numbers in () are change from D0.

The mode shapes identified for the undamaged test (D0) and the D3 damaged test are presented in Figure 4.6. Observing Figure 4.6, there is very little difference in the overall shape of the undamaged and damaged mode shapes. There are subtle observable differences in most of the mode shapes, but the largest difference occurs in the first torsional mode (mode 1). The first torsional mode not only exhibits a change in the vertical displacement, but also a change in horizontal displacement. The fundamental bending mode (mode 2) appears to be largely unaffected by the damage with little or no observable differences in the identified undamaged and damaged mode shapes. In particular, there is no change in the horizontal displacement of the fundamental bending mode.

In order to better quantify the correlation between mode shapes measured in different tests, a modal assurance criterion (MAC) (Ewins 1985) was used. The MAC, Eq. 4.8, takes advantage of the orthogonal property of mode shapes to compare different modes. If the modes are identical, a value of one will be obtained. If the modes are dissimilar, a value of zero will be obtained. Ewins (1985) notes that in practice, modes are considered correlated if a value greater than 0.9 is calculated and uncorrelated if a value less than 0.05 is calculated. The MAC that compares mode i and j has the form given in Eq. 4.8 where $(\Phi)_k$ is an element of the mode shape vector and n represents the number of points at which the two mode shapes are compared.

$$MAC(i,j) = \frac{\left|\sum_{k=1}^{n}\left(\Phi_j\right)_k\left(\Phi_i\right)_k\right|^2}{\left(\sum_{k=1}^{n}\left(\Phi_j\right)_k\left(\Phi_j\right)_k\right)\left(\sum_{k=1}^{n}\left(\Phi_i\right)_k\left(\Phi_i\right)_k\right)} \qquad 4.8$$

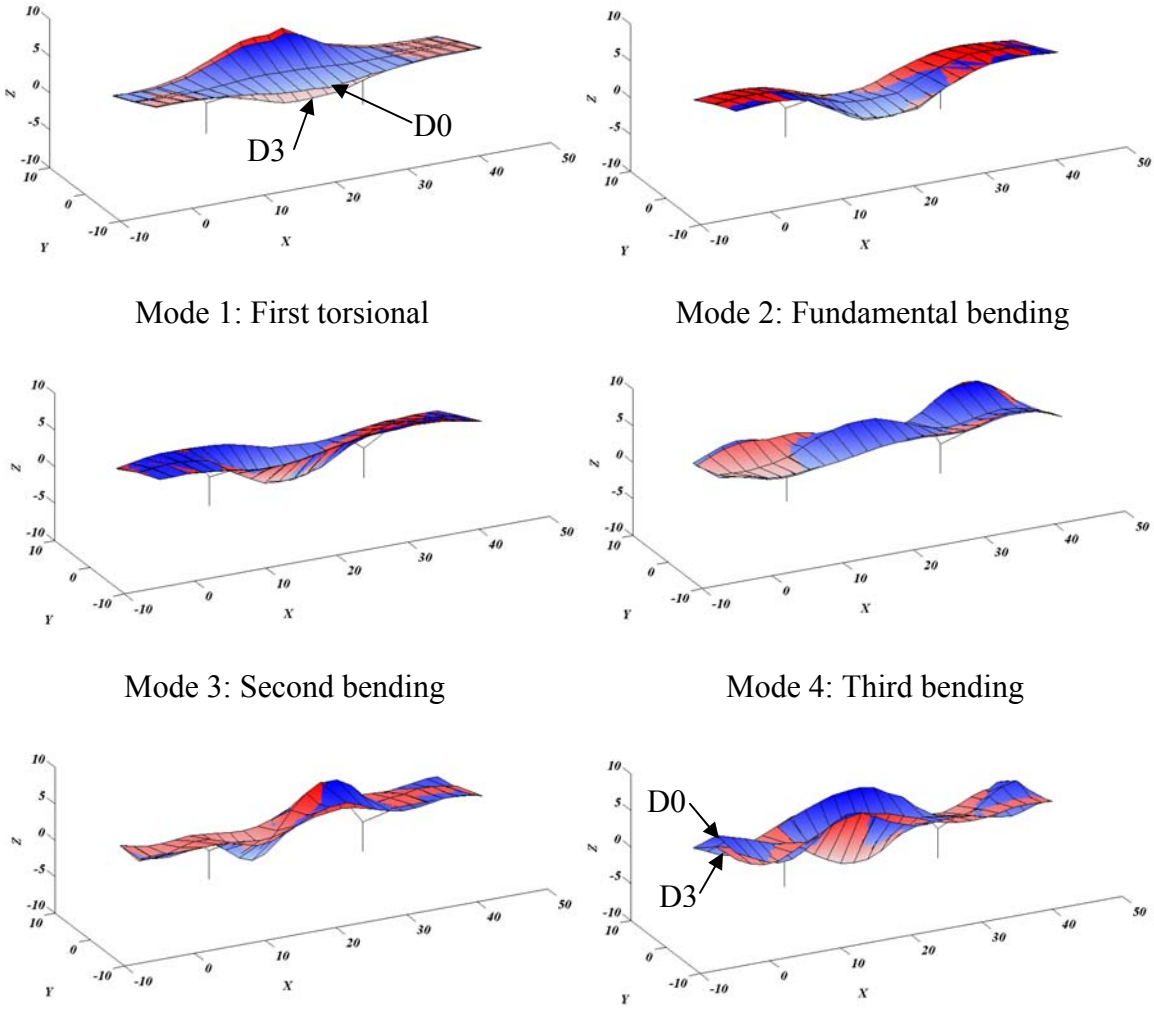

Figure 4.6. Comparison of undamaged (D0) and damaged (D3) mode shapes (m)

MAC values for each of the damage tests compared to the undamaged test are presented in Figure 4.7. One observation is that the MAC values seem to improve as the level of damage increases. The results for the first torsional mode (mode 1) significantly improve as the level of damage is increased. After the first damage scenario, D1, is inflicted, the first torsional mode (mode 1) seems to be highly coupled with the fundamental bending mode (mode 2). The first torsional mode and fundamental bending mode uncouple when the level of damage is increased to D2, and the correlation between the undamaged and damaged first torsional mode significantly improves. This observation suggests that the first torsional mode may be more sensitive to lower levels of damage.

The MAC values in Figure 4.7 indicate that the fundamental bending mode is largely unaffected by damage by showing excellent correlation between the undamaged mode shape and the damaged mode shape for all the damage scenarios. Because the fundamental bending mode's motion is predominantly vertical in nature, its strong correlation for all the damage scenarios may be attributed to its lack of a strong horizontal component of motion. This would suggest that the horizontal components of mode shapes are more sensitive to damage than the vertical components, and that mode shapes with a strong horizontal component may be more effective with vibration-based damage detection techniques.

The results obtained in this study suggest that changes in mode shapes calculated using the MAC are not useful indicators of damage. While there are observable changes, there is no discernible pattern that would suggest the bridge is damaged.

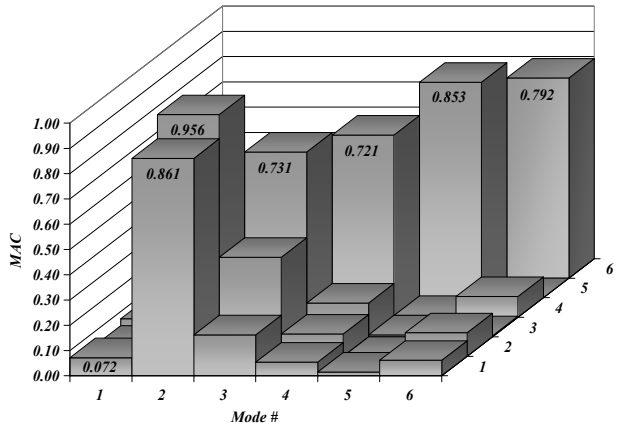

undamaged x D1 damage

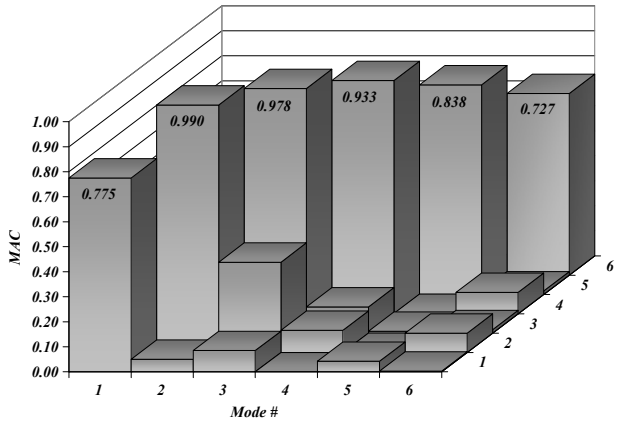

undamaged x D2 damage

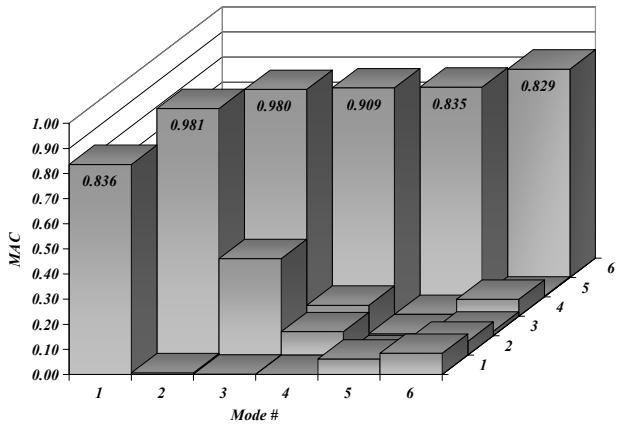

undamaged x D3 damage

Figure 4.7. MAC: undamaged vs. damaged tests

4.10 Application of Damage Detection Methods to Field Test Results

In this study, before the damage detection methods were applied, some preliminary conditioning of the field test results was performed. First, each beam in Figure 4.4 was divided into 100 uniform elements 0.45 m in length, and a cubic polynomial interpolation was used to estimate mode shape amplitudes between sensor locations. The cubic polynomial approximation of the mode shape was used obtain mode shape curvature values when needed. Second, because input forces were not measured as a part of this study, it was not possible to mass normalize the mode shapes as called for by the change in flexibility method and the change in uniform load surface curvature method. Instead, mode shapes were normalized using Eq. 4.9 for all the damage detection methods. This normalization procedure also satisfies the requirement of the damage index method and mode shape curvature method for consistently normalized mode shapes.

$$\{\varphi_n\}^T [I] \{\varphi_n\} = 1 \qquad 4.9$$

Finally, a unique aspect of the current study is the extension of the damage detection methods to three dimensions. Most researchers rely on the vertical response of bridges for extraction of modal parameters and damage detection, and any influence damage may have on the horizontal response of the bridge is lost. As part of this study, all the described damage detection methods are extended to include three dimensions by simply evaluating each method using the individual components of measured mode shapes: vertical (V), transverse (T), and longitudinal (L). In this study, transverse refers

to motion of the bridge deck perpendicular to the length of the bridge, and longitudinal refers to motion of the bridge deck parallel to the length of the bridge.

Table 4.2 summarizes the results obtained by applying each damage detection method with each identified mode. When all 72 measurement locations from the field test are considered in the damage evaluation process, a damage detection method was considered to have located the damage in a global sense if the maximum absolute value of the calculation occurred at the location where damage was induced in the finite element model. If a method was unable to identify damage on a global level (the maximum value occurs at an incorrect location), then the method was evaluated on its ability to identify damage locally on the damaged beam. Considering only the 24 measurement locations above the damaged beam (beam 3 in Figure 4.4), a damage detection method was considered to have located the damage in a local sense if the maximum absolute value of the calculation obtained using the smaller data set occurred at the inflicted damage location. In the present study, global damage identification means that the damage is distinguishable from the entire data set collected, while local damage identification means that the damage is distinguishable when only the portion of the data set collected directly above the damaged beam is considered.

Observing Table 4.2, it can be seen that each method is most effective when combined with the first torsional mode (mode 1). For damage scenario D1, each method was able to globally locate the damage using the longitudinal component of the first torsional mode. This observation suggests that the longitudinal response of the bridge is more sensitive to low levels of damage than the vertical or transverse response.

Table 4.2. Summary of damage detection results

Damage Scenario		Damage Index			Mode Shape Curvature			Change in Flexibility			Change in ULS Curvature		
		V	L	T	V	L	T	V	L	T	V	L	T
Mode 1 First torsional	D1	●	●	--	--	●	--	○	●	○	--	●	--
	D2	●	●	●	●	●	○	●	●	--	●	●	●
	D3	●	●	--	●	●	●	●	●	●	●	●	●
Mode 2 Fundamental bending	D1	--	--	--	○	--	--	○	--	--	○	--	--
	D2	○	--	--	○	--	--	○	--	--	○	--	--
	D3	○	--	--	○	○	--	○	○	--	○	○	--
Mode 3 Second bending	D1	○	--	--	--	○	○	○	--	--	○	--	--
	D2	--	○	--	--	--	--	○	--	○	--	○	--
	D3	--	--	--	--	--	--	○	○	--	--	--	--
Mode 4 Third bending	D1	--	--	--	--	--	--	--	--	○	--	--	--
	D2	--	--	--	--	--	--	--	--	--	--	--	--
	D3	--	--	--	--	--	--	--	--	○	--	--	--
Mode 5 Fourth bending	D1	--	--	○	--	--	--	--	○	○	--	--	--
	D2	--	--	--	--	--	--	--	--	--	--	--	--
	D3	--	--	--	--	--	--	--	--	○	--	--	--
Mode 6 Firth Bending	D1	--	○	○	○	○	○	○	--	--	--	○	--
	D2	--	○	--	--	--	○	○	○	○	--	--	○
	D3	--	●	--	--	●	--	○	--	○	--	●	--

●Damage located globally; ○Damage located locally;
-- Damage not located

There is an interest in the literature on using only the fundamental bending mode in combination with damage detection techniques to locate damage (Zhou et al. 2007). This desire is understood because of the ease involved with the fundamental mode's identification. However, its predominantly vertical behavior may be a weakness of the fundamental bending mode. Observing Table 4.2, it can be seen that the fundamental bending mode (mode 2) was unable to identify the induced damage on a global level when combined with either of the damage detection methods for any of the damage scenarios.

For completeness, various combinations of modes with each damage detection method were also studied. However, little improvement in the results was obtained using either method with the additional modes, particularly if the modes used lacked strong horizontal components.

A typical graphical representation of the results obtained using the change in uniform load surface curvature method and the first torsional mode for damage scenario D3 is presented in Figure 4.8. The first observation from Figure 4.8 is the high sensitivity of the longitudinal response of the bridge to damage. The magnitude of the changes calculated using the longitudinal component of the first torsional mode is greater than those calculated using the vertical or transverse component. Clearly the damage has occurred on beam 3, and the most likely location according to the change in magnitude is the middle of the beam, which corresponds exactly to where the damage was induced.

A comparison of the longitudinal components of the first torsional mode and the fundamental bending mode using the change in uniform load surface curvature method is

presented in Figure 4.9. As noted, the longitudinal component of the first torsional mode is more sensitive to damage than the longitudinal component of the fundamental bending mode. In fact, the longitudinal component of the fundamental bending mode incorrectly indicates that damage has occurred at the center of beam 2 (node 152). Because the fundamental bending mode is predominantly a vertical mode, this observation further verifies that modes exhibiting a strong horizontal component are better suited for use with vibration-based damage detection techniques.

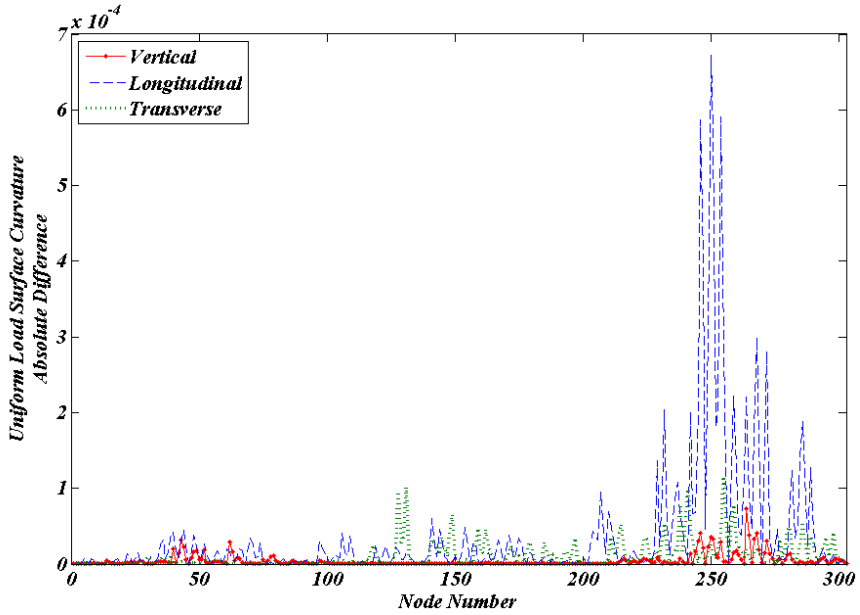

Figure 4.8. Localization results for damage scenario D3 using the first torsional mode (mode 1) and the change in uniform load surface curvature method.
Note: Node numbers in Figure 4.8 correspond to the beam numbers in Figure 4.4 as follows: from east to west, nodes 1-101, beam 1; nodes 102-202, beam 2; nodes 203-303, beam 3. The damage location corresponds to node 253.

It should be noted that the results obtained using the damage detection techniques would have been difficult to interpret had the location of the damage not been known *a priori*. With the exception of the damage index method, there is no criterion provided by any of the methods evaluated to distinguish damage from other results. Overall, the damage index and change in flexibility methods were found to perform best.

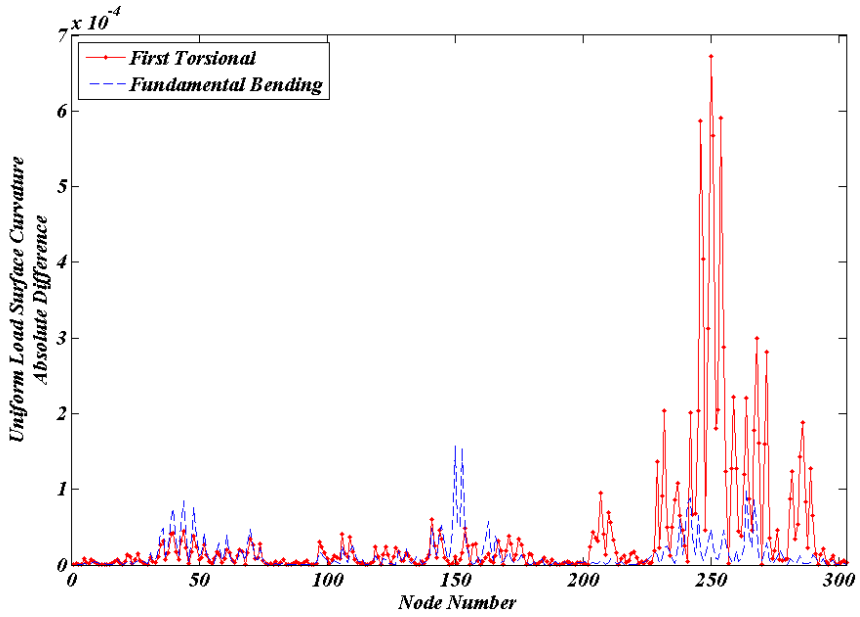

Figure 4.9. Comparison of the longitudinal components of the first torsional (mode 1) and fundamental bending (mode 2) modes for damage scenario D3 using the change in uniform load surface curvature method
Note: Node numbers in Figure 4.9 correspond to the beam numbers in Figure 4.4 as follows: from east to west, nodes 1-101, beam 1; nodes 102-202, beam 2; nodes 203-303, beam 3. The damage location corresponds to node 253.

4.11 Summary and Conclusions

The goal of this study was to compare various vibration-based damage detection techniques based on their ability to locate damage induced on an in-situ, full-scale bridge using triaxial vibration measurements obtained using inexpensive geophones. Unlike previous studies, which rely heavily on the vertical response of bridges for damage detection, the current study has incorporated the three-dimensional response of a bridge into the evaluated damage detection techniques. It is been found that the transverse and longitudinal responses are also capable of identifying damage. The longitudinal response of a bridge appears to be particularly sensitive to damage, even in the early stages of crack propagation.

This study found the first torsional mode of vibration to be better suited for use with the vibration-based damage detection techniques evaluated. When combined with the longitudinal component of the first torsional mode, each damage detection method evaluated was able to successfully locate the damage on a global level. This was true even for the lowest damage scenario. Using only the fundamental bending mode, damage could only be located locally on the damaged beam. The poor performance of the fundamental bending mode is attributed to its lack of a strong horizontal component. These observations indicate that the horizontal response of a bridge is more sensitive to damage than the vertical response, and that modes exhibiting a strong horizontal component should be used with vibration-based damage detection techniques.

Similarly to previous researchers, this study has found natural frequencies and mode shapes to be relatively poor indicators of damage when used alone. The more

complex damage detection methods described were found to be much better indicators of damage. Each method evaluated was able to locate the inflicted damage for each scenario tested. Incorporation of multiple modes was found to have little effect on the results obtained using either method particularly if the modes did not exhibit a strong horizontal component.

One of the significant obstacles in implementing continuous monitoring systems is the cost of the sensors. The results of this study have demonstrated that low-cost geophones can be used to characterize the dynamic response of a bridge, and the obtained results can be successfully implemented with vibration-based damage detection techniques. Furthermore, because geophones do not require a power source, another obstacle in implementing remote monitoring systems has been overcome using geophones. Throughout the described tests, the only power source used was a battery to power the seismograph. In an actual bridge monitoring system, the data logger could easily be powered using a small solar panel.

Finally, data sets obtained from in-situ, full-scale bridge tests both in an undamaged and damaged condition are scarce. The authors are unaware of any other data set that contains triaxial vibration records collected over a relatively dense measurement grid on an in-situ, full-scale bridge in undamaged and damaged conditions. Thus, this study has provided a valuable data set for continued research in the area of vibration-based damage detection related to bridges.

4.12 Acknowledgements

The authors would like to thank Jeff Walker of Bell and Associates Construction, Phil Large of Wilbur Smith and Associates, and Terry Leatherwood, Henry Pate, and Ed Wasserman of the Tennessee Department of Transportation for their help and cooperation.

4.13 Notation

The following symbols were used in this chapter:

β_{ij}	=	damage index relating the change in modal strain energy at location *j* in the *i*th mode
$\Phi_i''(x)$	=	second derivative of the ith identified undamaged mode shape at location *x*
$\Phi_i''^*(x)$	=	second derivative of the ith identified damaged mode shape at location *x*
L	=	length of beam segment being analyzed using the damage index method
E	=	modulus of elasticity of the material
I	=	moment of inertia of the cross-section
$M(x)$	=	bending moment at location *x*
$\upsilon(x)$	=	curvature at location *x*
$\Delta\Phi_i''$	=	absolute difference in damaged and undamaged modal curvature
ω_i	=	ith undamaged natural frequency
ω_i^*	=	ith damaged natural frequency
φ_i	=	ith unit mass normalized undamaged mode shape
φ_i^*	=	ith unit mass normalized damaged mode shape
$[F]$	=	undamaged flexibility matrix
$[F]^*$	=	damaged flexibility matrix
$[\Delta F]$	=	change in flexibility matrix
$\Delta U''$	=	absolute curvature change of the uniform load surface
U''	=	curvature of the undamaged uniform load surface
U''^*	=	curvature of the damaged uniform load surface
Δf	=	frequency resolution in the frequency domain
t	=	time variable
(Φ)	=	mode shape vector
$[I]$	=	identity matrix

4.14 References

Dobrin, M.B. and Savit C.H. (1988). *Introduction to Geophysical Prospecting*, 4th Ed., McGraw-Hill, New York.

Doebling, S.W., Farrar, C.R., Prime, M.B., and Shevitz, D.W. (1996). *Damage Identification and Health Monitoring of Structural and Mechanical Systems from Changes in Their Vibration Characteristics: A Literature Review*. Rep. No. LA 13070-MS, Los Alamos National Laboratory, Los Alamos, N.M.

Doebling, S.W., Farrar, C.R., and Prime, M.B. (1998). "A summary review of vibration-based damage identification methods." *The Shock and Vibration Digest.*, 30(2), 91–105.

Ewins, D.J. (1985). *Modal Testing: Theory and Practice*. John Wiley, New York.

Farrar, C.R., Baker, W.E., Bell, T.M., Cone, K.M., Darling, T.W., Duffey, T.A., Eklund, A., and Migliori, A. (1994). *Dynamic Characterization and Damage Detection in the I-40 Bridge Over the Rio Grande.* Rep. No. LA-12767-MS, Los Alamos National Laboratory, Los Alamos, N.M.

Farrar, C.R. and Jauregui, D.A. (1996). *Damage Detection Algorithms Applied to Experimental and Numerical Modal Data from the I-40 Bridge*. Rep. No. LA-13074-MS, Los Alamos National Laboratory, Los Alamos, N.M.

Farrar, C.R., Doebling, S.W., Cornwell, P.J., and Straser, E.G. (1997). "Variability of modal parameters measured on the Alamosa Canyon bridge." *Proceedings of the 15th International Modal Analysis Conference*, Orlando, FL, 257–263.

Farrar, C.R., Doebling, S.W., and Prime, M.B. Cornwell, P.J., Kam, M., Straser, E.G., Hoerst, B.C., Shevitz, D.W., and Jauregui, D.A. (1998). *A Comprehensive Monitoring System for Damage Identification and Location in Large Structural and Mechanical Systems*. Rep. No. LA-UR-98-233, Los Alamos National Laboratory, Los Alamos, N.M.

Federal Highway Administration (FHWA) (2001). *Reliability of Visual Inspection*. Rep. No. FHWA-RD-01–020, Washington, D.C.

Halling, M.W., Muhammad, I., and Womack, K.C. (2001). "Dynamic field testing for condition assessment of bridge bents." *Journal of Structural Engineering*, 127(2), 161-167.

Krämer, C., De Smet, C.A.M., and De Roeck, G. (1999). "Z24 bridge damage detection tests." *Proceedings of the 17th International Modal Analysis Conference,* Kissimmee, FL, USA.

Liu, C.Y. and DeWolf, J.T. (2007). "Effect of temperature on modal variability of a curved concrete bridge under ambient loads." *Journal of Structural Engineering*, 133(12), 1742-1751.

Maeck, J., Peeters, B., and De Roeck, G. (2001). "Damage identification on the Z24 bridge using vibration monitoring." *Smart Materials and Structures*, 10(3), 512-517.

The Mathworks, Inc. (2007). MATLAB®. Version R2007a.

Morassi, A. and Tonon, S. (2008). "Dynamic testing for structural identification of a bridge." *Journal of Bridge Engineering*, 13(6), 573-585.

Pandey, A.K., Biswas, M., and Samman, M.M. (1991). “Damage detection from changes in curvature mode shapes.” *Journal of Sound and Vibration*, 145(2), 321-332.

Pandey, A.K. and Biswas, M. (1994). “Damage detection in structures using changes in flexibility.” *Journal of Sound and Vibration*, 169(1), 3-17.

Pothisiri, T. and Hjelmstad, K.D. (2003). "Structural damage detection and assessment from modal response." *Journal of Engineering Mechanics*, 129(2), 135-145.

Ren, W.X., Zatar, W., and Harik, I.E. (2004). "Ambient vibration-based seismic evaluation of a continuous girder bridge." *Engineering Structures*, 26(5), 631-640.

Richardson, M.H. and Formenti, D.L. (1985). “Parameter estimation from frequency response measurements using rational fraction polynomials.” *Structural Measurement Systems Technical Note 85-3*.

Robinson, E.S. and Coruh, C. (1988). *Basic Exploration Geophysics*, John Wiley & Sons, New York.

Siddique, A.B., Sparling, B.F., and Wegner, L.D. (2007). "Assessment of vibration-based damage detection for an integral abutment bridge." *Canadian Journal of Civil Engineering*, 34(3), 438-452.

Sohn, H., Farrar, C.R., Hemez, F.M., Shunk, D.D., Stinemates, D.W., and Nadler, B.R. (2004). *A Review of Structural Health Monitoring Literature: 1996–2001*. Rep. No. LA-13976-MS, Los Alamos National Laboratory, Los Alamos, N.M.

Stubbs, N., Kim, Y.I., and Farrar, C.R. (1995). “Field verification of a nondestructive damage localization and severity estimation algorithm.” *Proceedings of the 13th International Modal Analysis Conference*, Bethel, CT, 210-218.

Xia, P.Q. and Brownjohn, J.M.W. (2004). "Bridge structural condition assessment using systematically validated finite-element model." *Journal of Bridge Engineering*, 9(5), 418-423.

Zhang, Z. and Aktan, A.E. (1995). "The damage indices for the constructed facilities." *Proceedings of the 13th International Modal Analysis Conference*, Bethel, CT, 1520-1529.

Zhao, J. and DeWolf, J.T. (2002). "Dynamic monitoring of steel girder highway bridge." *Journal of Bridge Engineering*, 7(6), 350-356.

Zhou, Z., Wegner, L.D., and Sparling, B.F. (2007). "Vibration-based detection of small-scale damage on a bridge deck." *Journal of Structural Engineering*, 133(9), 1257-1267.

Chapter 5. Damage Detection on a Full-Scale Five-Girder Bridge Using an Array of Triaxial Geophones

This chapter is revised based on a paper submitted to the ASCE *Journal of Bridge Engineering* by William Ragland, Dayakar Penumadu, and Richard Williams:

Ragland, W.S., Penumadu, D., and Williams, R.T. (In review). "Damage detection on a full-scale five-girder bridge using an array of triaxial geophones." *Journal of Bridge Engineering*.

My primary contributions to the paper included: (i) development of the problem into a work, (ii) gathering and reviewing literature, (iii) arrangement, design and conduction of the field tests, (iv) processing, analyzing, and interpretation of the experimental data, (v) development of computer codes for implementation of the damage detection techniques, and (vi) most of the writing.

5.1 Abstract

Vibration-based damage detection is a nondestructive evaluation approach based on structural damage being reflected in a structure's dynamic response. While vibration-based damage detection techniques have been shown to accurately locate damage in various mechanical systems and simple structures, varying levels of success have been reported when applying vibration-based damage detection techniques to bridges. Furthermore, there are only a handful of studies that evaluate vibration-based damage detection techniques using a data set collected entirely on a full-scale bridge. This paper describes results from an in-situ, full-scale, five-girder bridge test that was subjected to

controlled levels of known damage. Various vibration-based damaged detection techniques are evaluated based on their ability to locate the induced damage both locally and globally. Using triaxial vibration records obtained over a relatively dense measurement grid using inexpensive geophones, established vibration-based damage detection techniques were extended to include the three dimensional response of the bridge, a unique aspect of the current study. Results show that most of the damage detection techniques evaluated are capable of successfully locating the induced damage on a global level. Contrary to expectations, it was observed from the present test that the horizontal response of the bridge was more sensitive to induced damage than the vertical response.

5.2 Introduction

As the nation's infrastructure continues to age, methods of reliably assessing its overall health have become increasingly more important. While the condition of all types of infrastructure is important, the primary focus of this work is the nation's bridge inventory. Currently, bridges in the United States are inspected and rated during biennial inspections which rely heavily on visual techniques. However, in a report released by the Federal Highway Administration (FHWA), visual inspections were found to be relatively unreliable (FHWA 2001). For this reason, researchers have been working on the development of more objective methods for nondestructively inspecting and rating bridge condition.

Vibration testing has been used as a means of assessing structural health for some time. Results obtained through vibration testing serve as the basis for several areas of research such as structural health monitoring (Krämer et al. 1999, Zhao and DeWolf 2002), finite element model updating and calibration (Xia and Brownjohn 2004, Morassi and Tonon 2008), condition assessment of structures (Xia et al. 2008, Ren et al. 2004), and structural damage detection (Farrar and Jauregui 1996, Lauzon and DeWolf 2006, Sanayei et al. 2006, Zhou et al. 2007). The focus of this paper is vibration-based damage detection on in-situ, full-scale bridges.

Vibration-based damage detection is a nondestructive structural health monitoring approach that focuses on changes in the dynamic characteristics of a structure, such as natural frequency and mode shape, as indicators of damage. Several different global evaluation techniques and associated quantitative damage indices have been published in recent years. Detailed reviews of these techniques as applied to bridges and other structures can be found in Doebling et al. (1996, 1998) and Sohn et al. (2004). In summary, the methods discussed monitor shifts in natural frequency, absolute changes in mode shapes, changes in mode shape curvature or strain energy, and variations in stiffness and flexibility matrices.

Recently, a large construction project often referred to as SmartFix 40 realigned I-40 through downtown Knoxville, TN, while increasing the roadway's capacity to meet current demand. In order to decrease the amount of time required for construction, a small section of I-40 was closed for a period of 14 months. Due to the closing, the rare opportunity to perform full-scale bridge testing in an in-situ state and subjected to

controlled amounts of damage at a chosen location became a reality. The experimental testing methods, analysis procedures, and results obtained on an in-situ, full-scale, five-girder bridge are presented are presented in the current study, and the ability of various vibration-based damage detection methods to locate experimentally induced damage is evaluated.

The testing of the bridge discussed in this paper is of interest for several reasons. First of all, the bridge was tested in an in-situ, full-scale, operating condition before any structural demolition or removal of the surrounding soil had taken place. Furthermore, unlike previous studies that relied heavily on the vertical response of the bridge, triaxial vibration records were obtained in this study which has allowed the use of vibration-based damage detection techniques to be extended to three dimensions. The bridge tested also has direct practical relevance because it is of a similar design to many existing bridges and new bridges being constructed in Tennessee. Thus, results obtained in this study may prove applicable in the implementation of monitoring systems for a large number of bridges. The method used to induce damage is also believed to simulate a realistic crack that could threaten the bridge's overall structural integrity. Additionally, the damage was also located in a region closer to a support to determine if the vibration-based damage detection techniques evaluated could successfully locate damage that does not occur near mid-span of the bridge. Considering these points, the purpose of this paper is to use triaxial vibration measurements obtained using highly sensitive, inexpensive geophones on an incrementally damaged, in-situ, full-scale bridge to investigate a new three-dimensional approach to vibration-based damage detection.

5.3 Geophones as Sensors

One of the challenges involved when implementing vibration-based damage detection techniques with full scale bridges is obtaining inexpensive, detailed modal parameters from vibration measurements. To overcome this obstacle, inexpensive geophones (approximately $50 each) are used in this study to obtain triaxial vibration records over a relatively dense measurement grid.

A geophone is a passive directional sensor that measures the speed of motion in the direction of its sensitive axis. In basic terms, a geophone is a coil suspended by springs around a permanent magnet, all of which is contained in a protective casing. When the coil moves relative to the magnet, a voltage is induced in the coil that depends on the relative velocity between the coil and magnet.

Traditionally, geophysicists, rather than bridge engineers, use geophones to measure elastic waves propagating through several kilometers of geologic materials. Detailed technical descriptions of the various types of geophones can be found in geophysical textbooks (Dobrin and Savit 1988, Robinson and Coruh 1988).

Accelerometers are commonly used for dynamic testing of civil engineering structures. However, geophones offer important advantages over accelerometers when considered for implementation in bridge monitoring systems. First of all, an accelerometer generally requires charge amplification electronics to produce a signal suitable for recording, and thus a power source is needed for the amplifier and associated hardware. In comparison, geophones are passive devices that produce a voltage that can be recorded without additional amplification or conditioning. Because they do not

require an external power supply or an amplifier, geophones are ideal candidates for implementation in remote bridge monitoring systems. Furthermore, geophones may more easily be incorporated into a wireless sensor system for bridge monitoring in the future.

5.4 Full-Scale Bridge Used for Experiments

Constructed in 1967, the I-40 westbound bridge over 4th Avenue, Figure 5.1, consisted of three spans comprised of a concrete deck supported by five rolled steel girders. Due to the alignment of 4th Avenue, the bridge was constructed on a forty-five degree skew. The overall horizontal alignment of the bridge was straight, while there was a slight decrease in elevation from the east abutment to the west abutment. When in operation, the bridge carried two lanes of traffic. An elevation of the bridge is shown in Figure 5.2, and a typical cross section is shown in Figure 5.3.

Figure 5.1. I-40 westbound over 4th Avenue
(47I00400066)

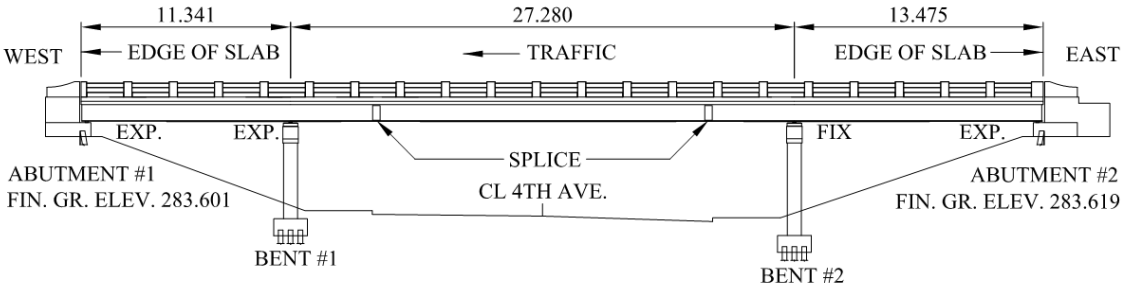

Figure 5.2. I-40 westbound over 4th Avenue: elevation (m)

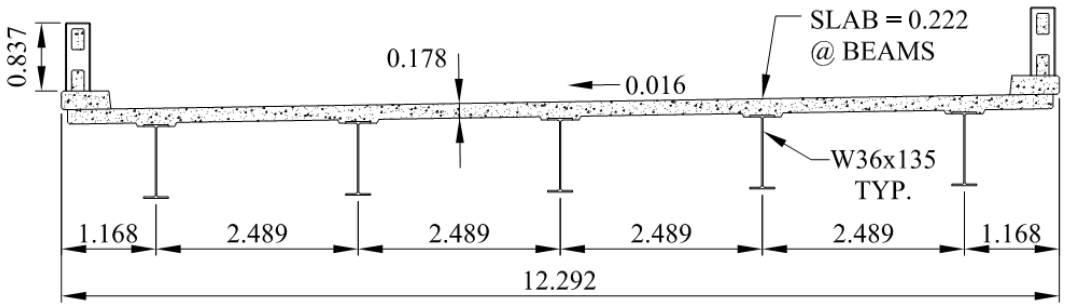

Figure 5.3. I-40 westbound over 4th Avenue: typical cross-section (m)

The I-40 westbound bridge over 4th Avenue consisted of three spans. From east to west, the bridge spanned approximately 13, 27, and 11m as shown in Figure 5.2. Three rolled W36x135 were connected with bolted splice plates to form one continuous beam over the entire bridge length. Cover plates were added to the top and bottom of each beam in the end spans. For the center span, a cover plate was added to the bottom of each beam, and headed studs were used on top of each beam to promote composite action with the concrete deck. Connections that allowed for longitudinal expansion, marked "Exp" in Figure 5.2, and connections that prevented longitudinal expansion,

marked “Fixed” in Figure 5.2, were installed on the bottom of the beams at each location where the beams were supported by either a concrete bent or abutment. Intermediate diaphragms, C12x20.7, are located at 7.6 m on center perpendicular to each beam, and end diaphragms, C15x33.9, are provided at each end of the bridge parallel to the bridge skew.

5.5 Test Setup

Mark Products LRS-1000 10Hz vertical geophones and Mark Products L-28LBH 4.5Hz horizontal geophones were used for the vibration measurements. One vertical and one horizontal geophone were rigidly attached to a 1.6 cm thick, 11.5 cm diameter steel plate which rested on the bridge deck. The bridge was excited by dropping a 22.7 kg sandbag at a total of 9 different locations corresponding to the quarter points of the center span along beams 1, 3, and 5 in Figure 5.4.

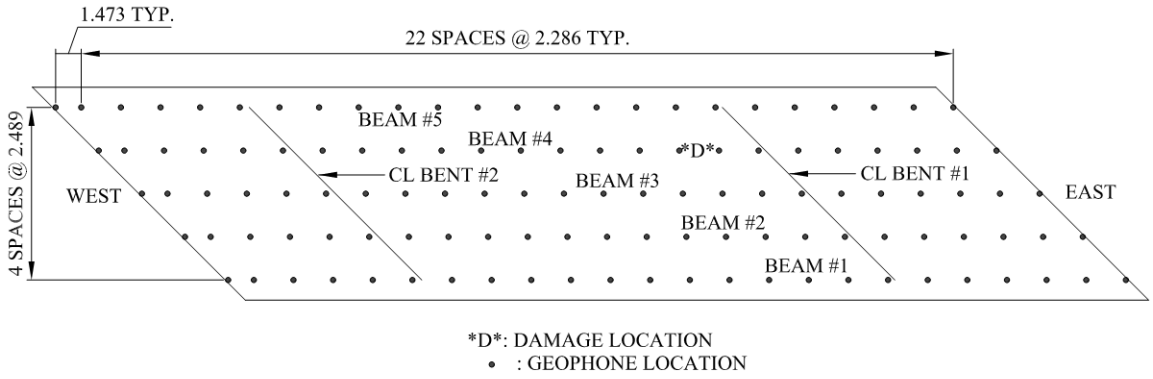

Figure 5.4. I-40 westbound over 4th Avenue: geophone layout

During the testing, data was recorded in the three global coordinate directions at a total of 120 measurement locations using a Geometrics 48-channel StrataView® seismograph. Because the seismograph was only able to record 48 geophone signals at one time (24 vertical and 24 horizontal), the 120 measurements locations were divided into five groups. For each group, the steel plates were spaced at 2.3 m center-to-center (except for the last pair of plates, which was 1.5 m) on the bridge deck along the beam line below as shown in Figure 5.4. In order to obtain triaxial vibration records, the sandbag was dropped and then dropped again after rotating the horizontal geophones by 90°. Once the data had been recorded in three directions, the line of geophones was shifted to the next position. This process was repeated until all 120 measurement locations were covered. During each test, data was sampled at a rate of 1000 Hz for a total of three seconds. Using these sampling parameters, a frequency resolution of 0.33 Hz was obtained over a frequency range of 0-500 Hz. All results presented in this paper were obtained from the data sets collected when the sandbag was dropped at the midpoint of beams 3 and 5 in Figure 5.4.

5.6 Damage Scenarios

While the bridge exhibited some defects, the first test performed is considered to represent an undamaged state. The goal of this study is to identify the additional damage induced as part of the experiment based on comparisons with a baseline measurement. Additional studies could be performed to assess the overall condition of the bridge using

only the baseline measurement by comparing the field test results with bridge inspection reports and/or a finite element model.

For this research, damage was induced by incrementally cutting a main girder upward from the bottom flange as shown in Figure 5.5. This method of inducing damage was meant to simulate a crack that may occur due to fatigue or excessive vehicle weight. Because vibration-based damage detection has been shown to be less reliable at locating damage occurring near a support using a laboratory model (Zhou et al. 2007), it was decided to locate the cut near a support in this study to assess the ability of each evaluated damage detection technique to identify damage occurring in a near-support region on a full-scale bridge. It was also decided to cut and interior beam, thus beam #4 was cut at the location indicated in Figure 5.4.

Figure 5.5. Damage scenarios
From Left to Right, undamaged (D0), bottom flange cut (D1),
bottom flange plus ¼ of the web cut (D2), bottom flange plus ½ the web cut (D3)

5.7 Modal Analysis

For this study, the rational polynomial method (Richardson et al. 1985) as implemented in DIAMOND (Farrar et al. 1998) was used for extracting natural frequencies and mode shapes from measured field data. DIAMOND (Damage Identification and Modal Analysis of Data) is a MATLAB® (Mathworks 2007) based software package developed at Los Alamos National Laboratories for modal analysis, damage identification, and finite element model refinement.

Briefly, the rational polynomial method uses orthogonal polynomials to estimate the coefficients of a polynomial approximation to the frequency response function (FRF). The FRF of a system is the ratio of the Fourier transform of the measured input and response signals. Thus, the rational polynomial method is intended for use with measured inputs. However, recording the input excitation for an in-service bridge under ambient loading, such as wind or traffic, would be nearly impossible. For this reason, it was decided not to record input excitations as a part of this research. Because the input was not recorded, an assumption was made in order to implement the rational polynomial method. If an input force is known to have a flat spectrum, as would be the case for wind or traffic, then any peaks in the response spectrum are caused by structural resonances. Therefore, it was assumed that the impulsive loading source used during tests possessed a flat spectrum, at least over the frequency range of interest. This assumption allows the response spectrum matrix created by multiplying the spectrum of each measured response by the conjugate spectrum of a reference response to be analyzed instead of the FRF matrix.

This method of modal analysis is meant to simulate what would have to be used in an actual bridge monitoring system where inputs due to ambient sources, such as wind and traffic, are not easily measured. The results of this study indicate that the natural frequencies and operating shapes obtained using this procedure can be successfully combined with vibration-based damage techniques to locate damage on a full-scale bridge.

5.8 Damage Detection Methods

Various damage detection techniques have been presented in the literature, but most are simply a variation of a much smaller number. For this study, the methods compared by both Farrar and Jauregui (1996) and Zhou et al. (2007) are evaluated. By comparing the same methods as previous researchers a better understanding of these methods when applied to different bridge structures can be obtained. The various methods are briefly described in the following paragraphs.

Given mode shapes obtained before and after damage, the damage index method (Stubbs et al. 1995) attempts to identify damage in a structure using changes in modal strain energy between the undamaged and damaged structure. The damage index, β, relates the change in modal strain energy at location *j* in the *i*th mode using mode shape curvatures as shown in Eq. 5.1.

$$\beta_{ij} = \frac{\left(\int_a^b \left[\Phi_i''^*(x)\right]^2 dx + \int_a^L \left[\Phi_i''^*(x)\right]^2 dx \right) \int_a^L \left[\Phi_i''(x)\right]^2 dx}{\left(\int_a^b \left[\Phi_i''(x)\right]^2 dx + \int_a^L \left[\Phi_i''(x)\right]^2 dx \right) \int_a^L \left[\Phi_i''^*(x)\right]^2 dx} \qquad 5.1$$

In Eq. 5.1, $\Phi_i''(x)$ and $\Phi_i''^*(x)$ are the second derivatives of the ith mode shape of the undamaged and damaged structure, respectively. L is the length of the beam, and a and b are the end points of the segment of the beam being analyzed. Multiple modes can be used, in which case the damage index is calculated by summing damage indices from each mode. Upon calculating the damage index at each location on the beam, a normal distribution is fit to the indices, and values falling two or more standard deviations from the mean are considered likely damage locations.

The mode shape curvature method (Pandey et al. 1991) assumes that damage to a structure only affects its stiffness and mass. Mode shapes are determined for the structure before and after damage, and mode shape curvatures are estimated using some type of numerical differentiation. In order to develop this method, consider an example of a beam with uniform bending stiffness, EI, subjected to a bending moment, $M(x)$. The curvature, $\upsilon(x)$, of the beam at location x is then given by Eq. 5.2.

$$v(x) = \frac{M(x)}{EI} \tag{5.2}$$

$$\Delta\Phi'' = \left|\Phi_i''^*\right| - \left|\Phi_i''\right| \tag{5.3}$$

Observing Eq. 5.2, it is clear that curvature is inversely proportional to flexural stiffness and that a reduction in stiffness will result in an increase in curvature. Therefore, differences in undamaged and damaged mode shape curvatures, Eq. 5.3, should be greatest near damaged locations. When multiple modes are used, the absolute value of the difference in curvatures for each mode is summed to obtain a damage parameter for each location.

The change in flexibility method (Pandey and Biswas 1994) first approximates the flexibility matrix of the undamaged structure, Eq. 5.4, and the damaged structure, Eq. 5.5, using a given number, n, of modal frequencies, ω_i, and unit-mass-normalized mode shapes, φ_i.

$$[F] \approx \sum_{i=1}^{n} \frac{1}{\omega_i^{\,2}} \{\varphi_i\}\{\varphi_i\}^T \tag{5.4}$$

$$[F]^* \approx \sum_{i=1}^{n} \frac{1}{\omega_i^{*2}} \{\varphi_i\}^* \{\varphi_i\}^{*T} \tag{5.5}$$

$$[\Delta F] = [F] - [F]^* \tag{5.6}$$

The two flexibility matrices are then subtracted which results in the change in flexibility matrix, Eq. 5.6. The absolute maximum value of each column of the change in flexibility matrix is then determined, and the column corresponding to the largest change in flexibility is indicative of the damaged degree of freedom.

The uniform load surface, U_i, is obtained by summing all the columns of the flexibility matrix. The result is the deformed shape of the structure caused by applying a unit load to each degree of freedom on the structure simultaneously. The change in uniform load surface curvature method (Zhang and Aktan 1995) identifies damage as the location where the absolute difference between the undamaged and damaged uniform load surface curvatures is greatest, Eq. 5.7.

$$\Delta U_i'' = \left| U_i''^* - U_i'' \right| \tag{5.7}$$

5.9 Damage Effects on Conventional Modal Properties

A summary of the identified natural frequencies for undamaged and damaged bridge tests is presented in Table 5.1. It was expected that the natural frequencies would decrease with each progressive increase in damage (Figure 5.5). After the final damage scenario was induced, the largest decrease in natural frequency occurred in the third bending mode (mode 4). The natural frequencies of the fundamental bending mode (mode 1), first torsional mode (mode 2), and the second bending mode (mode 3) change very little as a result of the induced damage. Overall, the observed changes in natural frequency are not considered to be significant because researchers have shown that environmental conditions can cause changes in natural frequencies of similar order to those caused by the induced damage in this study (Farrar et al. 1997, Zhao and DeWolf 2002). Therefore, similar observations noted by previous researchers (Liu and DeWolf 2007, Siddique et al. 2007) are confirmed by this study, and changes in natural frequencies alone are deemed to be unreliable indicators of damage.

Because resolution in the frequency domain is directly proportional to the length of measured time series ($\Delta f=1/t$, where t is the length of the measured time series in seconds), it is expected that these results would slightly improve had longer vibration records been recorded. However, similar changes in natural frequencies were observed when comparing the results obtained from different sandbag drop locations. Thus, the observed changes in natural frequencies are considered to be reliable due to their repeatability.

Due to the proximity of the fundamental bending mode (mode 1) and the first torsional mode (mode 2) natural frequencies, the shorter vibration records obtained during the field tests necessitated the use of different sandbag drops to distinguish these two modes from one another. Modes 1, 3, and 4 were extracted from vibration records obtained when the sandbag was dropped at the midpoint of beam 3 in Figure 5.4. Mode 2 was extracted from the vibration records obtained when the sandbag was dropped at the midpoint of beam 5 in Figure 5.4. Therefore, it is recommended that longer vibration records than those obtained in this study are acquired to allow for the distinction of closely spaced modes. However, the results of this indicate that accurate modal parameters for full-scale bridges can be extracted from relatively short vibration records. In terms of remote data transmission, this may prove to be a useful observation.

Table 5.1. Comparison of natural frequencies (Hz)

Damage Test	Mode 1	Mode 2	Mode 3	Mode 4
D0, Undamaged	4.34	4.41	6.39	15.00
D1, Flange Cut	4.35 (0.28%)	4.44 (0.66%)	6.35 (-0.59%)	14.66 (-2.28%)
D2, Flange + 1/4 Web Cut	4.29 (-1.15%)	4.43 (0.40%)	6.38 (-0.19%)	14.66 (-2.31%)
D3, Flange + 1/2 Web Cut	4.26 (-1.87%)	4.40 (-0.18%)	6.40 (0.08%)	14.63 (-2.51%)

Note: Numbers in () are change from D0.

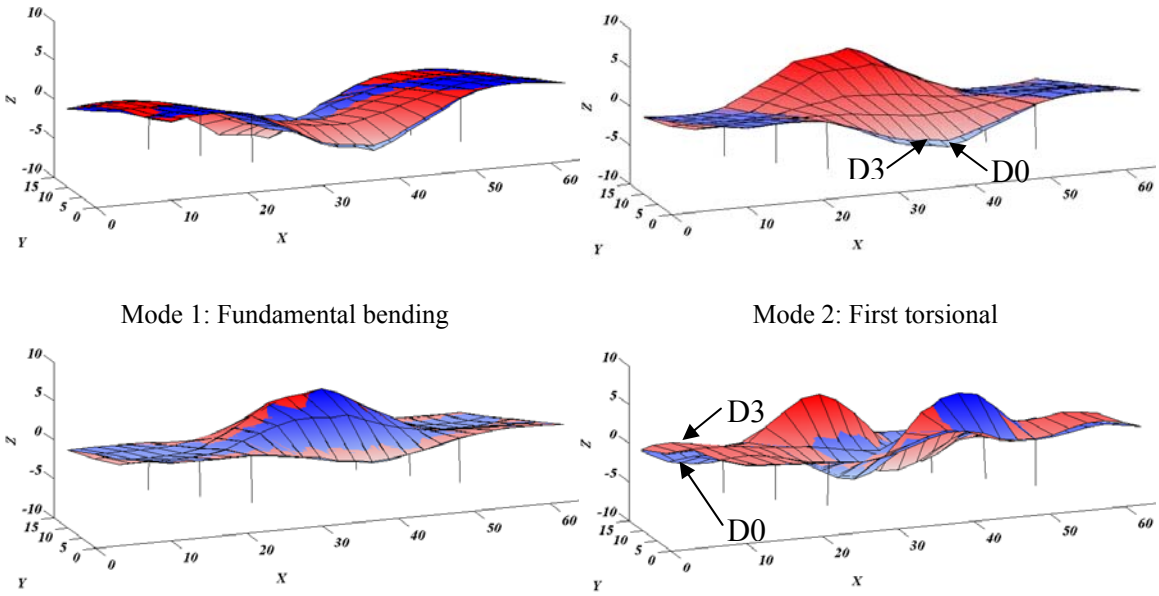

Figure 5.6. Comparison of undamaged (D0) and damaged (D3) mode shapes

The mode shapes identified for the undamaged test and D3 damaged test are presented in Figure 5.6. Observing Figure 5.6, there is very little difference in the overall shape of the undamaged and damaged mode shapes. While subtle observable differences exist in most of the mode shapes, the largest differences occur in the first torsional mode, and the third bending mode. Although not easily seen in Figure 5.6, the first torsional mode not only exhibits a change in the vertical displacement, but also a change in horizontal displacement. The fundamental bending mode appears to be largely unaffected by the damage with little to no observable difference in the identified undamaged and damaged mode shapes.

In order to better quantify the correlation between mode shapes measured in different tests, the modal assurance criterion (MAC) (Ewins 1985) was used. The MAC,

Eq. 5.8, takes advantage of the orthogonal property of mode shapes to compare different modes. If the modes are identical, a value of one will be obtained. If the modes are dissimilar, a value of zero will be obtained. Ewins (1985) notes that in practice, modes are considered correlated if a value greater than 0.9 is calculated and uncorrelated if a value less than 0.05 is calculated. The MAC that compares mode *i* and *j* has the form given in Eq. 5.8 where $(\Phi)_k$ is an element of the mode shape vector and *n* represents the number of points at which the two mode shapes are compared.

$$MAC(i,j) = \frac{\left|\sum_{k=1}^{n}(\Phi_j)_k(\Phi_i)_k\right|^2}{\left(\sum_{k=1}^{n}(\Phi_j)_k(\Phi_j)_k\right)\left(\sum_{k=1}^{n}(\Phi_i)_k(\Phi_i)_k\right)} \qquad 5.8$$

MAC values for each of the damage tests compared to the undamaged test are presented in Figure 5.7. Observing Figure 5.7, the fundamental bending mode (mode 1) and the second bending mode (mode 3) are largely unaffected by damage, showing excellent correlation between the undamaged mode shape and the damaged mode shape for all the damage scenarios. The third bending mode (mode 4) exhibits a change after the first damage scenario but slightly improves with each additional increase in the amount of damage. The first torsional mode (mode 2) is the only mode that continually worsens as the damage level is increased. This observation suggests that the first torsional mode shape is more sensitive to damage than the remaining identified mode shapes. Overall, changes in mode shapes calculated using the MAC are not considered to be reliable indicators of damage when used alone.

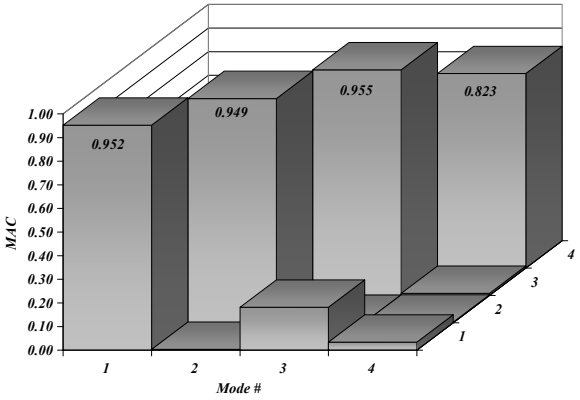

Undamaged x D1 damage

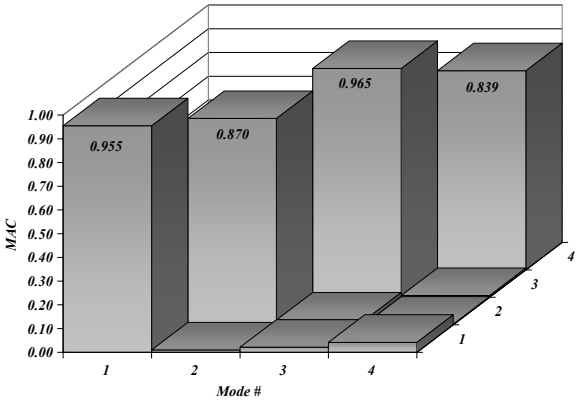

Undamaged x D2 damage

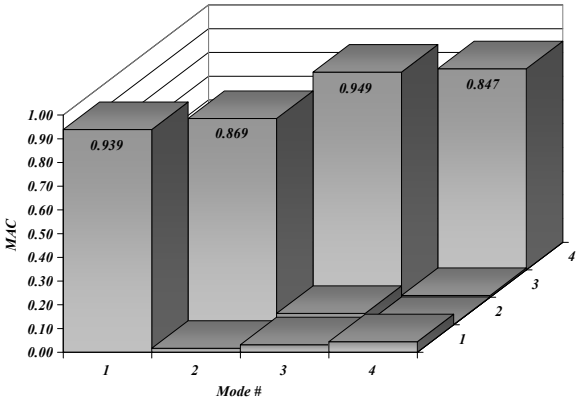

Undamaged x D3 damage

Figure 5.7. MAC: Undamaged vs. damaged tests

5.10 Application of Damage Detection Methods to Field Test Results

In this study, before the damage detection methods were applied, some preliminary conditioning of the field test results was performed. First, each beam in Figure 5.4 was divided into 100 uniform elements 0.52 m in length, and a cubic polynomial interpolation was used to estimate mode shape amplitudes between sensor locations. The cubic polynomial approximation of the mode shape was used obtain mode shape curvature values when needed. Second, because input forces were not measured as a part of this study, it was not possible to mass normalize the mode shapes as called for by the change in flexibility method and the change in uniform load surface curvature method. Instead, mode shapes were normalized using Eq. 5.9 for all the damage detection methods. This normalization procedure also satisfies the requirement of the damage index method and mode shape curvature method for consistently normalized mode shapes.

$$\{\varphi_n\}^T [I] \{\varphi_n\} = 1 \qquad 5.9$$

Finally, the damage detection methods are evaluated in three dimensions. Most researchers rely on the vertical response of bridges for extraction of modal parameters and damage detection, and any influence damage may have on the horizontal response of the bridge is lost. As part of this study, all the described damage detection methods are extended to include three dimensions by simply evaluating each method using the individual components of measured mode shapes: vertical (V), transverse (T), and longitudinal (L). In this study, transverse refers to motion of the bridge deck

perpendicular to the length of the bridge, and longitudinal refers to motion of the bridge deck parallel to the length of the bridge.

Table 5.2 summarizes the results obtained by applying each damage detection method with each identified mode. When all 120 measurement locations from the field test are considered in the damage evaluation process, a damage detection method was considered to have located the damage in a global sense if the maximum absolute value of the calculation occurred at the location where damage was induced in the finite element model. If a method was unable to identify damage on a global level (the maximum value occurs at an incorrect location), then the method was evaluated on its ability to identify damage locally on the damaged beam. Considering only the 24 measurement locations above the damaged beam (beam 4 in Figure 5.4), a damage detection method was considered to have located the damage in a local sense if the maximum absolute value of the calculation obtained using the smaller data set occurred at the inflicted damage location. In the present study, global damage identification means that the damage is distinguishable from the entire data set collected, while local damage identification means that the damage is distinguishable when only the portion of the data set collected directly above the damaged beam is considered.

Observing Table 5.2, none of the methods are particularly effective when combined with any of the identified modes. Note that none of the methods was successfully able to locate the induced damage on any level using the vertical component of any of the identified modes for any of the damage scenarios. However, using the horizontal components of the identified modes, most of the methods were able to

successfully locate the induced damage on a global scale, and all the methods were able to successfully locate the damage locally. This observation suggests that the horizontal response of the bridge is more sensitive to damage than the vertical response when the damage occurs as it was induced this study.

It can be seen in Table 5.2 that the second bending mode (mode 3) is the most consistent of all the modes at identifying the induced damage. This observation suggests that the fundamental bending mode (mode 1), which is commonly focused on, is perhaps not the best mode to use with vibration-based damage detection techniques.

Table 5.2. Summary of damage detection results

Mode		Mode 1 Fundamental bending			Mode 2 First torsional			Mode 3 Second bending			Mode 4 Third bending		
Damage Scenario		D1	D2	D3	D1	D2	D3	D1	D2	D3	D1	D2	D3
Damage Index	V	--	--	--	--	--	--	--	--	--	--	--	--
	L	○	●	--	○	●	--	○	○	○	--	--	○
	T	○	○	●	○	○	○	○	○	●	○	○	○
Mode Shape Curvature	V	--	--	--	--	--	--	--	--	--	--	--	--
	L	--	--	--	--	○	--	--	--	○	○	○	--
	T	○	--	○	○	--	--	○	●	○	○	○	○
Change in Flexibility	V	--	--	--	--	--	--	--	--	--	--	--	--
	L	--	--	--	--	○	--	○	○	○	○	●	○
	T	○	○	○	--	--	--	○	--	○	--	--	--
Change in ULS Curvature	V	--	--	--	--	--	--	--	--	--	--	--	--
	L	--	--	--	--	○	--	--	--	○	--	--	--
	T	--	--	○	○	--	--	○	○	○	○	○	○

●Damage located globally; ○Damage located locally;
-- Damage not located

A typical graphical representation of the results obtained using the damage index method and the first torsional mode (mode 2) for damage scenario D2 is presented in Figure 5.8. The first observation from Figure 5.8 is the high sensitivity of the longitudinal and transverse response of the bridge to damage. The damage index calculated using the longitudinal component of the first torsional mode correctly identifies the induced damage (element 335) on a global level. In terms of absolute value, the second highest damage index calculated using the transverse component of the first torsional mode occurs at the induced damage location, and the damage is considered to be located on a local level. Using the vertical component of the first torsional mode, the damage is incorrectly identified to have occurred at midpoint of beam 3 (element 250) on a global level, and the damage is also incorrectly located at the midpoint of the damaged beam on a local level. This result again suggests that the horizontal response of the bridge is more sensitive to damage than the vertical response.

It should be noted that the results obtained using the damage detection techniques would have been difficult to interpret had the location of the damage not already been known *a priori*. With the exception of the damage index method, there is no criterion provided by either method evaluated to distinguish damage from other results. Even when considering results obtained using the damage index method, the maximum absolute value was used to identify the most likely damage location because the criterion provided was found to be inadequate. However, when the results of the field study are considered as a whole, the damage index method was found to perform best.

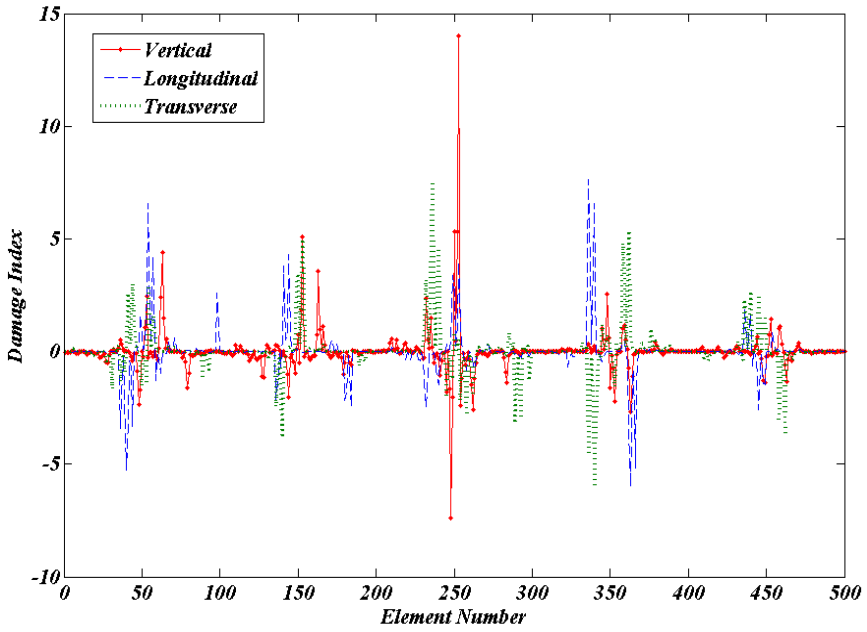

Figure 5.8. Localization results for damage scenario D2 using the first torsional mode (mode 2) and the damage index method.
Note: Element numbers in Figure 5.8 correspond to the beam numbers in Figure 5.4 as follows: from east to west, elements 1-100, beam 1; elements 101-200, beam 2; elements 201-300, beam 3; elements 301-400, beam 4; elements 401-500, beam 5. The damage location corresponds to element 335.

5.11 Summary and Conclusions

The goal of this study was to compare various vibration-based damage detection techniques based on their ability to locate damage induced near a support on an in-situ, full-scale bridge using triaxial vibration measurements obtained using inexpensive geophones. Unlike previous studies, which rely heavily on the vertical response of a bridge for damage detection, the current study has incorporated the three-dimensional response of a bridge into the evaluated damage detection techniques.

It was found that the transverse and longitudinal responses of the bridge are also capable of identifying damage and actually appear to be more sensitive to damage than the vertical response of the bridge. In fact, none of the damage detection methods evaluated was able to successfully locate the induced damage on a global or local level using the vertical component of any of the identified mode shapes. However, when combined with the horizontal components of the identified mode shapes, each method was able to successfully locate the damage on a global level using at least one of the identified mode shapes with the exception of the change in uniform load surface curvature method which was only able to locate the damage on a local level. When the results of the study are considered as a whole, the damage index method was found to perform best.

This study found the second bending mode of vibration (mode 3) to be more consistent at locating the induced damage when combined with the damage detection techniques evaluated. Because the fundamental bending mode is often focused on for use with vibration-based damage detection techniques, it should be noted that results obtained using the fundamental mode and the damage detection methods, with the exception of the damage index method, were fairly inconsistent. Considering that the horizontal response of the bridge seems to be more sensitive to damage, the inconsistency of the fundamental bending mode is attributed to its predominantly vertical behavior and lack of stronger horizontal components. These observations support the conclusion that the horizontal response of a bridge is more sensitive to damage than the vertical response, and that

modes exhibiting stronger horizontal components should be used with vibration-based damage detection techniques.

Similar to previous researchers, this study has found natural frequencies and mode shapes to be relatively poor indicators of damage when used alone. The more complex damage detection methods described were found to be much better indicators of damage. Incorporation of multiple modes was found to have little effect on the results obtained using either method.

One of the significant obstacles in implementing continuous monitoring systems is the cost of the sensors. The results of this study have demonstrated that low-cost geophones can be used to characterize the dynamic response of a bridge, and the obtained results can be successfully implemented with vibration-based damage detection techniques. Furthermore, because geophones do not require a power source, the obstacle of providing power to the sensors in a remote monitoring system is eliminated using geophones. Throughout the described tests, the only power source used was a battery to power the seismograph. In an actual bridge monitoring system, the data logger could easily be powered using a small solar panel.

Finally, data sets obtained from in-situ, full-scale bridge tests both in an undamaged and damaged condition are scarce. This study provides a data set that contains triaxial vibration records collected over a relatively dense measurement grid on an in-situ, full-scale bridge in undamaged and damaged conditions. Thus, this study has provided a valuable data set for continued research in the area of vibration-based damage detection related to bridges.

5.12 Acknowledgements

The authors would like to thank Jeff Walker of Bell and Associates Construction, Phil Large of Wilbur Smith and Associates, and Terry Leatherwood, Henry Pate, and Ed Wasserman of the Tennessee Department of Transportation for their help and cooperation.

5.13 Notation

The following symbols are used in this paper:

β_{ij} = damage index relating the change in modal strain energy at location *j* in the *i*th mode
$\Phi_i''(x)$ = second derivative of the i^{th} identified undamaged mode shape at location *x*
$\Phi_i''^*(x)$ = second derivative of the i^{th} identified damaged mode shape at location *x*
L = length of beam segment being analyzed using the damage index method
E = modulus of elasticity of the material
I = moment of inertia of the cross-section
$M(x)$ = bending moment at location *x*
$\upsilon(x)$ = curvature at location *x*
$\Delta\Phi_i''$ = absolute difference in damaged and undamaged modal curvature
ω_i = i^{th} undamaged natural frequency
ω_i^* = i^{th} damaged natural frequency
φ_i = i^{th} unit mass normalized undamaged mode shape
φ_i^* = i^{th} unit mass normalized damaged mode shape
$[F]$ = undamaged flexibility matrix
$[F]^*$ = damaged flexibility matrix
$[\Delta F]$ = change in flexibility matrix
$\Delta U''$ = absolute curvature change of the uniform load surface
U'' = curvature of the undamaged uniform load surface
U''^* = curvature of the damaged uniform load surface
Δf = frequency resolution in the frequency domain
t = time variable
(Φ) = mode shape vector
$[I]$ = identity matrix

5.14 References

Dobrin, M.B. and Savit C.H. (1988). *Introduction to Geophysical Prospecting*, 4th Ed., McGraw-Hill, New York.

Doebling, S.W., Farrar, C.R., Prime, M.B., and Shevitz, D.W. (1996). *Damage Identification and Health Monitoring of Structural and Mechanical Systems from Changes in Their Vibration Characteristics: A Literature Review.* Rep. No. LA 13070-MS, Los Alamos National Laboratory, Los Alamos, N.M.

Doebling, S.W., Farrar, C.R., and Prime, M.B. (1998). "A summary review of vibration-based damage identification methods." *The Shock and Vibration Digest*, 30(2), 91–105.

Ewins, D. J. (1985). *Modal Testing: Theory and Practice*. John Wiley, New York.

Farrar, C.R. and Jauregui, D.A. (1996). *Damage Detection Algorithms Applied to Experimental and Numerical Modal Data from the I-40 Bridge*. Rep. No. LA-13074-MS, Los Alamos National Laboratory, Los Alamos, N.M.

Farrar, C.R., Doebling, S.W., Cornwell, P.J., and Straser, E.G. (1997). "Variability of modal parameters measured on the Alamosa Canyon bridge." *Proceedings of the 15th International Modal Analysis Conference*, Orlando, FL, pp. 257–263.

Farrar, C.R., Doebling, S.W., and Prime, M.B. Cornwell, P.J., Kam, M., Straser, E.G., Hoerst, B.C., Shevitz, D.W., and Jauregui, D.A. (1998). *A Comprehensive Monitoring System for Damage Identification and Location in Large Structural and Mechanical Systems.* Rep. No. LA-UR-98-233, Los Alamos National Laboratory, Los Alamos, N.M.

Federal Highway Administration. (2001). *Reliability of Visual Inspection.* Rep. No. FHWA-RD-01–020, Washington, D.C.

Krämer, C., De Smet, C.A.M., and De Roeck, G. (1999). "Z24 bridge damage detection tests." *Proceedings of the 17th International Modal Analysis Conference,* Kissimmee, FL, USA.

Lauzon, R.G. and DeWolf, J.T. (2006). "Ambient vibration monitoring of a highway bridge undergoing a destructive test." *Journal of Bridge Engineering*, 11(5), 602-610.

Liu, C.Y. and DeWolf, J.T. (2007). "Effect of temperature on modal variability of a curved concrete bridge under ambient loads." *Journal of Structural Engineering*, 133(12), 1742-1751.

The Mathworks, Inc. (2007). MATLAB®. Version R2007a.

Morassi, A. and Tonon, S. (2008). "Dynamic testing for structural identification of a bridge." *Journal of Bridge Engineering*, 13(6), 573-585.

Pandey, A.K., Biswas, M., and Samman, M.M. (1991). "Damage detection from changes in curvature mode shapes." *Journal of Sound and Vibration*, 145(2), 321-332.

Pandey, A.K. and Biswas, M. (1994). "Damage detection in structures using changes in flexibility." *Journal of Sound and Vibration*, 169(1), 3-17.

Ren, W.X., Zatar, W., and Harik, I.E. (2004). "Ambient vibration-based seismic evaluation of a continuous girder bridge." *Engineering Structures*, 26(5), 631-640.

Richardson, M.H. and Formenti, D.L. (1985). “Parameter estimation from frequency response measurements using rational fraction polynomials.” *Structural Measurement Systems Technical Note 85-3*.

Robinson, E.S. and Coruh, C. (1988). *Basic Exploration Geophysics*, John Wiley & Sons, New York.

Sanayei, M., Bell, E.S., Javdekar, C.N., Edelmann, J.L., and Slavsky, E. (2006). “Damage localization and finite-element model updating using multiresponse NDT data.” *Journal of Bridge Engineering*, 11(6), 688-698.

Siddique, A.B., Sparling, B.F., and Wegner, L.D. (2007). “Assessment of vibration-based damage detection for an integral abutment bridge.” *Canadian Journal of Civil Engineering*, 34(3), 438-452.

Sohn, H., Farrar, C.R., Hemez, F.M., Shunk, D.D., Stinemates, D.W., and Nadler, B.R. (2004). *A Review of Structural Health Monitoring Literature: 1996–2001*. Rep. No. LA-13976-MS, Los Alamos National Laboratory, Los Alamos, N.M.

Stubbs, N., Kim, Y.I., and Farrar, C.R. (1995). “Field verification of a nondestructive damage localization and severity estimation algorithm.” *Proceedings of the 13th International Modal Analysis Conference*, Bethel, CT., 210-218.

Xia, P.Q. and Brownjohn, J.M.W. (2004). "Bridge structural condition assessment using systematically validated finite-element model." *Journal of Bridge Engineering*, 9(5), 418-423.

Xia, Y., Hao, H., Deeks, A.J., and Zhu, X.Q. (2008). “Condition assessment of shear connectors in slab-girder bridges via vibration measurements.” *Journal of Bridge Engineering*, 13(1), 43-54.

Zhang, Z. and Aktan, A. E. (1995). “The damage indices for the constructed facilities.” *Proceedings of the 13th International Modal Analysis Conference*, Bethel, CT., 1520-1529.

Zhao, J. and DeWolf, J.T. (2002). "Dynamic monitoring of steel girder highway bridge." *Journal of Bridge Engineering*, 7(6), 350-356.

Zhou, Z., Wegner, L.D., and Sparling, B.F. (2007). “Vibration-based detection of small-scale damage on a bridge deck.” *Journal of Structural Engineering*, 133(9), 1257-1267.

Chapter 6. Finite Element Modeling of a Full-Scale Five-Girder Bridge for Structural Health Monitoring

This chapter is revised based on a paper submitted to *Computers and Structures* by William Ragland, Dayakar Penumadu, and Richard Williams:

Ragland, W.S., Penumadu, D., and Williams, R.T. (In review). "Finite element modeling of a full-scale five-girder bridge for structural health monitoring." *Computers and Structures*.

My primary contributions to the paper included: (i) development of the problem into a work, (ii) gathering and reviewing literature, (iii) arrangement, design and conduction of the field test on the full-scale bridge, (iv) processing, analyzing, and interpretation of the experimental data, (v) development of computer codes for implementation of the damage detection techniques, (vi) development and calibration of the finite element model, and (vii) most of the writing.

6.1 Abstract

A limited number of studies exist that evaluate vibration-based damage detection techniques using a data set collected entirely on a full-scale bridge. Because in-service bridges can not be damaged to collect such data sets, finite element modeling is commonly used to simulate the effect of damage on the bridge to facilitate the study of vibration-based damage detection techniques. This paper describes the field testing and finite element modeling of an in-situ, full-scale, five-girder bridge that was subjected to controlled levels of known damage. The focus of the paper is finite element model

calibration to enable the study of damage scenarios including those not imposed during the field tests. Modal parameters were extracted from triaxial vibration records obtained over a relatively dense measurement grid using inexpensive geophones and were used to calibrate a three dimensional finite element model of the bridge. The calibration process and considerations that should be made during field tests for proper model calibration are discussed. Various vibration-based damaged detection techniques are evaluated based on their ability to locate the simulated damage. Results show that most of the damage detection techniques evaluated are capable of successfully locating the induced damage on a global level. It was observed from the present study that the horizontal vibration response of the bridge was particularly sensitive to the simulated damage. It is recommended that efforts be made to measure a bridge's horizontal vibration response (in addition to vertical vibration records) during field tests and this information be included in the finite element model calibration processes.

6.2 Introduction

According to the American Association of State Highway and Transportation Officials (AASHTO), the average age of a bridge in the United States is 43 years while most were only designed for a service life of 50 years (AASHTO 2008). Furthermore, as of 2008, the Federal Highway Administration (FHWA) reports that nearly one in four bridges in the United States is either structurally deficient or functionally obsolete (FHWA 2009). Considering these facts, methods of reliably assessing the overall health of the nation's bridge inventory are becoming increasingly important. Currently, bridges

in the United States are inspected and rated during biennial inspections which rely heavily on visual techniques. However, in a report released by the Federal Highway Administration, visual inspections were found to be relatively unreliable (FHWA 2001). For this reason, researchers have been working on the development of more objective methods for nondestructively inspecting and rating bridge condition.

Vibration-based damage detection is a nondestructive evaluation approach based on structural damage being reflected in a structure's dynamic response. While vibration-based damage detection techniques have been shown to accurately locate damage in various mechanical systems and simple structures, varying levels of success have been reported when applying vibration-based damage detection techniques to bridges. Several different global evaluation techniques and associated quantitative damage indices have been published in recent years. Detailed reviews of these techniques as applied to bridges and other structures can be found in Doebling et al. (1996, 1998) and Sohn et al. (2004). In summary, the methods discussed monitor shifts in natural frequency, absolute changes in mode shapes, changes in mode shape curvature or strain energy, and variations in stiffness and flexibility matrices.

Recently, a large construction project often referred to as SmartFix 40 realigned I-40 through downtown Knoxville, TN, while increasing the roadway's capacity to meet current demand. In order to decrease the amount of time required for construction, a small section of I-40 was closed for a period of 14 months. Due to the closing of I-40, a rare opportunity was presented to the authors to perform full-scale bridge testing in an in-situ state and subjected to controlled amounts of damage at a chosen location. The

experimental testing of an in-situ, full-scale, five-girder bridge and the finite element model calibration process used to facilitate the study of additional damage scenarios are presented in the current study. Using simulated vibration records from the calibrated model, various vibration-based damage detection methods are assessed based on their ability to locate the induced damage.

The testing and modeling of the bridge discussed in this paper are of interest for several reasons. First of all, the bridge was tested in an in-situ, full-scale, operating condition before any structural demolition or removal of the surrounding soil had taken place. Furthermore, unlike previous studies that relied heavily on the vertical response of the bridge, triaxial vibration records were obtained in this study which was found to be important for reliable calibration of the bridge model using the finite element method. The bridge tested also has direct practical relevance because it is of a similar design in terms of span, redundancy, and construction to many new and existing bridges in Tennessee and throughout the United States. Thus, results obtained in this study may be applicable in the implementation of monitoring systems for a large number of bridges. The purpose of this paper is to present a three-dimensional approach to finite element model calibration based on triaxial vibration measurements obtained using highly sensitive, inexpensive geophones on an undamaged full-scale bridge and to compare the predicted response of the damaged bridge model with measured data.

6.3 Geophones as sensors

One of the challenges involved when implementing vibration-based damage detection techniques with full-scale bridges is obtaining inexpensive, detailed modal parameters from vibration measurements. To overcome this obstacle, inexpensive geophones (approximately $50 each) are used in this study to obtain triaxial vibration records over a relatively dense measurement grid.

A geophone is a passive directional sensor that measures the speed of motion in the direction of its sensitive axis. In basic terms, a geophone is a coil suspended by springs around a permanent magnet, all of which is contained in a protective casing. When the coil moves relative to the magnet, a voltage is induced in the coil that depends on the relative velocity between the coil and magnet.

Traditionally, geophysicists, rather than bridge engineers, use geophones to measure elastic waves propagating through several kilometers of geologic materials. Detailed technical descriptions of the various types of geophones can be found in geophysical textbooks (Dobrin and Savit 1988, Robinson and Coruh 1988).

Accelerometers are commonly used for dynamic testing of civil engineering structures. However, geophones offer important advantages over accelerometers when considered for implementation in bridge monitoring systems. First, an accelerometer generally requires charge amplification electronics to produce a signal suitable for recording, and thus a power source is needed for the amplifier and associated hardware. In comparison, geophones are passive devices that produce a voltage that can be recorded without additional amplification or conditioning, and they are sensitive enough (orders of

magnitude higher than accelerometers) to measure the small amplitude vibrations associated with higher order modes of vibration. Because they do not require an external power supply or an amplifier, geophones are ideal candidates for implementation in remote bridge monitoring systems. Furthermore, geophones may more easily be incorporated into a wireless sensor system for bridge monitoring in the future.

6.4 Full-scale bridge used for experiments

Constructed in 1967, the I-40 westbound bridge over 4th Avenue, Figure 6.1, consisted of three spans comprised of a concrete deck supported by five rolled steel girders. Due to the alignment of 4th Avenue, the bridge was constructed on a forty-five degree skew. The overall horizontal alignment of the bridge was straight, while there was a slight decrease in elevation from the east abutment to the west abutment. When in operation, the bridge carried two lanes of traffic. An elevation of the bridge is shown in Figure 6.2, and a typical cross section is shown in Figure 6.3.

Figure 6.1. I-40 westbound over 4th Avenue
(47I00400066)

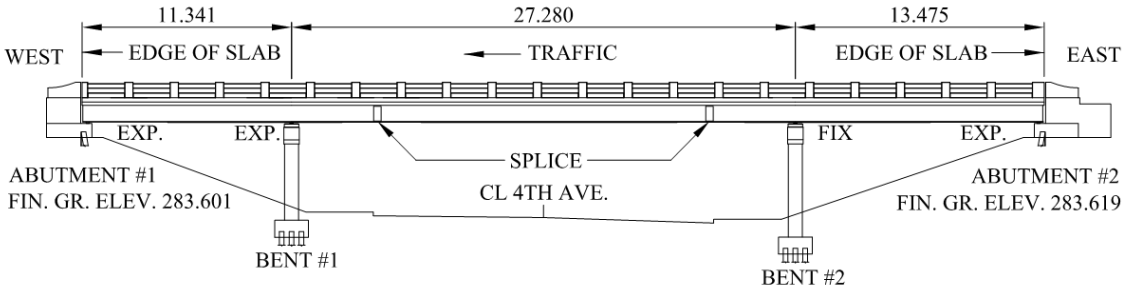

Figure 6.2. I-40 westbound over 4th Avenue: elevation (m)

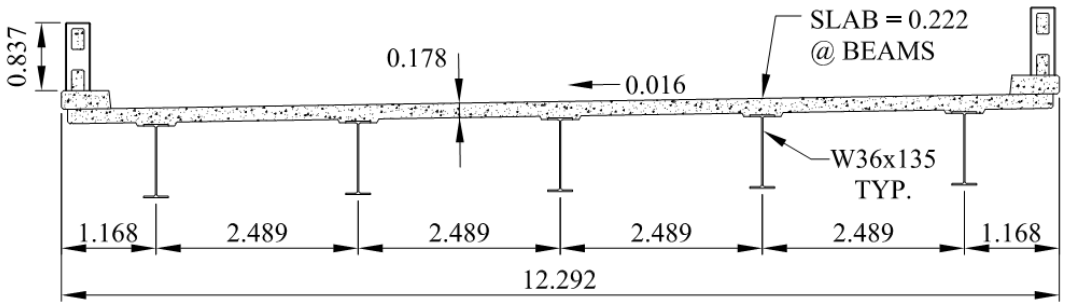

Figure 6.3. I-40 westbound over 4th Avenue: typical cross-section (m)

The I-40 westbound bridge over 4th Avenue consisted of three spans. From east to west, the bridge spanned approximately 13, 27, and 11m as shown in Figure 6.2. Three rolled W36x135 were connected with bolted splice plates to form one continuous beam over the entire bridge length. Cover plates were added to the top and bottom of each beam in the end spans. For the center span, a cover plate was only added to the bottom of each beam, and headed studs were used on top of each beam to promote

composite action with the concrete deck. Connections that allowed for longitudinal expansion, marked "Exp." in Figure 6.2, and connections that prevented longitudinal expansion, marked "Fixed" in Figure 6.2, were installed on the bottom of the beam at each location where a beam was supported by either a concrete bent or abutment. Intermediate diaphragms, C12x20.7, are located at 7.6 m on center perpendicular to each beam, and end diaphragms, C15x33.9, are provided at each end of the bridge parallel to the bridge skew.

6.5 Test Setup

Mark Products LRS-1000 10Hz vertical geophones and Mark Products L-28LBH 4.5Hz horizontal geophones were used for the vibration measurements. One vertical and one horizontal geophone were rigidly attached to a 1.6 cm thick, 11.5 cm diameter steel plate which rested on the bridge deck. The bridge was excited by dropping a fifty pound sandbag at a total of 9 different locations corresponding to the quarter points of the center span along beams 1,3, and 5 in Figure 6.4.

During the testing, data was recorded in the three global coordinate directions at a total of 120 measurement locations using a Geometrics 48-channel StrataView® seismograph. Because the seismograph was only able to record 48 geophone signals at one time (24 vertical and 24 horizontal), the 120 measurements locations were divided into five groups. For each group, the steel plates were spaced at 2.3 m center-to-center (except for the last pair of plates, which was 1.5 m) on the bridge deck along the beam line below as shown in Figure 6.4. In order to obtain triaxial vibration records, the

sandbag was dropped and then dropped again after rotating the horizontal geophones by 90°. Once the data had been recorded in three directions, the line of geophones was shifted to the next position. This process was repeated until all 120 measurement locations were covered. During each test, data was sampled at a rate of 1000 Hz for a total of three seconds. Using these sampling parameters, a frequency resolution of 0.33 Hz was obtained over a frequency range of 0-500 Hz. All results presented in this paper were obtained from the data set collected when the sandbag was dropped at the midpoint of beams 3 and 5 in Figure 6.4.

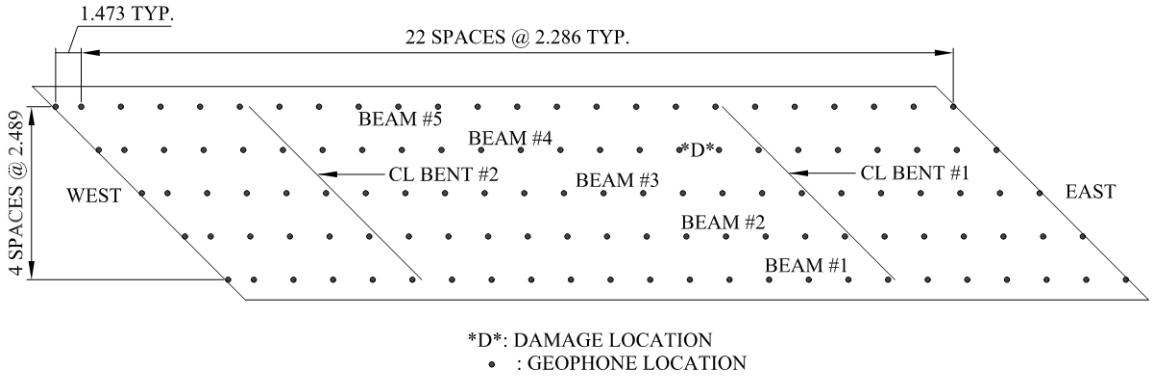

Figure 6.4. I-40 westbound over 4th Avenue: geophone layout (m)

6.6 Experimental Damage Scenarios

While the bridge exhibited some defects prior to the introduction of the controlled damage, the first test performed, and the associated vibration data, is considered to represent an undamaged, baseline condition. The goal of the present study is to identify the damage induced as part of the controlled field experiments based on comparisons with the baseline measurement.

For this research, damage was induced by incrementally cutting a main girder upward from the bottom flange as shown in Figure 6.5. This method of inducing damage was meant to simulate a crack that may occur due to fatigue or excessive vehicle weight. Because vibration-based damage detection has been shown to be less reliable at locating damage occurring near a support using a laboratory model (Zhou et al. 2007), the cut was located near a support in this study to assess the ability of each evaluated damage detection technique to identify damage occurring in a near-support region on a full-scale bridge. Thus, it was decided to cut beam #4 at the location indicated by "D" in Figure 6.4.

Figure 6.5. Damage scenarios
From left to right, undamaged (D0), bottom flange cut (D1),
bottom flange plus ¼ of the web cut (D2), bottom flange plus ½ the web cut (D3)

6.7 Modal Analysis

For this study, the rational polynomial method (Richardson et al. 1985) as implemented in DIAMOND (Farrar et al. 1998) was used for extracting natural frequencies and mode shapes from measured field data. DIAMOND (Damage Identification and Modal Analysis of Data) is a MATLAB® (Mathworks 2007) based software package developed at Los Alamos National Laboratories for modal analysis, damage identification, and finite element model refinement.

Briefly, the rational polynomial method uses orthogonal polynomials to estimate the coefficients of a polynomial approximation to the frequency response function (FRF). The FRF of a system is the ratio of the Fourier transform of the measured input and response signals. Thus, the rational polynomial method is intended for use with measured inputs. However, recording the input excitation for an in-service bridge under ambient loading, such as wind or traffic, would be nearly impossible. For this reason, it was decided not to record input excitations as a part of this research. Because the input was not recorded, an assumption was made in order to implement the rational polynomial method. If an input force is known to have a flat spectrum, as would be the case for wind or traffic, then any peaks in the response spectrum are caused by structural resonances. Therefore, it was assumed that the impulsive loading source used during tests possessed a flat spectrum, at least over the frequency range of interest. This assumption allows the response spectrum matrix created by multiplying the spectrum of each measured response by the conjugate spectrum of a reference response to be analyzed instead of the FRF matrix.

This method of modal analysis is meant to simulate what would have to be used in an actual bridge monitoring system where inputs due to ambient sources, such as wind and traffic, are not easily measured. The results of this study indicate that the natural frequencies and operating shapes obtained using this procedure can be successfully combined with vibration-based damage techniques to locate damage on a full-scale bridge.

6.8 Damage Detection Methods

Various damage detection techniques related to bridge health monitoring have been presented in the literature. For this study, methods considered by Farrar and Jauregui (1996) and Zhou et al. (2007) are evaluated. By comparing the same methods as previous researchers a better understanding of these methods when applied to different bridge structures can be obtained. The various methods are briefly described in the following paragraphs.

Given mode shapes obtained before and after damage, the damage index method (Stubbs et al. 1995) attempts to identify damage in a structure using changes in modal strain energy between the undamaged and damaged structure. The damage index, β, relates the change in modal strain energy at location *j* in the *i*th mode using mode shape curvatures as shown in Eq. 6.1.

$$\beta_{ij} = \frac{\left(\int_a^b \left[\Phi_i''^*(x)\right]^2 dx + \int_a^L \left[\Phi_i''^*(x)\right]^2 dx \right) \int_a^L \left[\Phi_i''(x)\right]^2 dx}{\left(\int_a^b \left[\Phi_i''(x)\right]^2 dx + \int_a^L \left[\Phi_i''(x)\right]^2 dx \right) \int_a^L \left[\Phi_i''^*(x)\right]^2 dx} \qquad 6.1$$

In Eq. 6.1, $\Phi_i''(x)$ and $\Phi_i''^*(x)$ are the second derivatives of the *i*th mode shape of the undamaged and damaged structure, respectively. L is the length of the beam, and a and b are the end points of the segment of the beam being analyzed. Multiple modes can be used, in which case the damage index is calculated by summing damage indices from each mode. Upon calculating the damage index at each location on the beam, a normal distribution is fit to the indices, and values falling two or more standard deviations from the mean are considered likely damage locations.

The mode shape curvature method (Pandey et al. 1991) assumes that damage to a structure only affects its stiffness and mass. Mode shapes are determined for the structure before and after damage, and mode shape curvatures are estimated using some type of numerical differentiation. In order to develop this method, consider an example of a beam with uniform bending stiffness, EI, subjected to a bending moment, $M(x)$. The curvature, $\upsilon(x)$, of the beam at location x is then given by Eq. 6.2.

$$v(x) = \frac{M(x)}{EI} \tag{6.2}$$

$$\Delta\Phi'' = \left|\Phi_i''^*\right| - \left|\Phi_i''\right| \tag{6.3}$$

Observing Eq. 6.2, it is clear that curvature is inversely proportional to flexural stiffness and that a reduction in stiffness will result in an increase in curvature. Therefore, differences in undamaged and damaged mode shape curvatures, Eq. 6.3, should be greatest near damaged locations. When multiple modes are used, the absolute value of the difference in curvatures for each mode is summed to obtain a damage parameter for each location.

The change in flexibility method (Pandey and Biswas 1994) first approximates the flexibility matrix of the undamaged structure, Eq. 6.4, and the damaged structure, Eq. 6.5, using a given number, n, of modal frequencies, ω_i, and unit-mass-normalized mode shapes, φ_i.

$$[F] \approx \sum_{i=1}^{n} \frac{1}{\omega_i^{\,2}} \{\varphi_i\}\{\varphi_i\}^T \tag{6.4}$$

$$[F]^* \approx \sum_{i=1}^{n} \frac{1}{\omega_i^{*2}} \{\varphi_i\}^* \{\varphi_i\}^{*T} \tag{6.5}$$

$$[\Delta F] = [F] - [F]^* \tag{6.6}$$

The two flexibility matrices are then subtracted which results in the change in flexibility matrix, Eq. 6.6. The absolute maximum value of each column of the change in flexibility matrix is then determined, and the column corresponding to the largest change in flexibility is indicative of the damaged degree of freedom.

The uniform load surface, U_i, is obtained by summing all the columns of the flexibility matrix. The result is the deformed shape of the structure caused by applying a unit load to each degree of freedom on the structure simultaneously. The change in uniform load surface curvature method (Zhang and Aktan 1995) identifies damage as the location where the absolute difference between the undamaged and damaged uniform load surface curvatures is greatest, Eq. 6.7.

$$\Delta U_i'' = \left| U_i''^* - U_i'' \right| \tag{6.7}$$

6.9 Finite Element Model

In the field of nondestructive bridge evaluation and damage detection, finite element models are used for multiple purposes such as planning field tests (Morassi and Tonon 2008), assessing bridge condition (Ren et al. 2004, Bozdag et al. 2006), providing baseline references for bridge monitoring (Ren and Peng 2005), estimating ultimate load carrying capacities (Cheng et al. 2003), and simulating damaged bridge conditions (Koh and Dyke 2007, Siddique et al. 2007). As part of this research, a finite element model of the test bridge was developed for several reasons but mainly to verify the field test results, to evaluate the ability to locate damage using a calibrated finite element model of an undamaged bridge, and to investigate damage scenarios other than those imposed during the field test.

The finite element model of the test bridge (Figure 6.6) was constructed using ABAQUS® (Dassault 2008). With the exception of the bent columns and diaphragm channels, the entire bridge was modeled using 4-noded reduced integration shell elements, S4R in ABAQUS. The bent columns and diaphragm channels were modeled using 3-noded quadratic beam elements, B32 in ABAQUS. The model simulates composite action between the girders and the concrete slab for the center span by constraining the degrees of freedom associated with the top flange of each girder to mirror those associated with the bottom of the concrete slab directly above each girder.

The bridge bents, deck, and parapet railing were modeled using the following material properties for concrete: E_c = 22.0 GPa (3,200 ksi), υ_c = 0.18, and ρ_c = 2.32 g/cm^3 (145 lb/ft^3). The steel girders and diaphragm members were modeled using the following material properties for steel: E_s = 200 GPa (29,000 ksi), υ_s = 0.30, and ρ_s = 7.85 g/cm^3 (490 lb/ft^3).

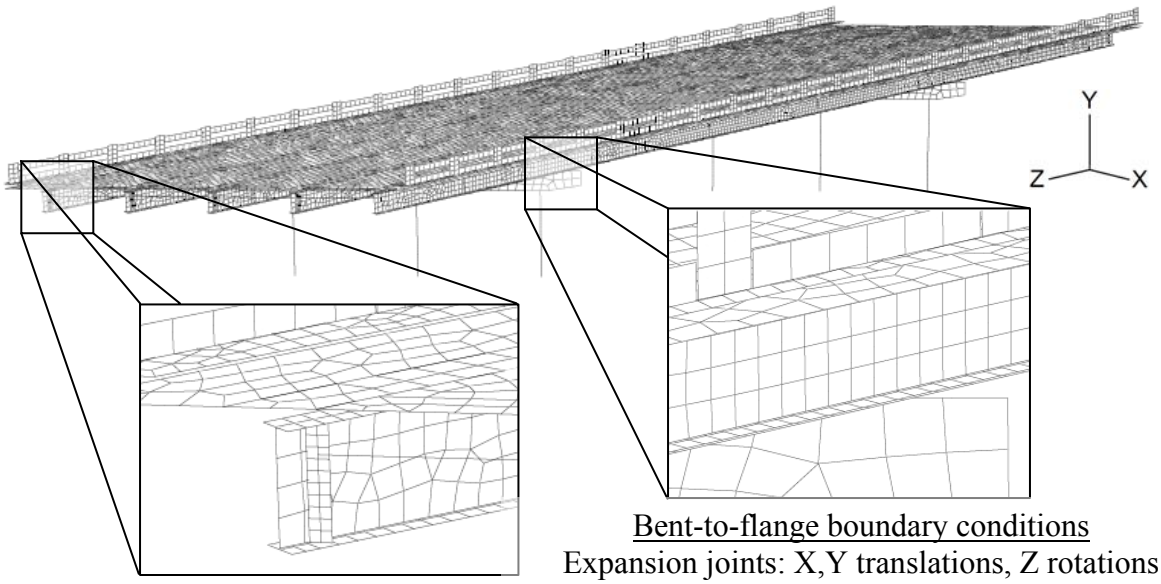

Figure 6.6. Finite element model of the test bridge

6.10 Modeling Damage Induced to the Test Bridge

In order to simulate the damage scenarios inflicted during the field test, two independent instances of the girder web and bottom flange were tied together at the damage location. (In the ABAQUS modeling environment, *instances*, or occurrences, of parts are assembled to create the overall model. If the same part is needed multiple times, separate *instances* of the part can be created without having to completely recreate the part.) Because the top flange of the girder was not affected by the cut used to simulate damage, it was modeled as one continuous instance over the length of the girder. By tying two independent instances together, the translational and rotational degrees of freedom of one instance were forced to equal those of the other instance. The model was carefully constructed so that nodes occurred at the quarter points of the girder web, the midpoint of the bottom flange, and each edge of the bottom flange. To model the undamaged scenario, D0, the nodes on each instance of the girder web and bottom flange remained tied. To simulate damage scenario D1, the nodes representing each bottom flange were untied which allowed for independent translation and rotation of each instance. Damage scenario D2 was simulated by releasing the bottom node of each girder web instance. Thus, the lower quarter of each girder was allowed to translate and rotate independently of the other. Finally, damage scenario D3 was simulated by releasing the bottom quarter node of each girder web. The lower half of each girder was then allowed to translate and rotate independently of the other.

Modeling the induced damage in this manner allows for the introduction of damage without changing any aspect of the model other than releasing the tie constraints.

The mesh remains unchanged throughout each simulated damage test. Therefore, the size of the stiffness matrix is preserved between tests and no new nodes are introduced to the model. Thus, any noted changes from one damage scenario to another are entirely attributed to the induced damage and not changes to the finite element model.

6.11 Model Correlation with Measured Modal Parameters

In order to calibrate the finite element model of the bridge, boundary conditions at each girder support were adjusted by releasing or constraining various degrees of freedom until the finite element model predictions matched the measured natural frequencies and mode shapes for the undamaged bridge (D0). The damaged data sets obtained during the field test were not used for calibration purposes. All comparisons of the damaged field tests and damaged finite element model are based strictly on simulated data (corresponding to class-A predictions).

The finite element model of the test bridge was calibrated by only adjusting the boundary conditions of the bridge at the bents and abutments. Adjustment of the concrete material properties (elastic modulus and density) was initially considered. However, it was found that changing the concrete material properties mainly affected natural frequencies and had little to no effect on the mode shapes obtained from the model. Thus, generic material properties for concrete were used as described earlier.

In order to better quantify the correlation between mode shapes identified from the undamaged field test and the finite element model, the modal assurance criterion (MAC) (Ewins 1985) was used. The MAC, Eq. 6.8, takes advantage of the orthogonal

property of mode shapes to compare different modes. If the modes are identical, a value of one will be obtained. If the modes are dissimilar, a value of zero will be obtained. Ewins (1985) notes that in practice, modes are considered correlated if a value greater than 0.9 is calculated and uncorrelated if a value less than 0.05 is calculated. The MAC that compares mode *i* and *j* has the form given in Eq. 6.8 where $(\Phi)_k$ is an element of the mode shape vector and *n* represents the number of points at which the two mode shapes are compared.

$$MAC(i,j) = \frac{\left|\sum_{k=1}^{n}(\Phi_j)_k(\Phi_i)_k\right|^2}{\left(\sum_{k=1}^{n}(\Phi_j)_k(\Phi_j)_k\right)\left(\sum_{k=1}^{n}(\Phi_i)_k(\Phi_i)_k\right)} \qquad 6.8$$

After multiple iterations, the model that best agreed with the measured natural frequencies and mode shapes had the following characteristics. At the fixed bent, nodes on the bottom flange of each girder were constrained to have the same displacements in the X, Y, and Z (Figure 6.6) direction as the nodes representing the center of the bent below each girder. At the expansion bent, nodes on the bottom flange of each girder were constrained to have the same displacements in the X and Y direction as the nodes representing the center of the bent below each girder. Rotational degrees of freedom about the Z-axis were constrained at each bent. At each abutment, displacements in the Y direction were constrained using springs (k_y=613 kN/mm) and rotations were constrained about the Z-axis. The base of each bent column was modeled as a fixed condition by constraining displacements in the X, Y, and Z direction and constraining rotations about the X, Y, and Z axes.

Using traditional roller type connections at the abutments to model the expansion supports (constrained displacements in the X and Y directions and constrained rotations about the Y and Z axes) produced a well correlated model if only the measured vertical response of the bridge was considered. However, when the horizontal response of the bridge was considered, the model was not well correlated as defined using the MAC. Thus, the boundary conditions previously described were found to provide the best overall model when compared with the field test results as a whole which demonstrates the importance of considering the horizontal response of a bridge when attempting to calibrate finite element models to field test results. This important observation has been missed by previous researchers.

Another important feature of the finite element model was found to be the aspects associated with including the diaphragm bracing. If the diaphragm bracing was not considered, the correlation of the second and third bending modes (modes 3 and 4) was poor. The diaphragm channels were connected to each girder with a steel plate that was welded to the full depth of the web and the width of the compression flange at each location. If the weld to the compression flange was not considered, the natural frequencies obtained from the model did not correlate well with those measured on the test bridge for the second bending mode (mode 3). Thus, inclusion of the diaphragm bracing was significant for this type of bridge structure.

Natural frequencies obtained from the finite element model and those measured on the test bridge for each damage scenario are presented in Table 6.1. Observing Table 6.1, a good agreement is noted between the numerical and measured frequencies. Also, it

is observed that similar to the measured natural frequencies, the natural frequencies obtained from the finite element model do not appreciably change with each progressive increase in the amount of induced damage (D1 to D3). In fact, the third bending mode (mode 4) from the finite element model is the only mode that shows a change in natural frequency.

Table 6.1. Comparison of natural frequencies identified from the field test and finite element model

Damage Test		Mode 1	Mode 2	Mode 3	Mode 4
D0, Undamaged	Field Test	4.34	4.41	6.39	15.00
	F.E. Model	4.29	4.41	6.12	15.06
	% Diff.	-1.06%	0.12%	-4.19%	0.40%
D1, Flange Cut	Field Test	4.35	4.44	6.35	14.66
	F.E. Model	4.29	4.41	6.12	15.06
	% Diff.	-1.34%	-0.54%	-3.65%	2.67%
D2, Flange + 1/4 Web Cut	Field Test	4.29	4.43	6.38	14.66
	F.E. Model	4.29	4.41	6.12	15.03
	% Diff.	0.09%	-0.30%	-4.08%	2.55%
D3, Flange + 1/2 Web Cut	Field Test	4.26	4.40	6.40	14.63
	F.E. Model	4.29	4.41	6.12	15.00
	% Diff.	0.82%	0.25%	-4.40%	2.52%

The mode shapes identified from the finite element model that correspond to the mode shapes identified from the undamaged field test are presented in Figure 6.7. MAC values comparing the identified modes from the finite element model and the field tests are summarized in Table 6.2. To calculate the MAC, translational components in the X, Y, and Z directions were extracted from the finite element model mode shapes at locations corresponding to the geophone locations on the test bridge to form a mode shape vector that could be compared with the mode shapes determined from the field tests. Observing Table 6.2, a relatively good agreement is noted between the numerical and measured mode shape for all the damage scenarios. It should be noted again that only the undamaged (D0) field test data were used during the finite element model calibration process. The correlation of the damaged mode shapes was calculated using damaged mode shapes obtained by damaging the calibrated undamaged model as described earlier. Thus, the strong correlation that exists between the damaged experimental and numerical mode shapes suggests that the calibrated finite element model accurately represents the three dimensional dynamic response of the bridge used in this study.

Overall, the differences in the experimental and numerical results presented in Table 6.1 and Table 6.2 can be considered small. Any discrepancies in the measured and analytical results are mainly attributed to the idealization of the boundary conditions and the use of generic concrete material properties. Therefore, the model was considered to be well correlated to the results obtained in the field.

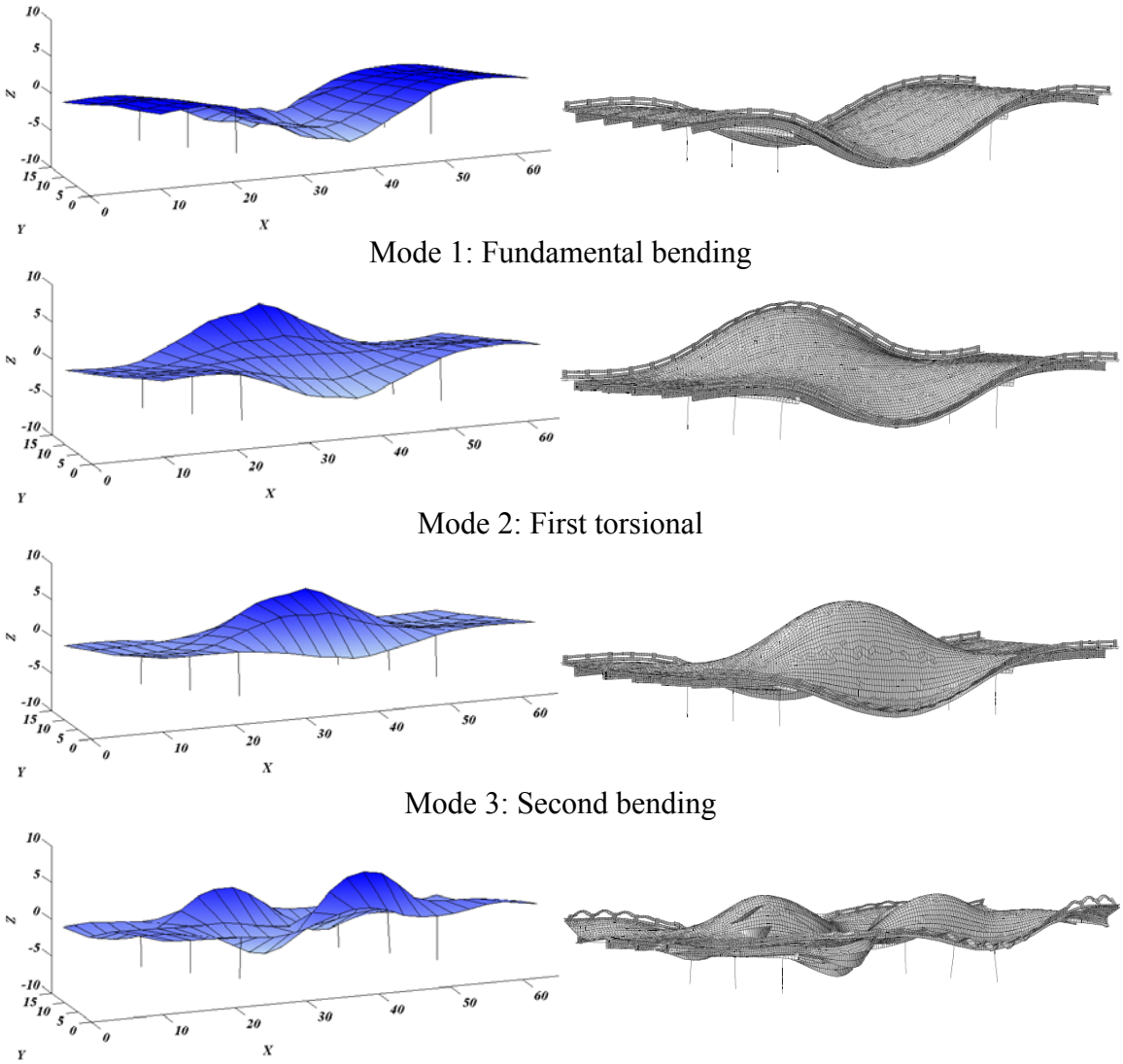

Mode 1: Fundamental bending

Mode 2: First torsional

Mode 3: Second bending

Mode 4: Third bending

Figure 6.7. Comparison of identified undamaged mode shapes
field test (left), finite element model (right)

Table 6.2. MAC: Field test vs. finite element model

Mode	1	2	3	4
Undamaged, D0				
1	0.974	0.001	0.095	0.051
2	0.001	0.963	0.004	0.000
3	0.070	0.001	0.985	0.008
4	0.010	0.000	0.024	0.900
D1 Damage				
1	0.940	0.028	0.124	0.031
2	0.000	0.924	0.003	0.002
3	0.165	0.000	0.947	0.027
4	0.007	0.000	0.025	0.849
D2 Damage				
1	0.945	0.043	0.103	0.038
2	0.018	0.912	0.003	0.001
3	0.013	0.011	0.958	0.033
4	0.016	0.005	0.025	0.866
D3 Damage				
1	0.944	0.062	0.149	0.039
2	0.026	0.896	0.035	0.004
3	0.021	0.032	0.922	0.035
4	0.019	0.002	0.026	0.867

6.12 Numerical Damage Scenarios

An important characteristic that any reliable damage detection technique should possess is the ability to identify different types of damage imposed in various ways and at various locations. Thus, the calibrated finite element model of the test bridge was used to simulate additional damage scenarios other than those imposed during the field tests. Using simulated data from the calibrated model, the damage detection techniques were evaluated on their ability to detect damage inflicted on the finite element model in various ways, locations, and combinations. The various numerical scenarios evaluated are summarized in Table 6.3. Note that for damage scenario N4, a 2.2 cm cover plate used to strengthen the bottom flange of the girder was also cut in addition to the bottom flange.

Table 6.3. Summary of finite element model damage scenarios

Scenario Designation	Damage Location	Damage Description
N1	Beam 4, same as field test	Bottom flange cut
N2	Beam 4, same as field test	Bottom flange plus one-quarter of web cut
N3	Beam 4, same as field test	Bottom flange plus one-half of web cut
N4	Beam 1, mid-span of the center span	Cover plate plus bottom flange cut
N5	Beam 1, mid-span of the center span	Cover plate, bottom flange, plus one-quarter of web cut
N6	Beam 1, mid-span of the center span	Cover plate, bottom flange, plus one-half of web cut
N7	N1 and N4 combined	
N8	N2 and N5combined	
N9	N3 and N6 combined	

6.13 Time-History and Simulated Modal Analyses

To obtain acceleration records from the finite element model, a sandbag drop was simulated by applying an impulsive concentrated load to the concrete deck at mid-span of the bridge's center span directly above beam 1 in Figure 6.4. The time-history response of the bridge was then obtained using modal superposition and the first forty modes identified from the model. Simulated acceleration records were obtained in the X, Y, and Z directions at 120 locations on the model's concrete deck corresponding to the geophone locations on the test bridge. Each time-history was obtained for a total of 20 s at a rate of 100 Hz. Using these sampling parameters, a frequency resolution of 0.05 Hz was obtained over a frequency range of 0-50 Hz. Once the time-histories were obtained, the modal analysis procedures described earlier were followed to facilitate the evaluation of the damage detection techniques.

6.14 Application of Damage Detection Methods to Finite Element Model Results

Preliminary processing of the finite element model results was performed before the damage detection methods were applied. First, each beam in Figure 6.4 was divided into 100 uniform elements 0.52 m in length, and a cubic polynomial interpolation was used to estimate mode shape amplitudes between the simulated geophone locations. The cubic polynomial approximation of the mode shape was used obtain mode shape curvature values when needed. Second, it was not possible to mass normalize the mode shapes as called for by the change in flexibility method and the change in uniform load surface curvature method because input forces were not measured during this study.

Instead, mode shapes were normalized using Eq. 6.9 for all of the damage detection methods. This normalization procedure also satisfies the requirements of the damage index method and mode shape curvature method for consistently normalized mode shapes. This normalization approach was implemented to simulate real bridge conditions where ambient excitation sources, such as wind or traffic, are not easily characterized.

$$\{\varphi_n\}^T [I] \{\varphi_n\} = 1 \qquad 6.9$$

Finally, the damage detection methods were evaluated in three dimensions. Previously published research relied mainly on the vertical response of bridges for the extraction of modal parameters and damage detection. The influence of the natural/induced damage on the horizontal response of the bridge was not considered. As a part of the present study, all of the described damage detection methods were extended to three dimensions by applying each method individually to the three components of the measured mode shapes: the vertical (V), transverse (T), and longitudinal (L) directions. Here, transverse refers to motion of the bridge deck perpendicular to the length of the bridge, and longitudinal refers to motion of the bridge deck parallel to the length of the bridge.

Table 6.4 summarizes the results obtained by applying each damage detection method to each identified mode. When all 120 measurement locations from the field test are considered in the damage evaluation process, a damage detection method was considered to have located the damage in a global sense if the maximum absolute value of the calculation occurred at the location where damage was induced in the finite element model. If a method was unable to identify damage on a global level (the

maximum value occurs at an incorrect location), then the method was evaluated on its ability to identify damage locally on the damaged beam. Considering only the 24 measurement locations above the damaged beam (beam 4 in Figure 6.4), a damage detection method was considered to have located the damage in a local sense if the maximum absolute value of the calculation obtained using the smaller data set occurred at the inflicted damage location. In the present study, global damage identification means that the damage is distinguishable from the entire data set collected, while local damage identification means that the damage is distinguishable when only the portion of the data set collected directly above the damaged beam is considered.

Examining Table 6.4, the ideal result would be darkened circles/squares/diamonds in every row and column. It can be seen that most of the damage detection methods were effective when evaluated using a favorable mode. Also note that the longitudinal and transverse components of the identified modes are capable of locating the induced damage. When comparing the damage detection methods using the field test results, Ragland et al. (In review) observed that the horizontal response of the bridge was more sensitive to the induced damage than the vertical response. In fact, the vertical response was insufficient to locate the induced damage using any of the evaluated damage detection methods. The favorable results obtained using the vertical response obtained from the finite element model are attributed to the lack of noise in the model data set, which is inherent to real data. However, the magnitude of the damage indices calculated using the horizontal components of the identified mode shapes from the finite element model were commonly larger than those calculated using the vertical components. This

was particularly true when damage was located near a support as it was in the field test (scenarios N1-N3, N7-N9). Therefore, the horizontal response of the bridge seems to be more sensitive to the induced damage than the vertical response.

Not all damage detection methods performed best using the same mode. For example, the damage index method was found to perform best using the second bending mode (mode 3). In contrast, the mode shape curvature and change in uniform load surface curvature methods performed best when evaluated with the first torsional mode (mode 2) for this particular bridge. While the change in flexibility method was not particularly effective when evaluated with any of the identified modes, it was most effective when combined with the second bending mode (mode 3). Thus, all the damage detection methods studied were found to perform best when evaluated with modes higher than the fundamental bending mode.

Because the damage detection methods studied were found to perform best using the first torsional mode and the second bending mode (modes 2 and 3), the fundamental bending mode (mode 1) does not appear to be the most critical mode for use with vibration-based damage detection techniques. The relatively poor results obtained with the fundamental bending mode when compared to the other modes are attributed to its predominantly vertical behavior and comparatively weak horizontal components.

Table 6.4. Summary of damage detection results using numerical data

Damage Scenario		Damage Index			Mode Shape Curvature			Change in Flexibility			Change in ULS Curvature		
		V	L	T	V	L	T	V	L	T	V	L	T
Mode 1 Fundamental bending	N1	○	●	--	●	●	--	--	--	○	○	--	--
	N2	○	●	--	●	●	--	--	--	○	○	--	--
	N3	○	●	--	●	●	--	--	--	○	○	--	--
	N4	●	○	--	●	○	--	●	--	--	●	--	--
	N5	●	○	--	●	--	--	●	--	--	●	--	--
	N6	●	○	●	--	--	--	--	--	--	●	--	●
	N7	■	□	--	■	--	--	■	--	◊	■	--	--
	N8	■	□	■	□	--	--	■	--	◊	■	--	--
	N9	■	□◊	■	■	■	■◊	■	◊	--	■	◊	■
Mode 2 First torsional	N1	○	●	--	●	●	--	--	--	--	●	●	--
	N2	●	●	--	●	●	--	--	--	--	●	●	--
	N3	●	●	--	●	●	--	--	--	--	●	●	--
	N4	○	○	○	●	●	●	●	--	--	●	●	●
	N5	○	○	●	●	●	●	--	--	--	●	●	●
	N6	●	●	●	●	●	●	●	--	--	●	●	●
	N7	□	□	□	■	■	■	■	--	--	■	■	■
	N8	□	□◊	□◊	■	--	■◊	■	--	◊	■	--	■◊
	N9	■	□	□	■	--	□	■	--	◊	□	--	□◊
Mode 3 Second bending	N1	●	●	--	●	●	--	--	--	--	●	●	--
	N2	●	●	--	--	--	--	○	○	--	●	●	--
	N3	●	●	--	--	○	--	○	●	--	○	--	--
	N4	●	●	●	●	--	●	●	--	--	●	○	--
	N5	●	●	●	●	●	●	●	--	--	●	○	○
	N6	●	●	●	●	●	●	●	--	--	●	○	○
	N7	■◊	■◊	■	■◊	□◊	■	■◊	□◊	--	■◊	□◊	□
	N8	■◊	□♦	■	■◊	■◊	■	■◊	◊	--	■	♦	□
	N9	■◊	■◊	■	□	◊	--	□◊	□◊	--	□♦	□♦	□
Mode 4 Third bending	N1	--	○	--	--	●	--	--	--	--	--	●	○
	N2	○	--	--	--	●	--	--	--	--	--	--	--
	N3	●	○	--	●	●	--	○	--	--	○	○	--
	N4	●	●	--	●	●	--	●	--	--	--	--	○
	N5	●	●	--	●	●	○	●	--	--	●	--	○
	N6	●	●	--	--	--	--	--	●	--	--	--	--
	N7	■◊	□◊	--	■	□♦	--	□	□◊	--	--	--	--
	N8	■	□	--	■	--	--	□	--	--	--	--	--
	N9	■	■	--	■	□◊	--	--	--	--	■	♦	◊

●Damage located globally; ○Damage located locally;
■Beam 1 damage located globally; □Beam 1 damage located locally
♦Beam 4 damage located globally; ◊Beam 4 damage located locally
-- Damage not located

Damage scenarios N4-N6 are meant to simulate mid-span damage to an exterior girder which is believed by the authors to be a likely mechanism for failure in a real bridge. This type of damage adversely affects the overall symmetry of the bridge which increases the motion of the torsional modes in comparison to the vertical modes. For this reason, the first torsional mode was the most successful at locating damage induced at mid-span of an exterior girder. Referring to scenarios N4-N6 in Table 6.4, every component of the first torsional mode (mode 2) correctly locates the damage for each scenario on a global level when combined with the mode shape curvature and change in uniform load surface curvature methods. The second bending mode (mode 3) also successfully locates the damage for scenarios N4-N6 using the damage index and mode shape curvature methods. As before, the first torsional mode and the second bending mode (modes 2 and 3) were found to be more appropriate for identifying damage using the damage detection techniques evaluated here. The poor performance of the fundamental bending mode is again attributed to its lack of strong horizontal components.

An example graphical representation is presented in Figure 6.8 for the results obtained using the damage index method and the second bending mode (mode 3) for damage scenario N8. Here the damage was induced at two locations corresponding to element numbers 50 and 335. Using each component of the second bending mode, the damage is correctly identified to have occurred near element 50 on a global level. However, the damage at element 335 is clearly defined only when observed using the longitudinal component. Using the longitudinal component of the second bending mode, the two maximum absolute values for the longitudinal damage index occur at both

locations where damaged was induced in the finite element model. This result again suggests that the horizontal response of the bridge is more sensitive to damage than the vertical response.

The results obtained using the damage detection techniques would have been difficult to interpret had the location of the damage not been known *a priori*. Further study is warranted to determine the statistical significance of the damage indices calculated using the methods discussed here. However, when the results of this study are considered as a whole, the damage index method was found to perform best.

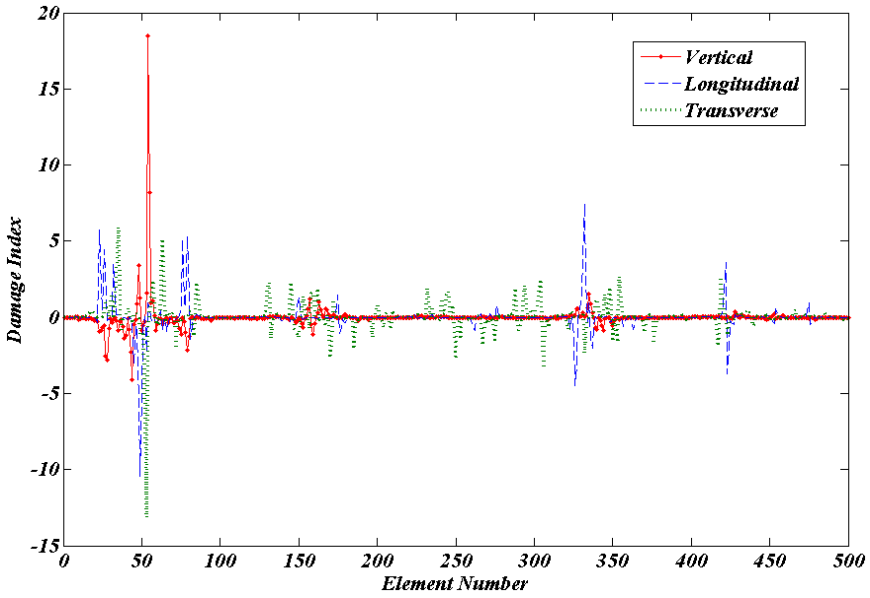

Figure 6.8. Localization results for damage scenario N8 using the second bending mode (mode 3) and the damage index method
Note: Element numbers in Figure 6.8 correspond to the beam numbers in Figure 6.4 as follows: from east to west, elements 1-100, beam 1; elements 101-200, beam 2; elements 201-300, beam 3; elements 301-400, beam 4; elements 401-500, beam 5. The damage locations correspond to element numbers 50 and 335.

6.15 Summary and Conclusions

The goal of this study was to compare various vibration-based damage detection techniques using simulated triaxial vibration measurements obtained from a calibrated finite element model. The model was calibrated against natural frequencies and mode shapes extracted from triaxial vibration records obtained from an in-situ, full-scale bridge. Unlike previous studies, which relied heavily on the vertical response of a bridge for damage detection, the current study has incorporated the three-dimensional response of a bridge into the damage detection techniques.

The fundamental bending mode is commonly the focus of vibration-based damage detection research, but the results obtained in this study using the fundamental mode were not as consistent as those obtained using other modes. This study found the second bending mode (mode 3) and the first torsional mode (mode 2) to more consistently locate the induced damage. The relative insensitivity of the fundamental bending mode to damage is attributed to its predominantly vertical motion and lack of strong horizontal components. The observations here support the conclusion that modes exhibiting stronger horizontal components should be used with vibration-based damage detection techniques.

Using simulated data from the calibrated finite element model, it was found that the first torsional mode was better suited for identifying damage located at mid-span of an exterior girder. Considering the relative symmetry of the bridge analyzed, it is not surprising that damage appreciably affecting the bridge's symmetry is more easily identified using torsional modes. This observation further supports the suggestion that

modes other than the fundamental bending mode should be included when vibration-based damage detection techniques are used.

Through the finite element model calibration efforts, it was learned that the horizontal response of the bridge should be included in the calibration process to obtain an accurate representation of the three dimensional response of the bridge. The horizontal response was found to be much more sensitive to the manner in which boundary conditions were applied than the vertical response. Using the MAC as a calibration tool, a well calibrated model was constructed using traditional roller type boundary conditions to model the expansion supports at each abutment when only the vertical response of the bridge was considered. The same model was not well correlated to the field test results when the horizontal response of the bridge was considered. Instead, the use of springs to model the expansion supports at the abutments provided the best overall model when compared with the field test results. Therefore, studies using calibrated finite element models to obtain damaged data sets should include the horizontal response of the bridge in the calibration process.

It was also found that including higher order modes in the calibration process is important to obtain a well correlated model. Overall, the highest order mode identified (mode 4) was found to be much more sensitive to changes made to the finite element model boundary conditions than the other modes.

The diaphragm bracing was found to have a significant impact on the dynamic response of the bridge. If the diaphragm bracing was not considered, the correlation of the higher order experimental and analytical modes was relatively poor. The natural

frequencies obtained from the finite element model did not correlate well with those measured for the second bending mode (mode 3) if small details such as welding the diaphragm connection plate to the compression flange of each girder were not considered. Thus, inclusion of the diaphragm bracing in the finite element model was significant for this type of bridge structure.

Developing a well calibrated finite element model of the bridge considered in this research required substantial effort to match the measured undamaged response. Once a suitable model of the bridge was developed, it provided a relatively accurate damaged response when compared to the measured damaged response of the test bridge. Thus, the use of calibrated finite element models shows promise for implementation in structural health monitoring of bridges.

6.16 Acknowledgements

The authors would like to thank Jeff Walker of Bell and Associates Construction, Phil Large of Wilbur Smith and Associates, and Terry Leatherwood, Henry Pate, and Ed Wasserman of the Tennessee Department of Transportation for their help and cooperation.

6.17 Notation

The following symbols are used in this paper:

β_{ij} = damage index relating the change in modal strain energy at location *j* in the *i*th mode
$\Phi_i''(x)$ = second derivative of the ith identified undamaged mode shape at location *x*
$\Phi_i''^*(x)$ = second derivative of the ith identified damaged mode shape at location *x*
L = length of beam segment being analyzed using the damage index method
E = modulus of elasticity of the material
I = moment of inertia of the cross-section
$M(x)$ = bending moment at location *x*
$\upsilon(x)$ = curvature at location *x*
$\Delta\Phi_i''$ = absolute difference in damaged and undamaged modal curvature
ω_i = ith undamaged natural frequency
ω_i^* = ith damaged natural frequency
φ_i = ith unit mass normalized undamaged mode shape
φ_i^* = ith unit mass normalized damaged mode shape
$[F]$ = undamaged flexibility matrix
$[F]^*$ = damaged flexibility matrix
$[\Delta F]$ = change in flexibility matrix
$\Delta U''$ = absolute curvature change of the uniform load surface
U'' = curvature of the undamaged uniform load surface
U''^* = curvature of the damaged uniform load surface
Δf = frequency resolution in the frequency domain
t = time variable
(Φ) = mode shape vector
k_y = spring constant
$[I]$ = Identity matrix

6.18 References

American Association of State Highway and Transportation Officials (2008). *Bridging the Gap: Restoring and Rebuilding the Nation's Bridges*. Washington, D.C.

Bozdag, E., Sunbuloglu, E., and Ersoy, H. (2006). "Vibration analysis of new Galata Bridge-experimental and numerical results." *Computers and Structures*, 84, 283-292.

Cheng, J., Jiang, J.J., Xiao, R.C., and Xiang, H.F. (2003). "Ultimate load carrying capacity of the Lu Pu steel arch bridge under static wind loads." *Computers and Structures*, 81, 61-73.

Dassault Systèmes, Inc., SIMULIA Corp., (2008). ABAQUS®. Version 6.8.

Dobrin, M.B. and Savit C.H. (1988). *Introduction to Geophysical Prospecting*, 4th Ed., McGraw-Hill, New York.

Doebling, S.W., Farrar, C.R., Prime, M.B., and Shevitz, D.W. (1996). *Damage Identification and Health Monitoring of Structural and Mechanical Systems from Changes in Their Vibration Characteristics: A Literature Review.* Rep. No. LA 13070-MS, Los Alamos National Laboratory, Los Alamos, N.M.

Doebling, S. W., Farrar, C. R., and Prime, M. B. (1998). "A summary review of vibration-based damage identification methods." *The Shock and Vibration Digest.*, 30(2), 91–105.

Ewins, D. J. (1985). *Modal Testing: Theory and Practice*. John Wiley, New York.

Farrar, C. R. and Jauregui, D.A. (1996). *Damage Detection Algorithms Applied to Experimental and Numerical Modal Data from the I-40 Bridge*. Rep. No. LA-13074-MS, Los Alamos National Laboratory, Los Alamos, N.M.

Farrar, C. R., Doebling, S. W., and Prime, M.B. Cornwell, P. J., Kam, M., Straser, E. G., Hoerst, B. C., Shevitz, D.W., and Jauregui, D.A. (1998). *A Comprehensive Monitoring System for Damage Identification and Location in Large Structural and Mechanical Systems.* Rep. No. LA-UR-98-233, Los Alamos National Laboratory, Los Alamos, N.M.

Federal Highway Administration (2001). *Reliability of Visual Inspection.* Rep. No. FHWA-RD-01–020, Washington, D.C.

Federal Highway Administration (FHWA) (2009). *Deficient Bridges by State and Highway System.* Washington, D.C. Accessed October 10, 2009. <http://www.fhwa.dot.gov/bridge/deficient.htm>

Koh, B.H. and Dyke, S.J. (2007). "Structural health monitoring for flexible bridge structures using correlation and sensitivity of modal data." *Computers and Structures*, 85, 117-130.

The Mathworks, Inc. (2007). MATLAB®. Version R2007a.

Morassi, A. and Tonon, S. (2008). "Dynamic testing for structural identification of a bridge." *Journal of Bridge Engineering*, 13(6), 573-585.

Pandey, A.K. Biswas, M., and Samman, M.M., (1991). "Damage detection from changes in curvature mode shapes." *Journal of Sound and Vibration*, 145(2), 321-332.

Pandey, A.K. and Biswas, M. (1994). "Damage detection in structures using changes in flexibility." *Journal of Sound and Vibration*, 169(1), 3-17.

Ragland, W.S., Penumadu, D., and Williams, R.T. (In review). "Damage detection on a full-scale five-girder bridge using an array of triaxial geophones." *Journal of Bridge Engineering.*

Ren, W. X., Zhao, T., and Harik, I. E. (2004). "Experimental and analytical modal analysis of a steel arch bridge." *Journal of Structural Engineering*, 130(7), 1022-1031.

Ren, W.X. and Peng, X.L. (2005). “Baseline finite element modeling of a large span cable-stayed bridge through field ambient vibration tests.” *Computers and Structures*, 83, 536-550.

Richardson, M.H. and Formenti, D.L., (1985). “Parameter estimation from frequency response measurements using rational fraction polynomials.” *Structural Measurement Systems Technical Note 85-3*.

Robinson, E.S. and Coruh, C. (1988). *Basic Exploration Geophysics*, John Wiley & Sons, New York.

Siddique, A. B., Sparling, B. F., and Wegner, L. D. (2007). "Assessment of vibration-based damage detection for an integral abutment bridge." *Canadian Journal of Civil Engineering*, 34(3), 438-452.

Sohn, H., Farrar, C. R., Hemez, F. M., Shunk, D. D., Stinemates, D. W., and Nadler, B. R. (2004). *A Review of Structural Health Monitoring Literature: 1996–2001*. Rep. No. LA-13976-MS, Los Alamos National Laboratory, Los Alamos, N.M.

Stubbs, N., Kim, Y.I., and Farrar, C.R., (1995). “Field verification of a nondestructive damage localization and severity estimation algorithm.” *Proceedings of the 13th International Modal Analysis Conference.*, Society of Experimental Mechanics, Bethel, CT., 210-218.

Zhang, Z., and Aktan, A. E. (1995). “The damage indices for the constructed facilities.” *Proceedings of the 13th International Modal Analysis Conference*, Society of Experimental Mechanics, Bethel, CT., 1520-1529.

Zhou, Z., Wegner, L. D., and Sparling, B.F. (2007). “Vibration-based detection of small-scale damage on a bridge deck.” *Journal of Structural Engineering*, 133(9), 1257-1267.

Chapter 7. Nondestructive Evaluation of Full-Scale Bridges Using Geophones

This chapter is revised based on an invited paper submitted to the Transportation Research Board's *Seventh International Bridge Engineering Conference* and potentially eligible for publication in a *Transportation Research Record: Journal of the Transportation Research Board* by William Ragland, Dayakar Penumadu, and Richard Williams:

Ragland, W.S., Penumadu, D., and Williams, R.T. (In review) "Nondestructive evaluation of full-scale bridges using geophones." Submitted to the *Seventh International Bridge Engineering Conference*, Dec. 1-3, 2010, San Antonio, Texas.

My primary contributions to the paper included: (i) Development of the problem into a work, (ii) gathering and reviewing literature, (iii) Arrangement, design, and conduction of the field test on the full-scale bridge, (iv) processing, analyzing, and interpretation of the experimental data, and (v) most of the writing.

7.1 Abstract

Nondestructive damage identification for civil engineering structures has received the attention of many researchers over the past several years. Vibration-based damage detection is a nondestructive structural health monitoring approach that focuses on changes in the dynamic characteristics of a structure as indicators of damage. All vibration-based damage detection techniques require high signal to noise vibration data

for analysis which makes the sensors used to measure vibrations an important consideration. The objective of this paper is to demonstrate the use of inexpensive geophones for determining the modal parameters of bridges for use with vibration-based damage detection techniques. A geophone is a velocity transducer commonly used by seismologists for subsurface exploration. Researchers typically use accelerometers to measure bridge vibrations. However, compared to geophones, accelerometers are relatively expensive, have lower sensitivity, and require active excitation (geophones are passive sensors). In order to validate the use of geophones for modal parameter identification, a simple beam experiment was conducted, and the results compared with theoretical values and a finite element model. Modal parameters identified from a full-scale bridge test are presented, and the effects of parapet rails and temperature change on the bridge's modal parameters are discussed. For successful implementation of the proposed methodology using a remote, wireless approach, a solar powered, cell phone modem based data acquisition system is demonstrated. This study makes an important contribution because the cost of the sensors needed for implementation of vibration-based damage detection on a large scale is substantially reduced using high sensitivity geophones.

7.2 Introduction

Vibration-based damage detection focuses on changes in the dynamic characteristics of a structure, such as natural frequency and mode shape, as indicators of damage. Several different global evaluation techniques and associated quantitative

damage indices have been published in recent years. Detailed reviews of these techniques as applied to bridges and other structures can be found in Doebling et al. (1996, 1998) and Sohn et al. (2004). In summary, the methods discussed monitor shifts in natural frequency, absolute changes in mode shapes, changes in mode shape curvature or strain energy, and variations in stiffness or flexibility matrices.

All vibration-based damage detection techniques begin with the acquisition of vibration data. In most cases, engineers employ accelerometers for the purpose of measuring bridge vibrations. Other instruments and techniques used on bridges that appear in the literature include the use of anemometers, temperature sensors, strain gauges, displacement transducers, global positioning systems, weigh-in-motion systems, corrosion sensors, elasto-magnetic sensors, optic fiber sensors, tiltmeters, level sensors, total stations, seismometers, barometers, hygrometers, pluviometers, and video cameras (Ko and Ni 2005).

It has been shown that the effectiveness of vibration-based damage detection techniques decreases with an increase in sensor spacing (Zhou et al. 2007). Thus, the number of sensors used and sensor placement are important considerations that must be addressed when implementing vibration-based damage detection techniques for the purpose of bridge monitoring. Krämer et al. (1999) state that "if high sensitivity, low frequency sensors were cheap, and only a small amount of data was to be acquired, stored, and processed, then a large number of sensors would be desirable." The current study directly addresses this issue by implementing high sensitivity, low frequency, inexpensive geophones to obtain triaxial vibration records on a full-scale bridge for the

purpose of extracting modal parameters for use with vibration-based damage detection techniques.

7.3 Geophones as Sensors

A geophone is a directional sensor that measures the speed of motion in the direction of its sensitive axis. In basic terms, a geophone is a coil suspended by springs around a permanent magnet, all of which is contained in a protective casing. When the coil moves relative to the magnet, a voltage is induced in the coil that depends on the relative velocity between the coil and magnet.

Traditionally, geophysicists, rather than bridge engineers, use geophones to measure elastic waves propagating through several kilometers of geologic materials. Detailed technical descriptions of the various types of geophones can be found in geophysical textbooks (Dobrin and Savit 1988, Robinson and Coruh 1988).

Accelerometers are commonly used for dynamic testing of civil engineering structures. However, geophones offer important advantages over accelerometers when considered for implementation in bridge monitoring systems. First of all, an accelerometer generally requires charge amplification electronics to produce a signal suitable for recording, and thus a power source is needed for the amplifier and associated hardware. In comparison, geophones are passive devices that produce a voltage that can be recorded without additional amplification or conditioning. The lack of a requirement for an external power supply and amplifier overcomes one of the obstacles in implementing remote bridge monitoring systems, and makes geophones ideal candidates

for implementation in such systems. Furthermore, geophones may be more easily incorporated into a wireless sensor system for bridge monitoring.

7.4 Modal Analysis

In this research, the rational polynomial method (Richardson et al. 1985) as implemented in DIAMOND (Farrar et al. 1998) was used for extracting natural frequencies and mode shapes from measured field data. DIAMOND (Damage Identification and Modal Analysis of Data) is a MATLAB® (Mathworks 2007) based software package developed at Los Alamos National Laboratories for modal analysis, damage identification, and finite element model refinement.

Briefly, the rational polynomial method uses orthogonal polynomials to estimate the coefficients of a polynomial approximation to the frequency response function (FRF). The FRF of a system is the ratio of the Fourier transform of the measured input and response signals. Thus, the rational polynomial method is intended for use with measured inputs. Because input forces were not recorded in this research, an assumption was made in order to implement the rational polynomial method. If an input force is known to have a flat spectrum, then any peaks in the response spectrum are caused by structural resonances. Therefore, it was assumed that the impulsive sources used during tests possessed a flat spectrum, at least over the frequency range of interest. This assumption allows the response spectrum matrix created from Fourier amplitude spectra to be analyzed instead of the FRF matrix.

This method of modal analysis is meant to simulate what would have to be used in an actual bridge monitoring system where inputs due to ambient sources, such as wind and traffic, are not easily measured. The results of this study indicate that the natural frequencies and operating shapes obtained using this procedure could be combined with vibration-based damage detection techniques.

7.5 Simply Supported Beam Test

In order to validate the geophone correction and modal analysis procedures used, a simply supported HP12x53 (Figure 7.1) was tested and analyzed. Field test results were compared to theoretical values and finite element models constructed using ABAQUS® (Dassault 2008): one model utilizing a pin and roller support, and the other using springs to simulate the support conditions. Partial results from the simple beam test are presented in Table 7.1 and Figure 7.2. For a more complete discussion of the simple beam test, the reader is referred to Ragland et al. (In review).

Figure 7.1. Simply supported test beam (HP12x53) instrumented with geophones

Table 7.1. Comparison of HP12x53 natural frequencies (Hz)

Mode	Theoretical	Field Test (Rational Polynomial)	ABAQUS Shell Elements	
			Simple Support	Spring Support
1	6.60	7.17	6.59	7.17
2	26.41	25.53	25.82	25.42
3	59.42	55.24	55.91	55.24

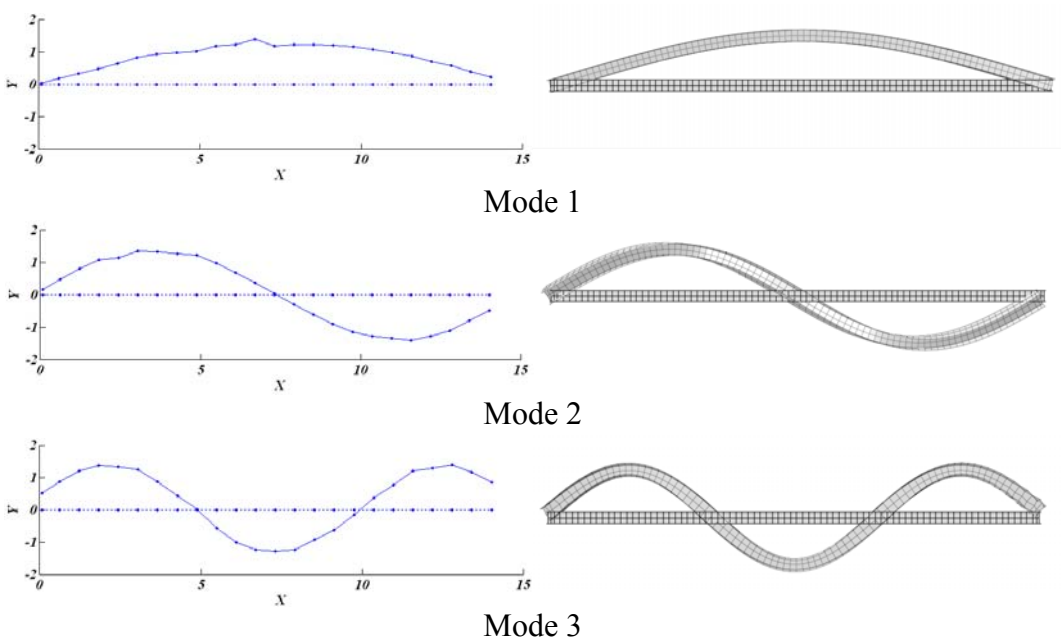

Figure 7.2. First three vertical bending modes of the HP12x53 test beam (m): DIAMOND using geophone data (left), ABAQUS (right)

The importance of accurately modeling the boundary conditions of a physical system (beam in this study) is apparent from inspection of Table 7.1. The first natural frequency is underestimated and the third natural frequency is overestimated theoretically and by using the simple support finite element model. However, using springs to model the boundary conditions provides a model that more closely represents the field test

results. Thus, the simple beam test results indicate that the manner in which boundary conditions are modeled has an appreciable effect on the modal frequencies.

7.6 Full-Scale Bridge Test

Constructed in 1967, the bridge tested (Figure 7.3) was reconditioned in 2008 and is part of 5th Avenue over the entrance ramp to James White Parkway from I-40 westbound in Knoxville, TN. The bridge consists of three spans comprised of a concrete deck supported by nine steel girders. Cross bracing in the form of steel channels was provided between all the girders. The bridge was constructed on a slight skew of five degrees. There is also a decrease in elevation from the west abutment (#1) to the east abutment (#2). The bridge carries four lanes of traffic with a sidewalk on each side. An elevation of the bridge is shown in Figure 7.4, and a typical cross section is shown in Figure 7.5.

From east to west, the bridge spans approximately 12, 15, and 12 m as shown in Figure 7.4. Two rolled W-shapes were connected with bolted splice plates to form one continuous beam over the entire bridge length. The seven interior beams are W27x84, while the two exterior beams are W36x135. Headed studs were used on top of the seven interior beams to promote composite action with the concrete deck. Connections that allowed for longitudinal (parallel to the bridge length) movement, marked "Exp" in Figure 7.4, and connections that prevented longitudinal movement, marked "Fix" in Figure 7.4, were installed at each location where a beam was supported by an interior bent. Each end of all the beams is integral with the abutment. Intermediate diaphragms,

C12x20.7, were located on average 5.3 m on center perpendicular to each beam, and end diaphragms, C15x33.9, were provided at each end of the bridge parallel to the bridge skew. During the bridge's reconditioning, two additional rows of C12x20.7 were added to the center span 3.8 m from each bent parallel to the bridge skew.

Figure 7.3. 5th Avenue over James White Parkway
(47SR1580051)

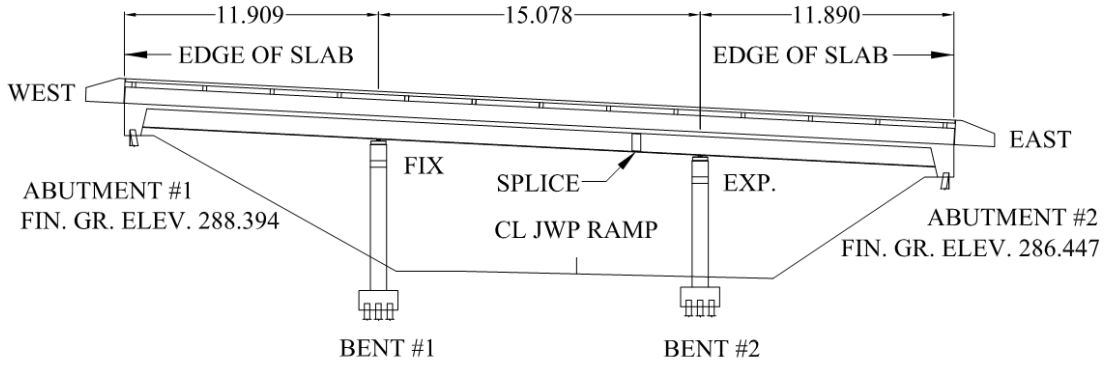

Figure 7.4. 5th Avenue over James White Parkway: elevation (m)

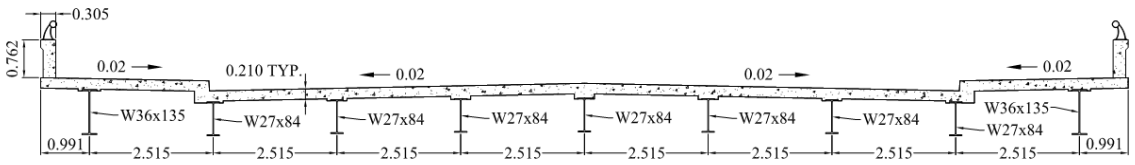

Figure 7.5. 5th Avenue over James White Parkway: typical cross-section (m)

7.7 Test Setup

Mark Products LRS-1000 10Hz vertical geophones and Mark Products L-28LBH 4.5Hz horizontal geophones were used for the vibration measurements. One vertical and one horizontal geophone were rigidly attached to a 1.6 cm thick, 11.5 cm diameter steel plate which rested on the bridge deck. The bridge was excited by dropping a 22.7 kg sandbag at a total of 3 different locations corresponding to the midpoint of the center span along beams B, E, and H in Figure 7.6.

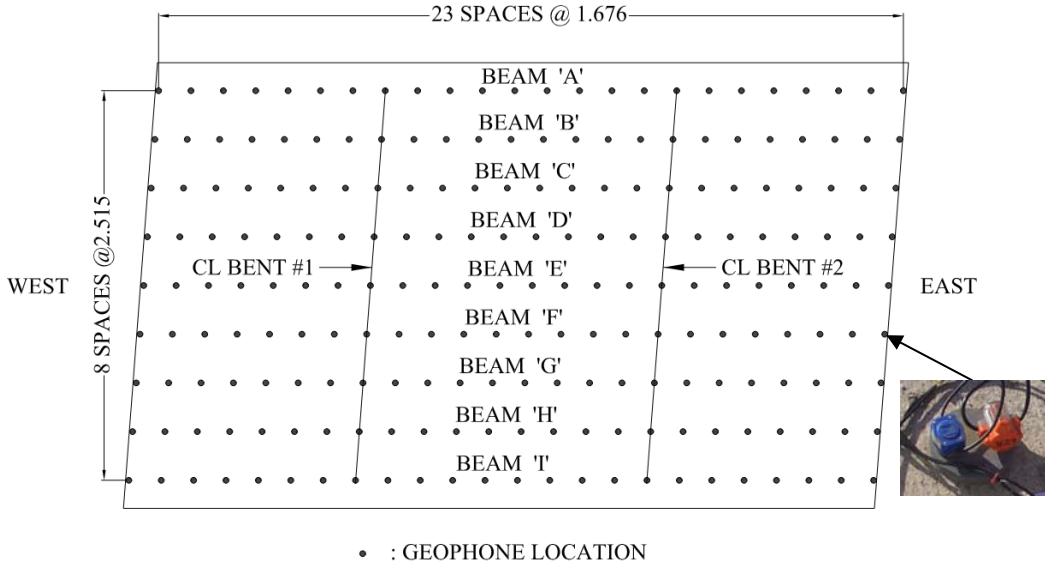

Figure 7.6. 5th Avenue over James White Parkway: geophone layout

Multiple tests were conducted on the bridge over the course of several months in order to evaluate the effects of temperature and the addition of a parapet rail on the bridge's modal parameters. A summary of the various tests conducted is presented in Table 7.2. At a minimum, data was recorded for fifteen seconds using a sampling rate of 125 Hz for each test which results in a frequency resolution of 0.067 Hz over a range of 0-62.5 Hz. During each test, data was recorded in the three global coordinate directions at the locations indicated in Table 7.2. When a full array of geophones was used, a total of 216 measurement locations were recorded using a Geometrics 48-channel StrataView® seismograph containing a 24-bit analog-to-digital (A/D) converter. Because the seismograph was only able to record 48 geophone signals at once (24 vertical and 24 horizontal each time), the 216 measurements locations were divided into nine groups. For each group, the geophones were spaced at 1.68 m center-to-center on the bridge deck along the beam line below as shown in Figure 7.6.

Table 7.2. Summary of field tests performed

Date (2009)	Designation	Temp. (°F)	Parapet Rail	Geophone Location	Data Logger Bit Depth	Sources
Jan. 22	Test 1	18-25	No	Full Array	24	Sandbag, Ambient
Feb. 17	Test 2	19-21	Yes	Full Array	24	Sandbag, Ambient
Apr. 21	Test 3	52-57	Yes	Beam 'A'	24, 16, 12	Sandbag, Ambient, Van
Apr. 30	Test 4	63-70	Yes	Full Array	24	Sandbag, Ambient
Aug. 26	Test 5	88	Yes	Beam 'A'	16	Traffic

In order to obtain triaxial vibration records when a full array of geophones was used, the sandbag was dropped and then dropped again after rotating the horizontal geophones by 90°. Once the data had been recorded in three directions, the line of geophones was shifted to the next position. This process was repeated until all 216 measurement locations were covered. For test 3, all coordinate directions were recorded simultaneously at the center 16 geophone locations along beam A in Figure 7.6. Test 5 was performed using two triaxial geophones and a more compact data acquisition system. For test 5, one triaxial geophone was placed at the midpoint of the west and center spans along beam A.

If multiple test setups were to be used to acquire the data for the full geophone array, it was important to verify that the same amount of energy was passed to the bridge each time the sandbag was dropped. If the source proved to be unrepeatable, the magnitude and phase relationship between various sensor setups would vary resulting in unintelligible mode shapes. However, as shown in Figure 7.7, dropping a sandbag at the same location imparts approximately the same amount of energy into the bridge each time which preserves the magnitude and phase relationships various sensor setups. This would not be the case under ambient loading such as wind or traffic. Due to the randomness of ambient loads, the magnitude and phase relationship between various sensor setups would vary widely making the identification of mode shapes difficult. Because a bridge will most likely be excited by traffic under service conditions, all the sensors used to characterize the bridge's dynamic response need to be recorded simultaneously, and geophones provide an economical way to accomplish this task.

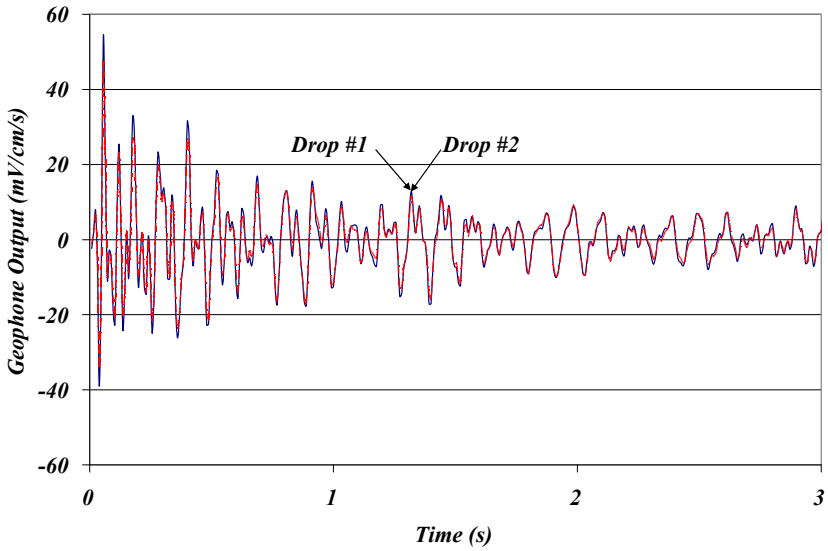

Figure 7.7. Comparison of vertical geophone signals from repeated drops

7.8 Parapet Rail Effects on Conventional Modal Properties

As a part of the current study, the test bridge was evaluated to determine the effects of adding a parapet rail on the bridge's modal properties. The bridge was first tested before the parapet rail was poured (test 1) and then tested again after the rail was poured (test 2). In an effort to minimize the effects of temperature on the obtained results, the post-rail test was performed when the ambient temperature was a close as possible to the pre-rail test.

In order to quantify the correlation between mode shapes measured before and after the parapet rail was poured, a modal assurance criterion (MAC) (Ewins 1985) was used. The MAC, Eq. 7.1, takes advantage of the orthogonal property of mode shapes to compare different modes. If the modes are identical, a value of one will be obtained. If the modes are dissimilar, a value of zero will be obtained. Ewins (1985) notes that in

practice, modes are considered correlated if a value greater than 0.9 is calculated and uncorrelated if a value less than 0.05 is calculated. The MAC that compares mode *i* and *j* has the form given in Eq. 7.1 where $(\Phi)_k$ is an element of the mode shape vector and *n* represents the number of points at which the two mode shapes are compared.

$$MAC(i,j) = \frac{\left|\sum_{k=1}^{n}(\Phi_j)_k(\Phi_i)_k\right|^2}{\left(\sum_{k=1}^{n}(\Phi_j)_k(\Phi_j)_k\right)\left(\sum_{k=1}^{n}(\Phi_i)_k(\Phi_i)_k\right)} \quad 7.1$$

Natural frequencies for the fundamental bending mode (mode 1), the first torsional mode (mode 2), and the second bending mode (mode 3) measured before and after the parapet rail pour, as well as the correlation between the pre and post parapet rail mode shapes, are presented in Table 7.3. The corresponding mode shapes for the frequencies presented in Table 7.3 are shown in Figure 7.8. Note that each grid intersection in Figure 7.8 represents a measurement location.

Table 7.3. Pre and post parapet rail natural frequencies and mode shape correlation

Date	Designation	Avg. Temp. (°F)	Parapet Rail	Mode 1 (Hz)	Mode 2 (Hz)	Mode 3 (Hz)
Jan. 22	Test 1	21.5	No	7.74	8.88	9.59
Feb. 17	Test 2	20	Yes	7.71	9.07	9.30
Percentage Difference (%)				-0.39%	2.14%	-3.02%
MAC				0.953	0.869	0.823

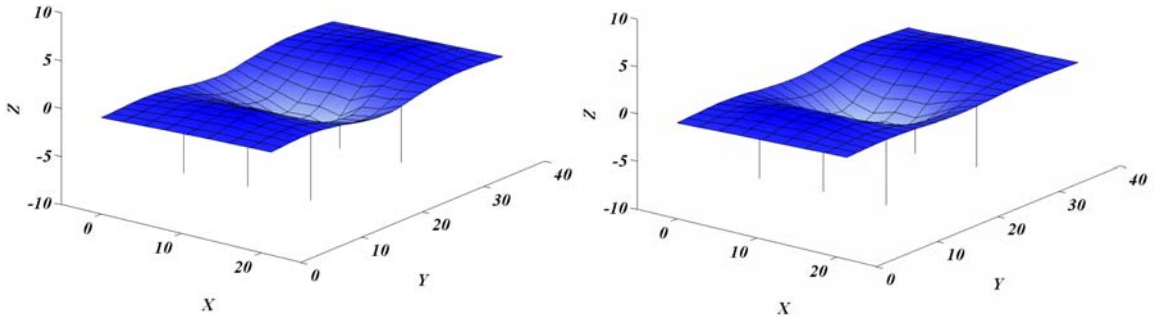

Mode 1: Fundamental bending

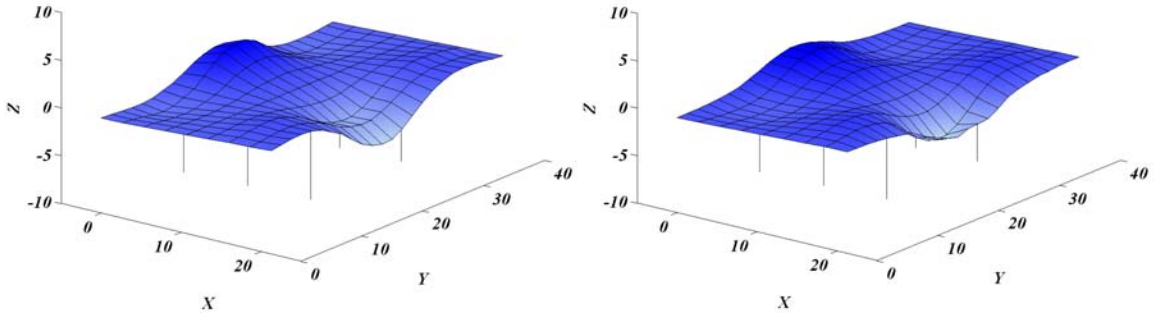

Mode 2: First torsional

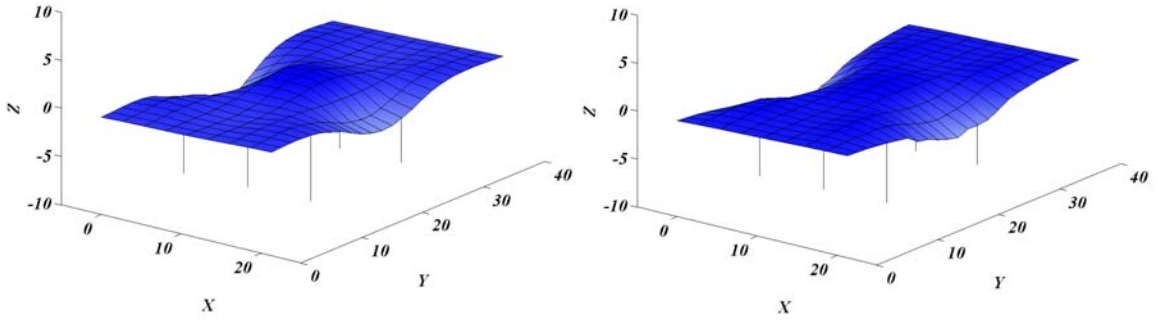

Mode 3: Second bending

Figure 7.8. Comparison of mode shapes obtained before (left) and after (right) pouring the parapet rail

Observing Table 7.3, it can be seen that the addition of the parapet rail has a larger effect on the higher order modes than the fundamental bending mode (mode 1). The first torsional mode (mode 2) and second bending mode (mode 3) show significantly larger percentage changes in natural frequency than the fundamental bending mode (mode 1). Also, the correlation between pre and post parapet rail mode shapes decreases as the modal order increases. These observations suggest that the addition of the parapet rail has a greater effect on higher order modes of vibration.

It was expected that the addition of the parapet rail would stiffen the bridge resulting in an increase in natural frequency. However, observing Table 7.3 and Figure 7.8, it can be seen that the addition of the parapet rail only stiffens the asymmetric, torsional mode. The symmetric bending modes exhibit no additional stiffness in terms of natural frequency from the addition of the parapet rail. The added mass of the parapet seems to have offset any additional stiffness the parapet may have added to the symmetric bending modes. Therefore, it appears that the addition of the parapet only has stiffening effects on asymmetric modes, such as the first torsional mode.

7.9 Temperature Effects on Conventional Modal Properties

Multiple tests were performed on the test bridge to determine the effects of temperature on the bridge's modal properties. Previous researchers have shown that environmental conditions can cause significant percentage changes in natural frequencies (Farrar et al. 1997). Because the focus of this study is determining modal parameters for

use with vibration-based damage detection techniques, it is important to understand how the modal properties of a bridge are affected by changing environmental conditions.

The natural frequencies obtained for the test bridge at various temperatures are presented in Table 7.4. Observing Table 7.4, it can be seen that changes in the ambient air temperature have an appreciable effect on the identified natural frequencies of the test bridge. In fact, a change in ambient air temperature from 20˚F to 88˚F results in greater changes in the identified natural frequencies than the addition of the parapet rail to the bridge. Considering this observation, it is unlikely that incipient damage to the bridge would result in natural frequency changes substantial enough to be a reliable indicator of damage. Therefore, similar observations noted by previous researchers (Liu and DeWolf 2007) are confirmed by this study, and changes in natural frequencies alone are deemed to be unreliable indicators of damage.

Table 7.4. Summary of field tests performed

Date	Designation	Avg. Temp. (°F)	Parapet Rail	Mode 1 Fundamental Bending (Hz)	Mode 2 First Torsional (Hz)	Mode 3 Second Bending (Hz)
Feb. 17	Test 2	20	Yes	7.71	9.07	9.30
Apr. 21	Test 3	56	Yes	7.71 0%	8.92 -1.65%	9.2 -1.08%
Apr. 30	Test 4	66.5	Yes	7.62 -1.17%	8.80 -2.98%	9.05 -2.69%
Aug. 26	Test 5	88	Yes	7.61 -1.30%	8.72 -3.86%	8.95 -3.76%
MAC (Tests 2 and 4)				0.959	0.833	0.932

Note: Percentages are differences from Test 2. MAC values compare modes obtained using a full array of geophones from Tests 2 and 4.

The correlation of the mode shapes identified from tests 2 and 4 using a full array of geophones is also presented in Table 7.4. Note that the bending mode shapes (modes 1 and 3) remain relatively well correlated for both tests. However, the torsional mode shape's correlation decreases with an increase in temperature. This observation suggests that the first torsional mode shape is more sensitive to changes in the bridge caused by temperature variations than the fundamental or second bending modes. Extending this observation, the first torsional mode may also be more sensitive to changes in the bridge caused by damage, such as girder cracking, than fundamental or second bending modes.

7.10 Remote Data Acquisition System Demonstration

In order to demonstrate that the proposed methodology could be implemented in a remote setting, a solar powered, cell phone modem based data acquisition system was compared to the wired system used to obtain full geophone array data sets. The remote data acquisition setup used is shown in Figure 7.9.

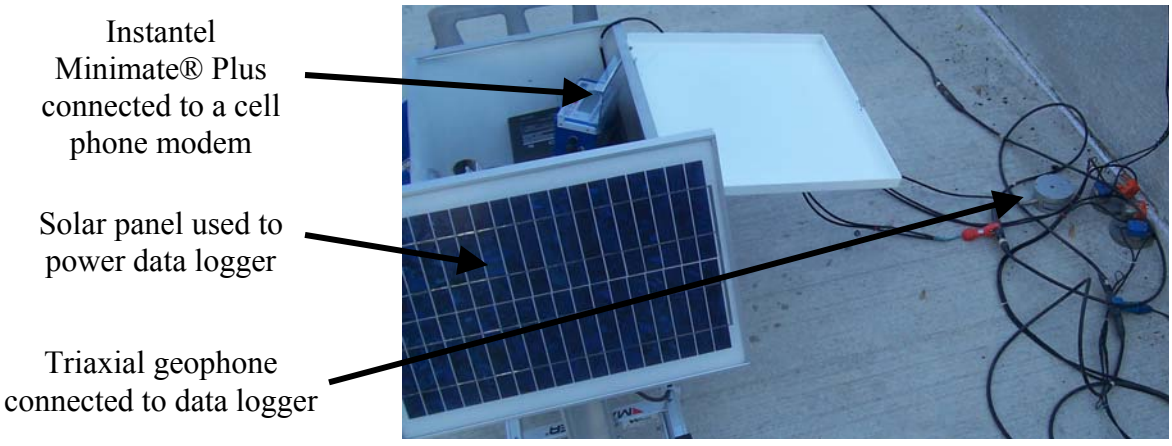

Figure 7.9. Remote data acquisition system

The system tested consisted of a triaxial geophone connected to an Instantel Minimate® Plus vibration monitor which was in turn connected to a cell phone modem and powered by a solar panel. Once the vibration monitor was triggered to record (manually for this study, but it could be set to use a preset vibration amplitude), data from the geophone was recorded for a preset time and sample rate. After acquisition, the data file was sent remotely via the cell phone modem to a server where the file could be downloaded for further evaluation.

As a part of the remote data acquisition system demonstration, systems incorporating various A/D conversion resolutions were also compared. The Instantel Minimate® Plus contained a 12-bit A/D converter, the Geometrics StrataView® seismograph contained a 24-bit A/D converter, and the Instantel Minitmate® Pro4 contained a 16-bit A/D converter. Overall, each conversion resolution was able to successfully measure the peak vibration amplitudes and produce time series and frequency spectra that were visually similar. However, upon closer inspection of the data files, it was found that the 12-bit data series contained several missing values of measured velocity in the digitized file. Therefore, it is recommended that data acquisition systems used for measuring bridge vibrations contain at least a 16-bit A/D converter.

Although on a small scale, the remote data acquisition system functioned extremely well. Data sent remotely to the server compared very well with data obtained using the larger wired system. While additional research is needed in the area of vibration-based damage detection on bridges, optimal sensor placement, and the optimal

number of sensors to be used, this demonstration has proven that geophones can successfully be implemented in remote bridge monitoring systems.

7.11 Summary and Conclusions

The goal of this study was to evaluate the use of inexpensive geophones for the purpose of dynamically characterizing full-scale bridges using output only data for the purpose of structural health monitoring. The effects of temperature and the addition of parapet rails on the bridge's dynamic response were also evaluated, and the incorporation of geophones into a remote bridge monitoring system was demonstrated on a small scale.

One of the significant obstacles in implementing remote monitoring systems is the cost of the sensors. The results of this study have demonstrated that low-cost geophones can be used to characterize the dynamic response of a bridge. Furthermore, because geophones do not require a power source, the obstacle of providing sensor power in a remote monitoring setting is eliminated using geophones. Throughout the described tests, the only power source used was a battery to power the seismograph which could easily be replaced with a solar panel as demonstrated in this study.

The density of sensors used in the current study resulted in mode shapes that are much more defined than those often reported in the literature. Thus, mode shape detail that may have been missed by other researchers has been identified in the current study. Because the more effective vibration-based damage detection techniques rely on changes in mode shapes and their derivatives, additional mode shape detail may prove to be invaluable in implementing these techniques in remote monitoring systems, and geophones provide an economical way to obtain the additional detail.

The current study demonstrated that the addition of a parapet rail to the test bridge affected its higher order modes more than its fundamental bending mode. It was also demonstrated that, in terms of natural frequency, the first torsional mode was stiffened by the addition of the parapet while the first and second bending modes were not. Thus, the addition of parapet rails seems to affect the stiffness of asymmetric modes more than symmetric modes.

Additionally, it was found that changes in the ambient air temperature significantly affected the natural frequencies of the test bridge. In fact, larger percentage changes in natural frequency resulted from changes in air temperature than the addition of the parapet rail. Considering these observations, changes in natural frequency were determined to be relatively unreliable indicators of damage when used alone.

The current study has also demonstrated that the rational polynomial method can be used for modal parameter identification using output-only data. The method is fairly straightforward and easy to understand making it more user friendly for parameter estimation than some of the other methods reported in the literature.

7.12 Acknowledgements

The authors would like to thank Jeff Walker of Bell and Associates Construction, Phil Large of Wilbur Smith and Associates, and Terry Leatherwood, Henry Pate, and Ed Wasserman of the Tennessee Department of Transportation for their help and cooperation. Special thanks are also extended to Dave Harrison and George Condjella of Seismic Surveys Inc. for their help and use of their equipment.

7.13 References

Dassault Systèmes, Inc., SIMULIA Corp. (2008). ABAQUS®. Version 6.8.

Dobrin, M.B. and Savit C.H. (1988). *Introduction to Geophysical Prospecting*, 4th Ed., McGraw-Hill, New York.

Doebling, S.W., Farrar, C.R., Prime, M.B., and Shevitz, D.W. (1996). *Damage Identification and Health Monitoring of Structural and Mechanical Systems from Changes in Their Vibration Characteristics: A Literature Review*. Rep. No. LA 13070-MS, Los Alamos National Laboratory, Los Alamos, N.M.

Doebling, S.W., Farrar, C.R., and Prime, M.B. (1998). "A summary review of vibration-based damage identification methods." *The Shock and Vibration Digest*, 30(2), 91–105.

Ewins, D.J. (1985). *Modal Testing: Theory and Practice*. John Wiley, New York.

Farrar, C.R., Doebling, S.W., Cornwell, P.J., and Straser, E.G. (1997). "Variability of modal parameters measured on the Alamosa Canyon bridge." *Proceedings of the 15th International Modal Analysis Conference*, Orlando, FL, 257–263.

Farrar, C.R., Doebling, S.W., and Prime, M.B. Cornwell, P.J., Kam, M., Straser, E.G., Hoerst, B.C., Shevitz, D.W., and Jauregui, D.A. (1998). *A Comprehensive Monitoring System for Damage Identification and Location in Large Structural and Mechanical Systems.* Rep. No. LA-UR-98-233, Los Alamos National Laboratory, Los Alamos, N.M.

Ko, J.M. and Ni, Y.Q. (2005). "Technology developments in structural health monitoring of large-scale bridges." *Engineering Structures,* 27(12), 1715-1725.

Krämer, C., De Smet, C.A.M., and De Roeck, G. (1999). "Z24 bridge damage detection tests." *Proceedings of the 17th International Modal Analysis Conference,* Kissimmee, FL, USA.

Liu, C.Y. and DeWolf, J.T. (2007). "Effect of temperature on modal variability of a curved concrete bridge under ambient loads." *Journal of Structural Engineering*, 133(12), 1742-1751.

The Mathworks, Inc. (2007). MATLAB®. Version R2007a.

Ragland, W.S., Penumadu, D., and Williams, R.T. (In review). "Nondestructive evaluation of a full-scale bridge using an array of triaxial geophones." *Journal of Structural Engineering*.

Richardson, M.H. and Formenti, D.L. (1985). "Parameter estimation from frequency response measurements using rational fraction polynomials." *Structural Measurement Systems Technical Note 85-3*.

Robinson, E.S. and Coruh, C. (1988). *Basic Exploration Geophysics*, John Wiley & Sons, New York.

Sohn, H., Farrar, C.R., Hemez, F. M., Shunk, D.D., Stinemates, D.W., and Nadler, B.R. (2004). *A Review of Structural Health Monitoring Literature: 1996–2001*. Rep. No. LA-13976-MS, Los Alamos National Laboratory, Los Alamos, N.M.

Zhou, Z., Wegner, L.D., and Sparling, B.F. (2007). "Vibration-based detection of small-scale damage on a bridge deck." *Journal of Structural Engineering*, 133(9), 1257-1267.

Chapter 8. Conclusions and Future Work

8.1 Summary and Conclusions

8.1.1 Simple Beam and UT Test Bridge

The goal of the initial studies involving the simple beam and UT test bridge was to evaluate the use of inexpensive geophones for the purpose of dynamically characterizing full-scale bridges using output only data. The motivation behind these studies was to determine a reliable and inexpensive method to accurately determine modal parameters for use with vibration-based damage detection techniques. The following observations were made from this study:

- Low-cost geophones can be used to characterize the dynamic response of a bridge. Because geophones do not require a power source, the obstacle of providing sensor power in a remote monitoring system is eliminated using geophones.

- It was demonstrated that the rational polynomial method can be used for modal parameter identification using output-only data. Assuming the input function has a relatively flat response over the frequency range of interest allows the response spectrum matrix created by multiplying the spectrum of each measured response by the conjugate spectrum of a reference response to be analyzed instead of a measured FRF matrix. This research demonstrated that this method of modal analysis produces accurate and reliable results. The method is fairly

straightforward and easy to understand making it more user friendly for parameter estimation than some of the other methods reported in the literature.

- The density of sensors used in the study resulted in mode shapes that are more defined than those often reported in the literature. Thus, mode shape detail that may have been missed by other researchers has been identified in the current study. Because the more effective vibration-based damage detection techniques rely on changes in mode shapes and their derivatives, additional mode shape detail may prove to be invaluable in implementing these techniques in remote monitoring systems, and geophones provide an economical way to obtain the additional detail.

8.1.2 Entrance to James White Parkway Over 4th Avenue

The goal of the three-girder bridge study was to compare various vibration-based damage detection techniques based on their ability to locate damage induced on an in-situ, full-scale bridge using triaxial vibration measurements obtained using inexpensive geophones. Unlike previous studies, which rely heavily on the vertical response of bridges for damage detection, the current study has incorporated the three-dimensional response of a bridge into the evaluated damage detection techniques. The following observations were made from this study:

- The transverse and longitudinal responses are also capable of identifying damage. The longitudinal response of the bridge appeared to be particularly sensitive to damage, even in the early stages of crack propagation.

- The first torsional mode of vibration was found to be better suited for use with the vibration-based damage detection techniques evaluated. When combined with the longitudinal component of the first torsional mode, each damage detection method evaluated was able to successfully locate the damage on a global level. This was true even for the lowest damage scenario.

- Using results based only on the fundamental bending mode, damage could only be located locally on the damaged beam. The poor performance of the fundamental bending mode is attributed to its lack of a strong horizontal component.

- Overall, observations from the study indicate that the horizontal response of a bridge is more sensitive to damage than the vertical response, and that modes exhibiting a strong horizontal component should be used with vibration-based damage detection techniques.

- The study has found natural frequencies and mode shapes to be relatively poor indicators of damage when used alone. The more complex damage detection methods described were found to be much better indicators of damage.

- When the results of the study are considered as a whole, the damage index method and change in flexibility method were found to perform best.

- Incorporation of multiple modes was found to have little effect on the results obtained using either method particularly if the modes did not exhibit a strong horizontal component.

- The results of this study demonstrated that low-cost geophones can be used to characterize the dynamic response of a bridge, and the obtained results can be successfully implemented with vibration-based damage detection techniques.

- It was demonstrated that the rational polynomial method can be used for modal parameter identification using output-only data, and the obtained results can be successfully implemented with vibration-based damage detection techniques.

- Data sets obtained from in-situ, full-scale bridge tests both in an undamaged and damaged condition are scarce. No other data set is known to exist that contains triaxial vibration records collected over a relatively dense measurement grid on an

in-situ, full-scale bridge in undamaged and damaged conditions. Thus, this study has provided a valuable data set for continued research in the area of vibration-based damage detection related to bridges.

8.1.3 I-40 Westbound Over 4th Avenue

The goal of the five-girder bridge study was to compare various vibration-based damage detection techniques based on their ability to locate damage induced near a support on an in-situ, full-scale bridge using triaxial vibration measurements obtained using inexpensive geophones. The following observations were made from this study:

- The transverse and longitudinal responses of the bridge are also capable of identifying damage.

- None of the damage detection methods evaluated was able to successfully locate the induced damage on a global or local level using the vertical component of any of the identified mode shapes.

- When combined with the horizontal components of the identified mode shapes, each method was able to successfully locate the damage on a global level using at least one of the identified mode shapes with the exception of the change in uniform load surface curvature method which was only able to locate the damage on a local level.

- The horizontal response of a bridge seems to be more sensitive to damage than the vertical response, and thus modes exhibiting stronger horizontal components should be used with vibration-based damage detection techniques.

- This study found the second bending mode of vibration to be more consistent at locating the induced damage when combined with the damage detection techniques evaluated.

- The results obtained using the fundamental mode and the damage detection techniques, with the exception of the damage index method, were fairly inconsistent. The inconsistency of the fundamental bending mode is attributed to its predominantly vertical behavior and lack of stronger horizontal components.

- Based on simulated data obtained from the calibrated finite element model, the observation from the three-girder bridge study that the first torsional mode was better suited for identifying damage located at mid-span of an exterior girder was confirmed. Considering the relative symmetry of the bridges tested, it is not surprising that damage affecting the bridge's symmetry is more easily identified using asymmetric modes such as the first torsional mode. This observation further suggests that modes other than the fundamental bending mode should be included when using vibration-based damage detection techniques.

- The horizontal response of a bridge should be included in the calibration process to obtain an accurate representation of the three dimensional response of the bridge. The horizontal response was found to be much more sensitive to the manner in which boundary conditions were applied than the vertical response. Using the MAC as a calibration tool, a well calibrated model was constructed using traditional roller type connections to model the expansion supports at each abutment when only the vertical response of the bridge was considered. However, when the horizontal response of the bridge was considered, the same model was not well correlated to the field test results as defined using the MAC.

- It was found that using springs to model the expansion supports at the abutments provided the best overall model when compared with the field test results as a whole.

- Studies using calibrated finite element models to obtain damaged data sets should include the horizontal response of the bridge in the calibration process to obtain a model that allows for the accurate assessment of vibration-based damage detection techniques using simulated data.

- The diaphragm bracing was also found to have a significant impact on the dynamic response of the bridge. If the diaphragm bracing was not considered, the correlation of the higher order experimental and analytical modes was poor.

- Inclusion of higher order modes in the calibration process is important to obtain a well correlated model. Overall, the highest order mode identified was found to be much more sensitive to changes made to the model than the other modes.

- Developing a well calibrated finite element model of the bridge considered in this research required substantial effort to match the measured undamaged response. Once a suitable model of the bridge was developed, it provided a relatively accurate damaged response when compared to the measured damaged response of the test bridge. Thus, the use of calibrated finite element models shows promise for implementation in structural health monitoring of bridges.

- This study has found natural frequencies and mode shapes to be relatively poor indicators of damage when used alone. The more complex damage detection methods described were found to be much better indicators of damage.

- Incorporation of multiple modes was found to have little effect on the results obtained using either method.

- When the results of the study are considered as a whole, the damage index method was found to perform best.

- This study further demonstrated that low-cost geophones can be used to characterize the dynamic response of a bridge, and the obtained results can be successfully implemented with vibration-based damage detection techniques.

- This study further demonstrated that the rational polynomial method can be used for modal parameter identification using output-only data, and the obtained results can be successfully implemented with vibration-based damage detection techniques.

- This study provides another valuable set data set for future research that contains triaxial vibration records collected over a relatively dense measurement grid on an in-situ, full-scale bridge in undamaged and damaged conditions.

8.1.4 5th Avenue Over the Entrance Ramp to James White Parkway

The goal of this study was to evaluate the use of inexpensive geophones for the purpose of dynamically characterizing full-scale bridges using output only data for the purpose of structural health monitoring. The following observations were made from this study:

- The results of this study again demonstrated that low-cost geophones can be used to characterize the dynamic response of a bridge.

- It was again demonstrated that the rational polynomial method can be used for modal parameter identification using output-only data.

- The addition of parapet rails to the test bridge affected its higher order modes more than its fundamental bending mode.

- It was found that, in terms of natural frequency, the first torsional mode was stiffened by the addition of the parapet while the first and second bending modes were not. Thus, the addition of the parapet rail seems to affect the stiffness of asymmetric modes more than symmetric modes.

- It was found that changes in the ambient air temperature appreciably affected the natural frequencies of the test bridge.

- Larger percentage changes in natural frequency resulted from changes in the ambient air temperature than the addition of the parapet rail.

- Changes in natural frequency are again deemed to be relatively unreliable indicators of damage when used alone.

- It was demonstrated that geophones can successfully be implemented in remote bridge monitoring systems.

8.2 Suggestions for Future Work

As a result of this study, some areas of possible future work have been identified in the following areas.

- One of the most cumbersome aspects of the research described was the wired geophone system. Ensuring that all the connections were in good contact was time consuming as well as frustrating. Therefore, future work in the development of a wireless geophone system is suggested.

- While the current research has employed a relatively dense array of sensors, the ideal bridge monitoring system would be built around a much smaller number of sensor locations. Therefore, future work in the development of an optimal sensor placement strategy is suggested.

- Results obtained in this research using a full array of geophones on the bridge deck were obtained on bridges closed to traffic. Therefore, future work using a full array of geophones on an in-service bridge, mounting the geophones on the underside of the bridge deck or to the girders, is suggested.

- The primary focus of this research was moderate span, concrete slab, on steel girder bridges. Therefore, it is suggested that future work be performed on

various bridge types such as reinforced concrete, prestressed concrete, truss, and long span steel girder.

- This research demonstrated that modal parameters could be extracted from relatively short vibration records and successfully implemented with vibration-based damage detection techniques. In hindsight, longer vibration records would have been preferable. In a remote monitoring system, the amount of data to be stored and transmitted is somewhat of a limiting constraint. Therefore, future work involving optimal data acquisition rates, lengths, and times is suggested.

- While the damage detection techniques evaluated in this research were found to perform satisfactorily at times, the interpretation of the results would have been difficult had the location of the damage not been know *a priori*. Based on the density of the sensors used in this study, better spatial resolution of the damage location was hoped for. The fact that the ideal bridge monitoring system would only incorporate a small number of sensors suggests that implementing the damage detection techniques evaluated in this research in a bridge monitoring system is impractical. Therefore, future work studying ways of identifying damage using the vibration records from a small number of sensors is suggested. For example, the present study has evaluated changes in the cross power spectrum of various combinations of the vertical and horizontal vibration components obtained on the undamaged and damaged bridge. Although further research is

needed, it appears the horizontal response of the bridge is once again more sensitive to the induced damage than the vertical response as seen in Figure 8.1, Figure 8.2, and Figure 8.3. These figures were constructed using vibration records obtained during the three-girder bridge test at the midpoint of beam 2 in Figure 4.4.

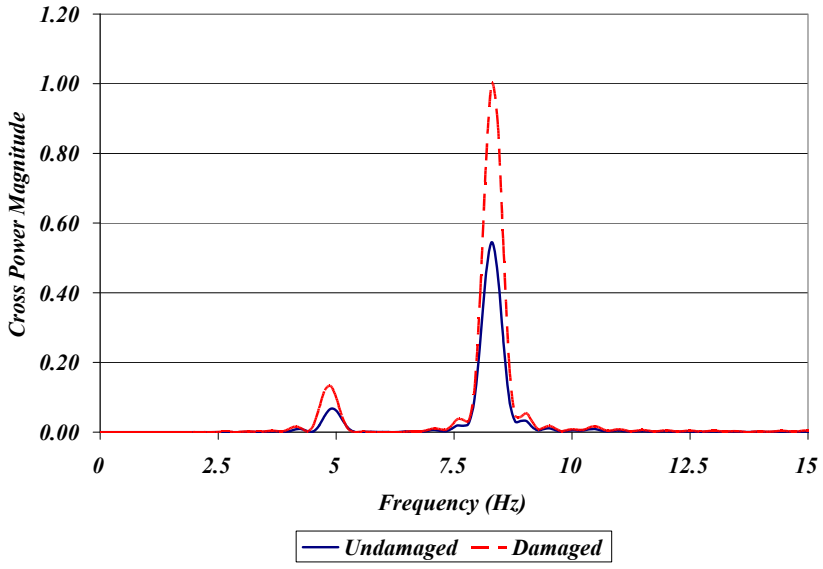

Figure 8.1. Cross power spectra of undamaged (D0) and damaged (D3) vertical vibration records obtained during the three-girder bridge test

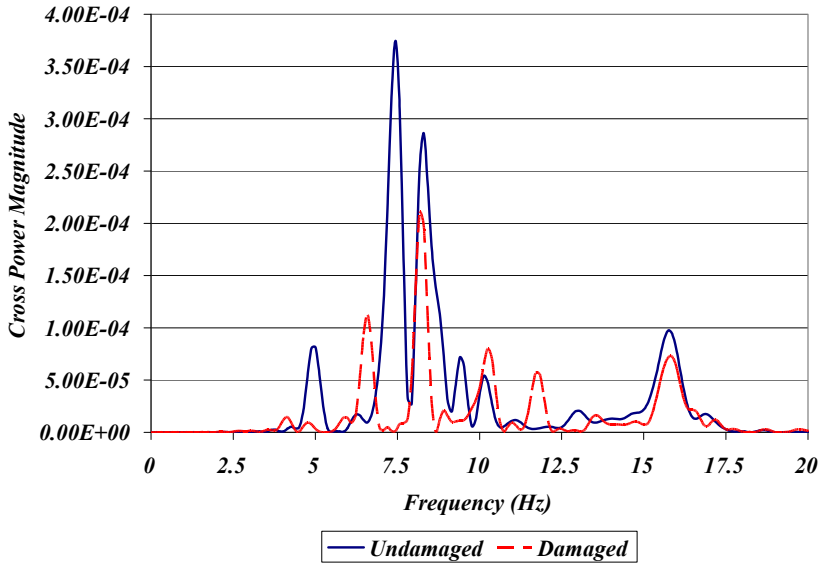

Figure 8.2. Cross power spectra of undamaged (D0) and damaged (D3) longitudinal vibration records obtained during the three-girder bridge test

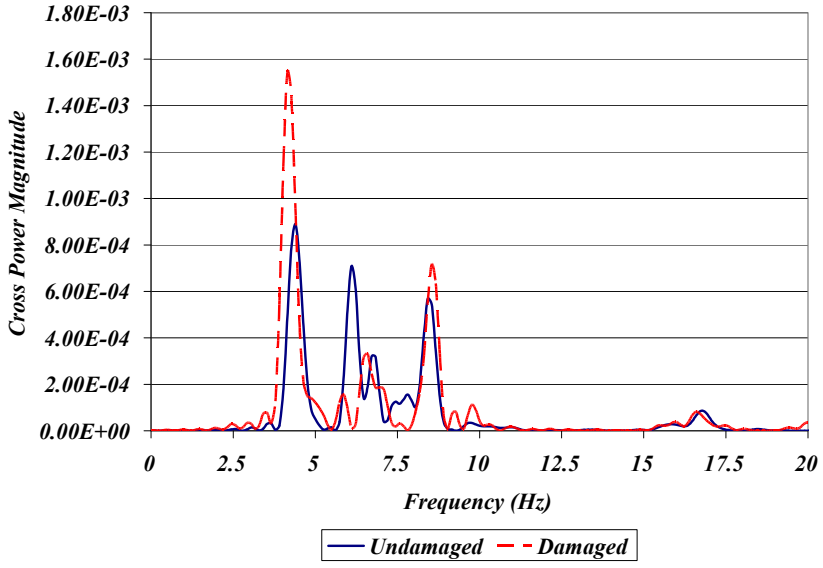

Figure 8.3. Cross power spectra of undamaged (D0) and damaged (D3) transverse vibration records obtained during the three-girder bridge test

Vita

William Steven Ragland II was born May 28, 1984, in Knoxville, Tennessee, to Steve and Joyce Ragland. William has one sister, Maggie. Originally from Crossville, Tennessee, William's family moved to Cookeville, Tennessee, in 1985. William attended Northeast Elementary School, Avery Trace Middle School, and is a 2002 graduate of Cookeville High School. On May 14, 2005, William married the love of his life, Rachel Elizabeth Trump, of Kingsport, Tennessee. William holds a Bachelor of Science in Civil Engineering (December 2005), a Master of Science in Civil Engineering (December 2006), and a Doctor of Philosophy in Civil Engineering (December 2009) from The University of Tennessee, Knoxville.